Politecnico di Milano

Industrial Engineering

Energy Engineering, Power Production

0D-1D THERMO-FLUID DYNAMIC MODELLING OF CYLINDER SCAVENGING PROCESS IN A FOUR STROKE IC ENGINE

Tesi di Laurea di:

Christian Leoni Matr. 892162

Gianmarco Latella Matr. 892266

Relatore: Prof. Angelo Onorati

Correlatore: Dott. Andrea Massimo Marinoni

ANNO ACCADEMICO 2018–2019

Extended abstract

Nowadays environmental topics, such as air pollution and global warming, are increasingly popular on the scientific debate. Focusing on the automotive sector, progressively stricter regulations have been applied on new designed cars, since internal combustion engines, together with tyres and brakes, are one of the major sources of local pollutants.
The aim of this thesis is to improve the performance of *Gasdyn*, a 1D engine simulation tool developed by the Energy Departement of Politecnico di Milano, in the prediction of pollutants emissions. In particular, we will concentrate our attention on the evaluation of *unburned hydrocarbons* emissions from SI engines, by means of a new model for *cylinder scavenging*.

Engine Gasdynamics Fundamental Equations

Gasdynamics in internal combustion engines is characterized by three dimensionality, unsteadiness and turbulence; thus, in order to completely represent the flowfield inside an IC engine, a 3D mathematical model should be applied. However, this kind of model involves the system of 3D Navier Stokes equations, which cannot be solved analytically but just numerically, with an enormous computational effort.

For these reasons, it is not possible to deal with the whole engine simulation with a 3D approach. This latter is adopted just for single pieces of equipment, while a 1D model has to be considered for the whole architecture, with the following fundamental assumptions:

- unsteady flow;
- one-dimensional flow: the longitudinal dimension of the duct-systems is significantly greater than the transversal one;
- compressible fluid: perfect gas model, with constant specific heats, or mixture of ideal gases, with specific heats depending both on temperature and composition;
- friction and heat transfer only at the gas-wall interface;
- non-adiabatic and non-isentropic flow;
- variable cross-section with assigned law.

In order to describe the fluid dynamics of flows inside pipes and cylinders, four conservation equations are applied:

- Mass Conservation:

$$\frac{\partial \rho}{\partial t} + \frac{\partial(\rho u)}{\partial x} + \frac{\rho u}{F}\frac{dF}{dx} = 0$$

- Momentum Conservation:

$$\frac{\partial u}{\partial t} + u\frac{\partial u}{\partial x} + \frac{1}{\rho}\frac{\partial p}{\partial x} + G = 0$$

- Energy Conservation:

$$\frac{\partial(\rho e_0)}{\partial t} + \frac{\partial(\rho u h_0)}{\partial x} + \frac{\rho u h_0}{F}\frac{dF}{dx} - \rho\dot{q} - \Delta H_{react} F dx = 0$$

- Transport of Species:

$$\frac{\partial}{\partial t}(\rho F Y_j) + \frac{\partial}{\partial x}(\rho u F Y_j) + \rho F \dot{Y_j} = 0$$

These equations are difficult to manage as they are; therefore, a matrix form is derived from them:

$$\frac{\partial}{\partial t}\vec{W}(x,t) + \frac{\partial}{\partial x}\vec{F}(\vec{W}) + \vec{B}(\vec{W}) + \vec{C}(\vec{W}) = 0$$

where: $\vec{W}(x,t)$ is the conserved variables vector, $\vec{F}(\vec{W})$ is the fluxes vector, $\vec{B}(\vec{W})$ and $\vec{C}(\vec{W})$ are the vectors of source terms.

$$\vec{W} = \begin{bmatrix} \rho F \\ \rho u F \\ \rho e_0 F \\ \rho \vec{Y} F \end{bmatrix} \qquad \vec{F} = \begin{bmatrix} \rho u F \\ (\rho u^2 + p) F \\ \rho u h_0 F \\ \rho u \vec{Y} F \end{bmatrix}$$

$$\vec{B} = \begin{bmatrix} 0 \\ -p\frac{dF}{dx} \\ 0 \\ 0 \end{bmatrix} \qquad \vec{C} = \begin{bmatrix} 0 \\ \rho G F \\ -(\rho\dot{q} + \Delta H_{react}) F \\ \rho \dot{Y} F \end{bmatrix}$$

Scavenging model for HC emissions

As far as it concerns pollutants emission, SI engines mainly emits Nitrogen Oxides (NO_x), Carbon Monoxide (CO) and Unburned Hydrocarbons (HC). Focusing on the last item, since it is the main target of the former analysis, the most important sources of HC are:

- crevices: fuel mass stored inside cylinder crevices cannot be reached by the flame front, thus unburned hydrocarbons are emitted in the exhaust;
- oil film: the fluid layer on the cylinder wall can absorb fuel hydrocarbons when the partial pressure is high, then release them during expansion stroke;
- quenching: when the flame front approaches cylinder walls it can be extinguished, if temperature is too low. This phenomenon is more likely at cold start and it results in unburned fuel emission;
- scavenging: during valve overlap period, part of the fresh mixture could directly flow from the intake through the exhaust port, so that part of the cylinder unburned fuel is emitted.

The purpose of this work is to enhance the predictivity of HC emissions due to cylinder scavenging. In the overlap period, three main gas exchange phenomena occur inside the cylinder: *short circuit* of unburned mixture directly through the exhaust port; *mixing* between unburned and burned mixtures; *inlet backflow*.
The model implemented in the original code describes the cylinder as a single zone volume, in which perfect mixing happens; thus, the residuals from

previous combustion and the unburned charge are not located in separated regions. This model is well predictive of CO and NO_x emissions, as well as HC from crevices and oil film. However, it is not capable to properly predict the HC emitted during the overlap period.

The proposed scavenging model considers four zones, as shown in figure 1:

1. cylinder unburned zone;
2. cylinder burned zone;
3. inlet duct;
4. exhaust duct;

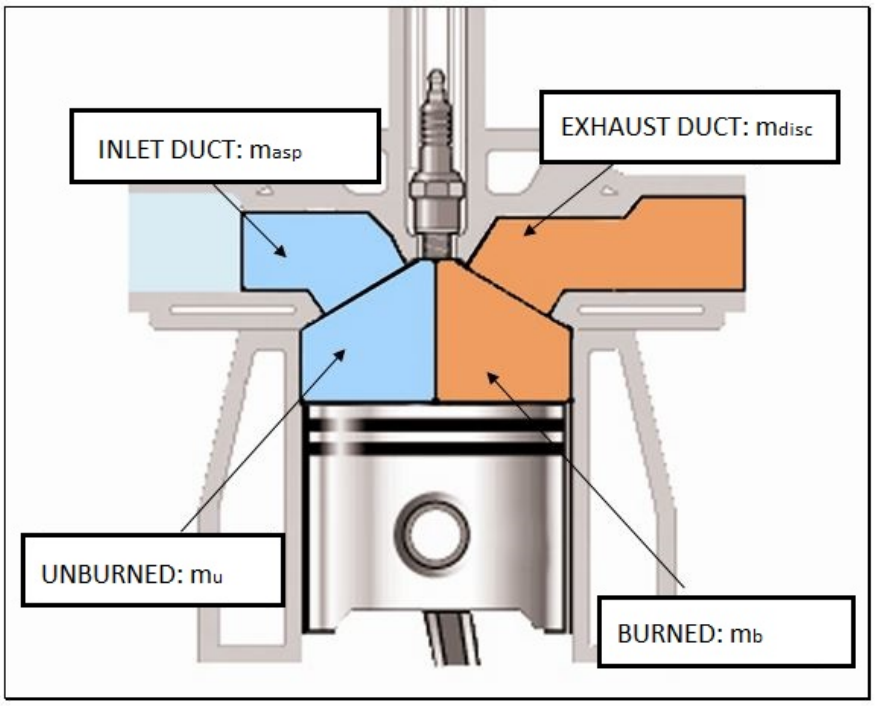

Figure 1: Cylinder-ducts system in the four zones model

These four control volumes can interact by means of six mass fluxes.

1. $Intake \rightarrow Unburned$
2. $Burned \rightarrow Exhaust$
3. $Unburned \rightarrow Burned : Mixing$
4. $Unburned \rightarrow Exhaust : Short\ Circuit$

} Primary Fluxes

5. $Intake \rightarrow Burned$
6. $Unburned \rightarrow Exhaust$

} Secondary Fluxes

This complex framework can be visualized in the picture below (3.11).

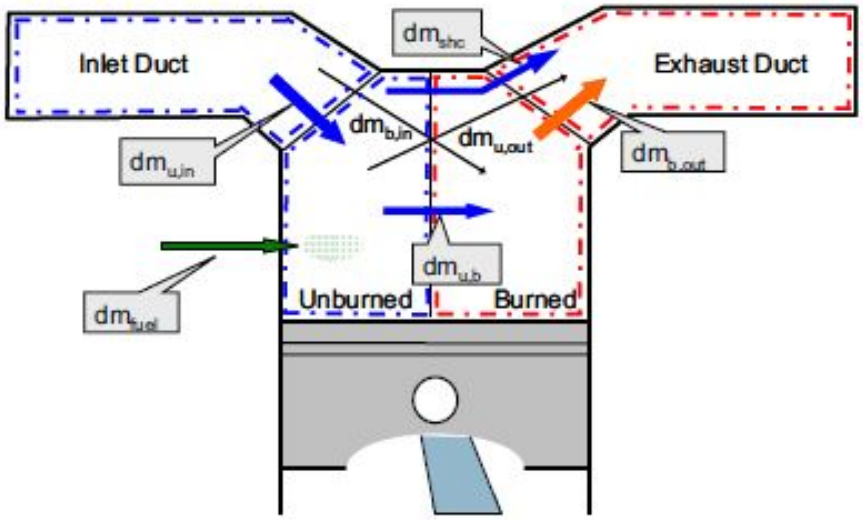

Figure 2: Four zone model fluxes [11]

Picture 2 distinguishes four kind of fluxes, represented by arrows:

- Primary fluxes of fresh mixture are portrayed in blue;
- The only primary flux of burned gases is in orange;
- The two secondary fluxes are represented in black;
- The fuel injected is in green.

Short circuit and mixing fluxes are evaluated by means of two calibration parameters, K_{SHC} and K_{MIX}, which depend on the turbulence intensity inside the cylinder and vary from 0 to 1. Specifically, these mass flow rates are expressed as:

$$dm_{SHC} = K_{SHC} \cdot min\ [dm_{IN};\ dm_{OUT}]$$

$$dm_{MIX} = K_{MIX} \cdot (dm_{IN} - dm_{SHC})$$

Sensitivity analysis results

First of all, the theoretical model validation is performed by means of a sensitivity analysis on two samples: a single cylinder, 2 valves spark ignition engine and a four cylinders, 16 valves spark ignition engine. The validation is done by comparing scavenging model results to original ones, focusing on two quantities: the average emitted mass of HC during a cycle [g], plotted for each rotational speed, and the HC instantaneous outgoing flux at a fixed regime [g/s].

Starting from the first sample, three cases are considered:

- perfect mixing, i.e. $K_{MIX} = 1,\ K_{SHC} = 0$;
- pure short circuit, i.e. $K_{MIX} = 0,\ K_{SHC} = 1$;
- turbulence intensity dependence, $K_{MIX} = K_{SHC} = f(u')$

Perfect mixing

In case of *perfect mixing*, the model behaves as the original code, as charts 3 and 4 show. This situation is absolutely reasonable, since a change in the zones number should not imply a significant difference in the final results.

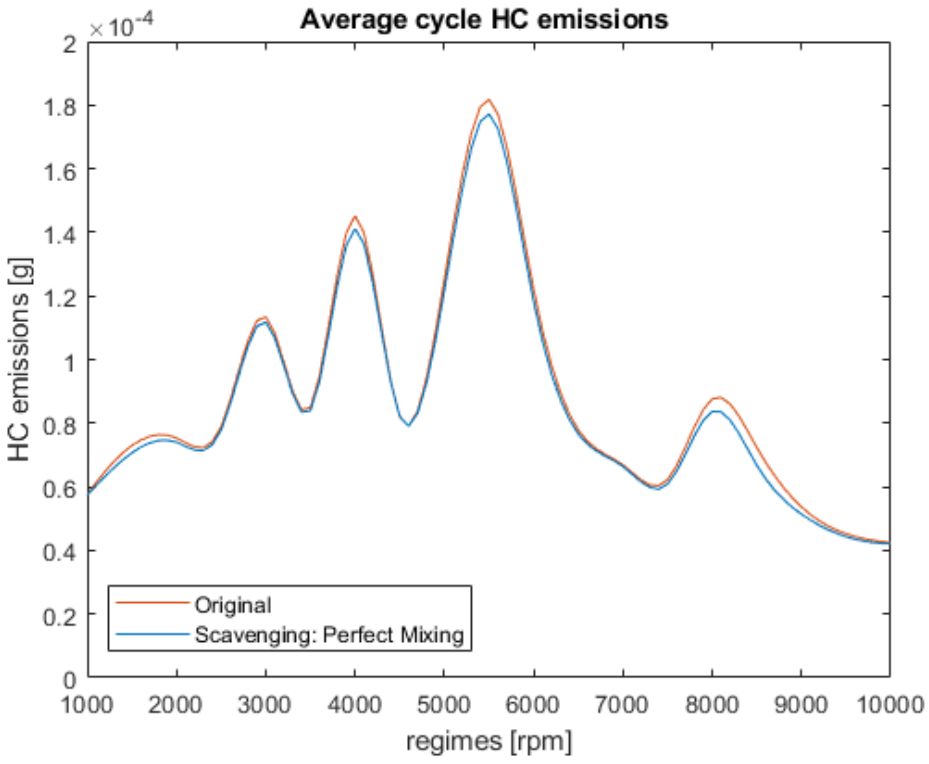

Figure 3: Average cycle HC emissions versus regime

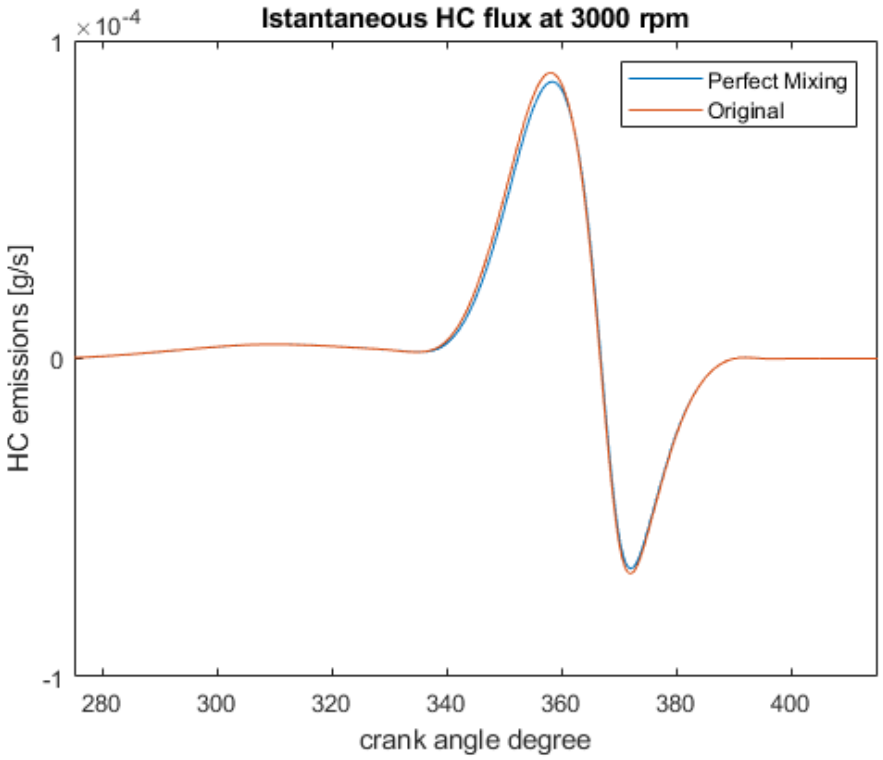

Figure 4: Istantaneous HC flux emitted at 3000 rpm

Pure short circuit

When *pure short circuit* is investigated, an increase of both cycle average and instantaneous HC emissions is expected, since a portion of the fresh charge by-passes the cylinder without any mixing with the burned volume. This situation is unwanted because it is the worse in terms of HC emissions and brake specific fuel consumption (BSFC), thus engine efficiency.

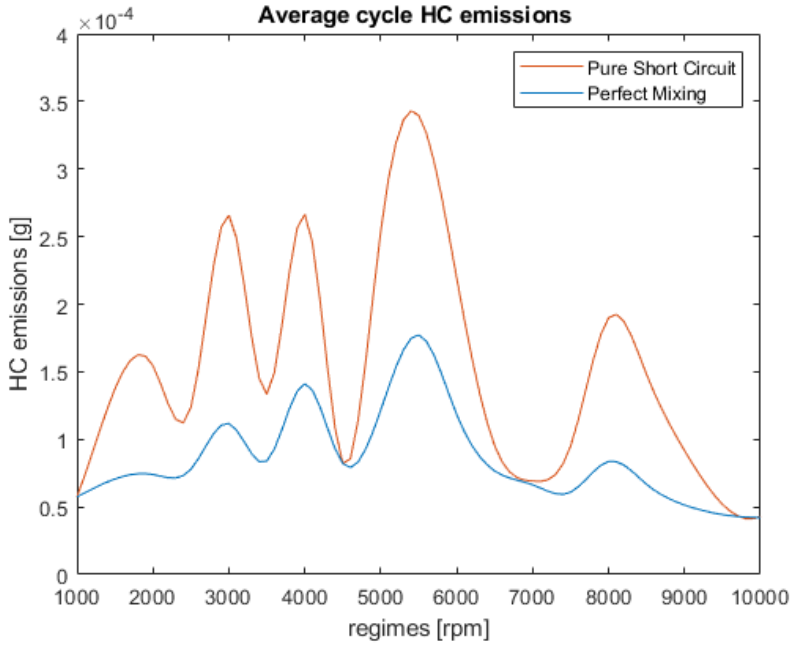

Figure 5: Average cycle HC emissions versus regime

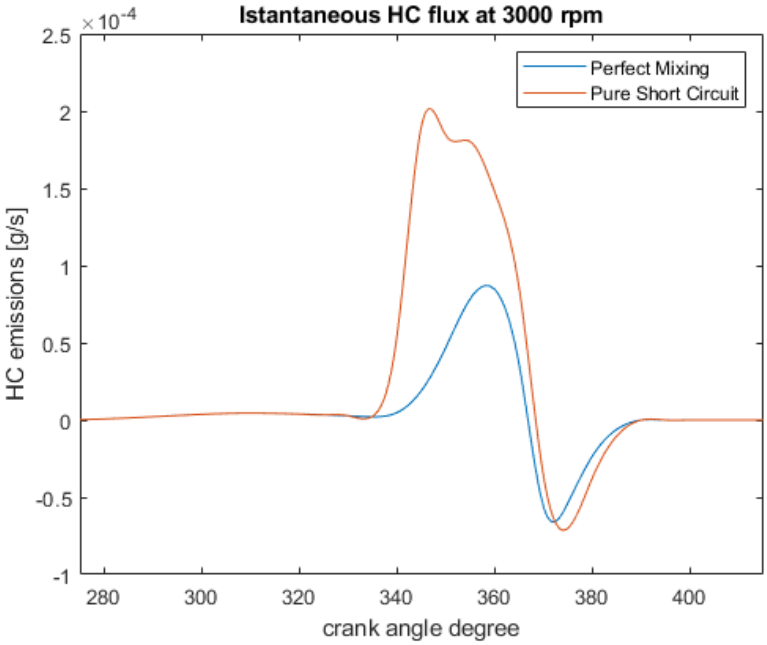

Figure 6: Istantaneous HC flux emitted at 3000 rpm

Turbulence intensity effect

Two limiting cases have been considered so far; now, the general situation is presented. According to [11], we can identify a correlation between cylinder turbulence intensity u' and the calibration coefficients, i.e. function $f_1(u')$ in table 1. However, this correlation does not capture the HC emission when the turbulence is too low. Therefore, $f_2(u')$ is proposed as alternative law.

Interval	$f_1(u')$	$f_2(u')$
$0 < u' < 3$	$K_{MIX} = K_{SHC} = 0$	$K_{MIX} = K_{SHC} = 0.5$
$3 < u' < 4$	$K_{MIX} = K_{SHC} = 0.5$	$K_{MIX} = K_{SHC} = 0.8$
$u' > 4$	$K_{MIX} = K_{SHC} = 0.9$	$K_{MIX} = K_{SHC} = 1$

Table 1: Calibration coefficients as function of the turbulence intensity

The single cylinder sample is characterized by a too low turbulence intensity at any engine speed, so that the performance of the proposed correlations for the scavenging model have to be analyzed on a more complex architecture: the four cylinders Alfa Romeo SI engine. The obtained results are reported in charts 7 and 8.

As expected, $f_1(u')$ considers neither mixing nor short circuit occurring in case of low turbulence intensity ($K_{MIX} = K_{SHC} = 0$ if $u' < 3$), resulting in a flat trend at low regimes. The main outcome of the sensitivity analysis is that $f_2(u')$ seems to behave better along the whole rotational speed range. Moreover, through-flow magnitude over mixing increases with the engine regime, since the difference between the scavenging model profiles and the original one enlarges with rotational speed.

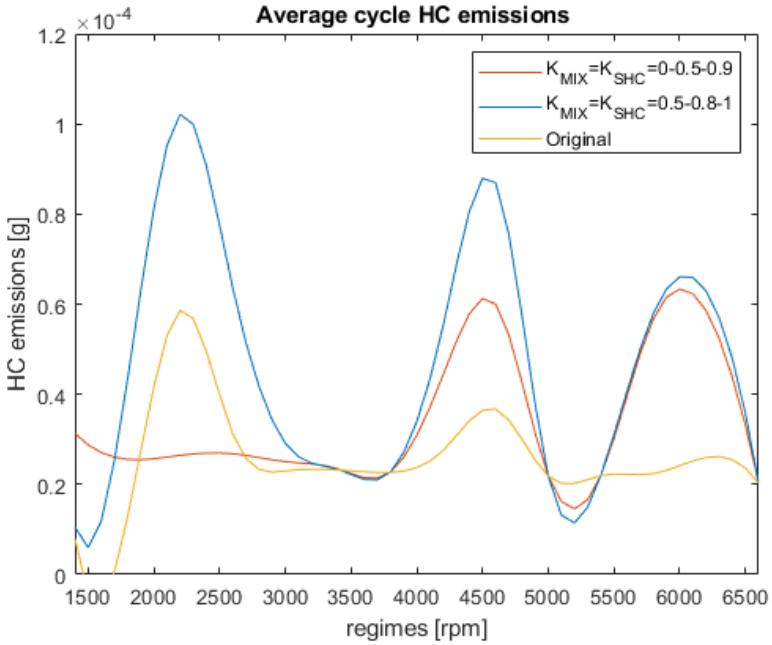

Figure 7: Average emitted mass of HC after cylinder 1

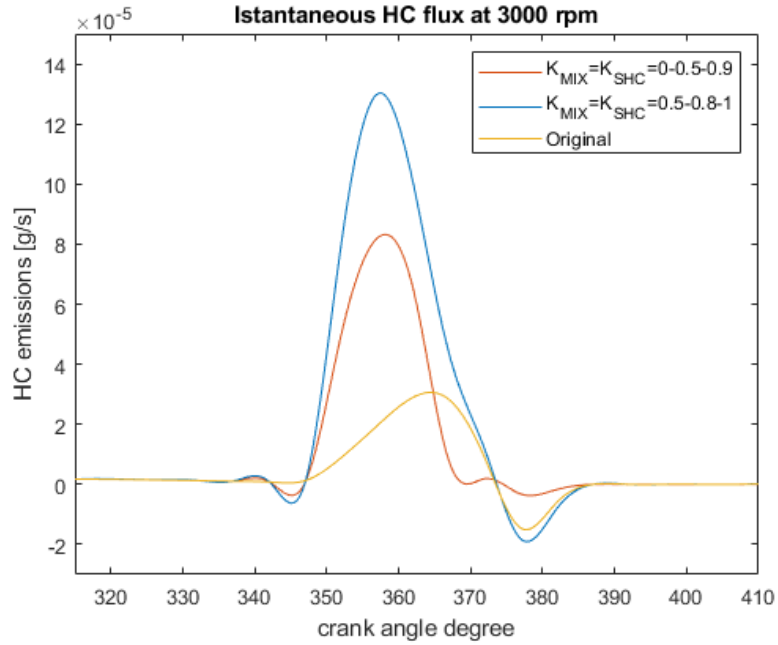

Figure 8: HC fluxes during overlap across the exhaust valve of cylinder 1

Experimental model validation

An experimental validation of the scavenging model is required to confirm the results of the sensitivity analysis.

The sample exploited for this purpose is the Lamborghini V10, 5.0 litres, 40 valves, spark ignition engine. This architecture is more complex than the two considered so far: a more accurate investigation of the influence of turbulence intensity on the calibration coefficients can be realized.

First of all, an engine performance validation is carried out, by comparing the *Gasdyn* calculated values to the experimental ones. Pressure is analyzed in many engine points: in intake and exhaust ducts, inside the cylinder, in aspiration manifold plenums. Moreover, volumetric efficiency, brake torque and brake power are considered for both the original and the scavenging model, without showing significant differences.

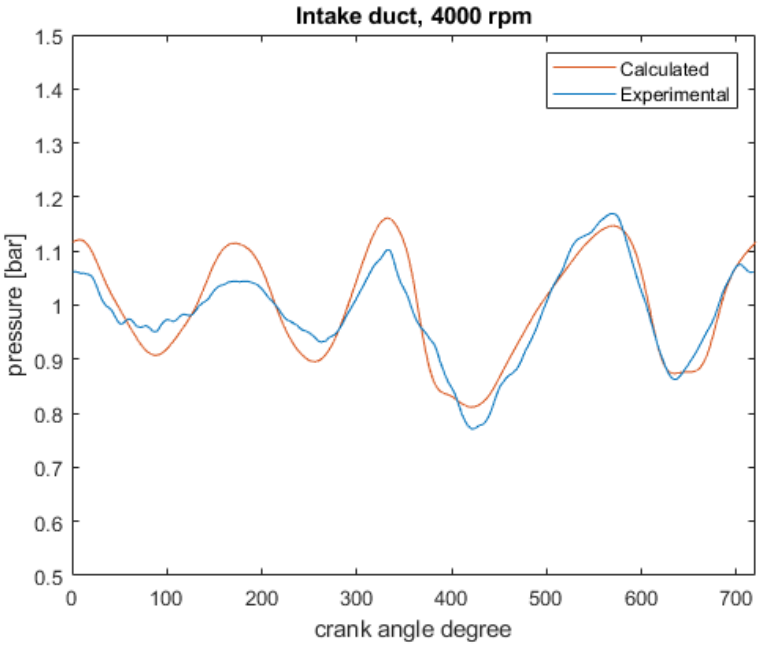

Figure 9: Pressure profile intake duct, 4000 rpm

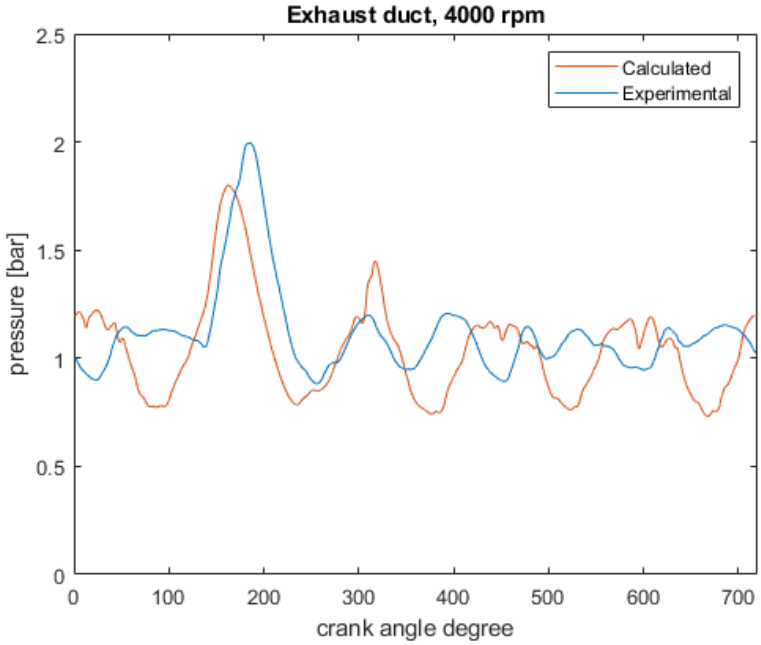

Figure 10: Pressure profile exhaust duct, 4000 rpm

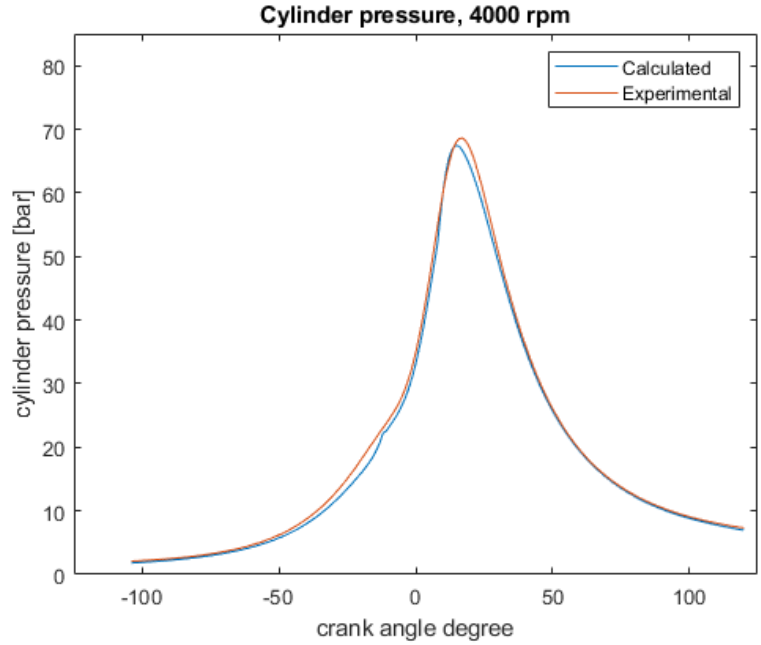

Figure 11: Cylinder pressure, 4000 rpm

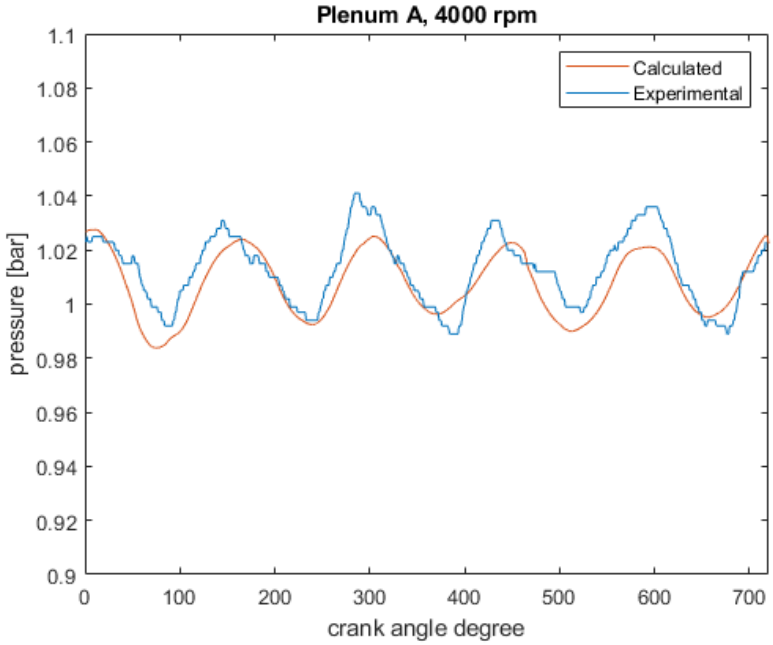

Figure 12: Pressure profile plenum A, 4000 rpm

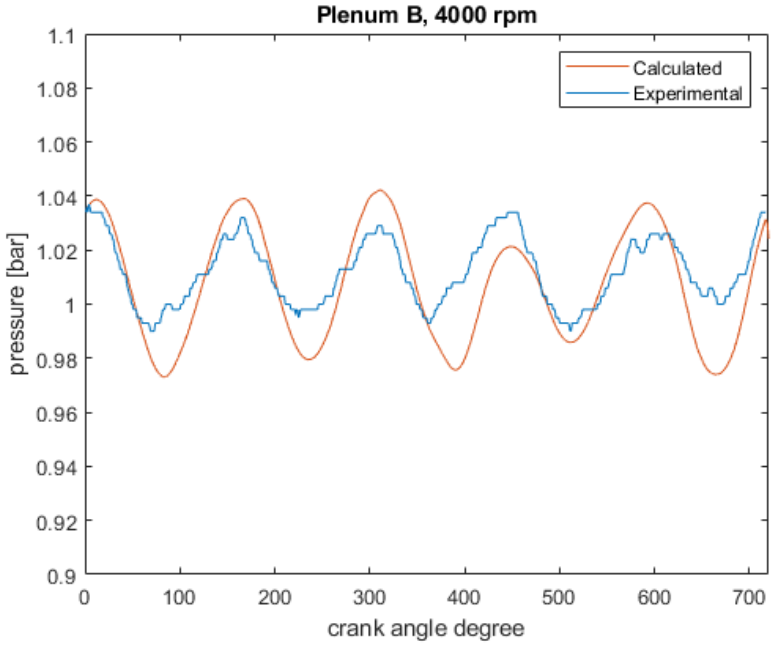

Figure 13: Pressure profile plenum B, 4000 rpm

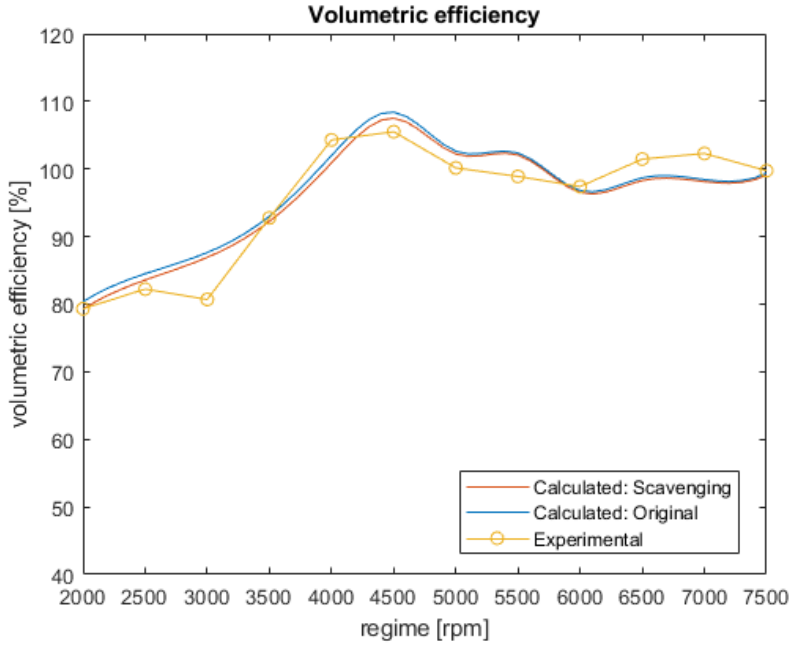

Figure 14: Volumetric efficiency versus engine rotational speed

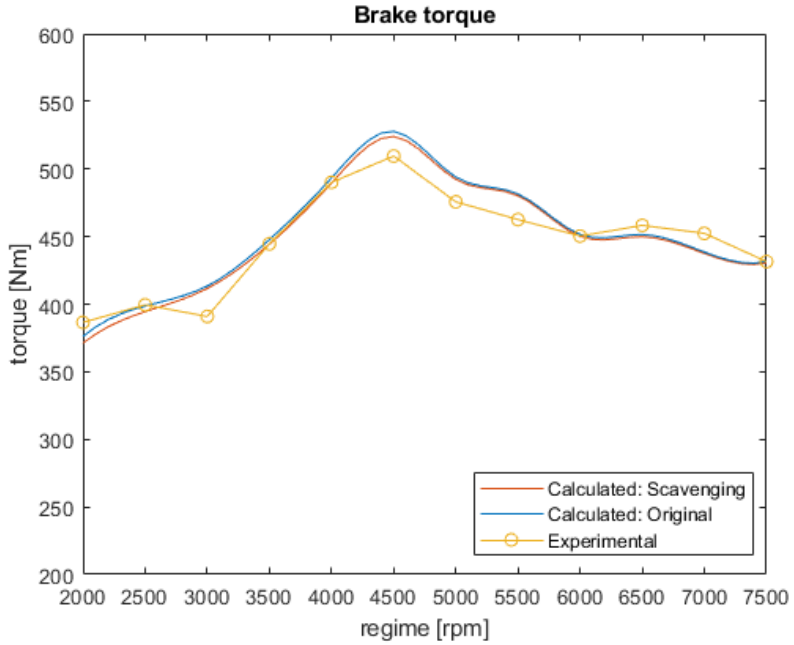

Figure 15: Torque versus engine rotational speed

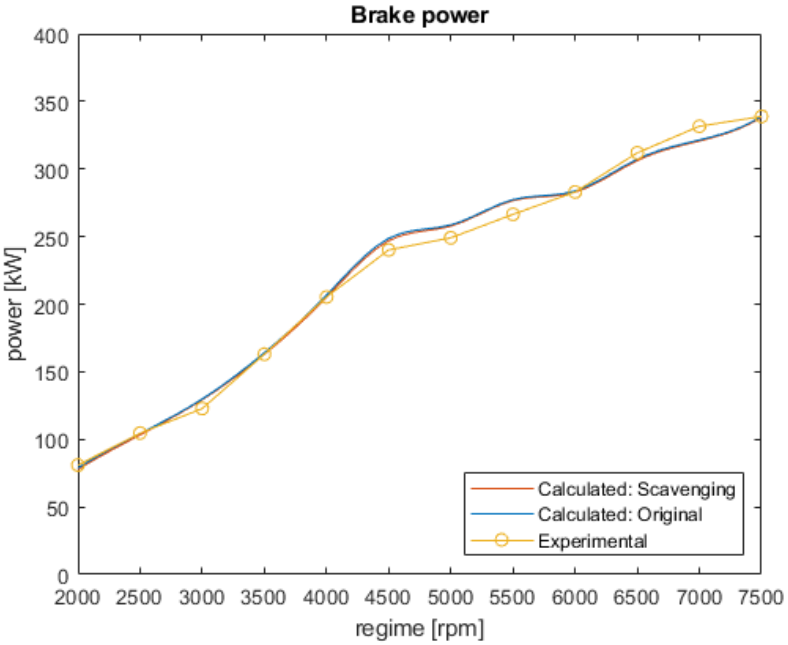

Figure 16: Power versus engine rotational speed

Once the engine sample is validated, the analysis on the HC emissions is performed. The average HC concentration in the exhaust duct is considered as reference quantity.

First of all, the original model results are compared to the experimental ones: from chart 17 it is clear that the old code is not satisfactory in the prediction of HC emitted.

Therefore, the scavenging model is applied to the same sample, providing the results portrayed in chart 18. Both the correlations are good to predict the peak of HC at 4000 rpm. However, $f_2(u')$ is better because of the following reasons:

1. higher HC peak emissions at 4000 rpm, closer to the experimental trend;

2. capability to capture the decreasing trend from 2000 to 3000 rpm.

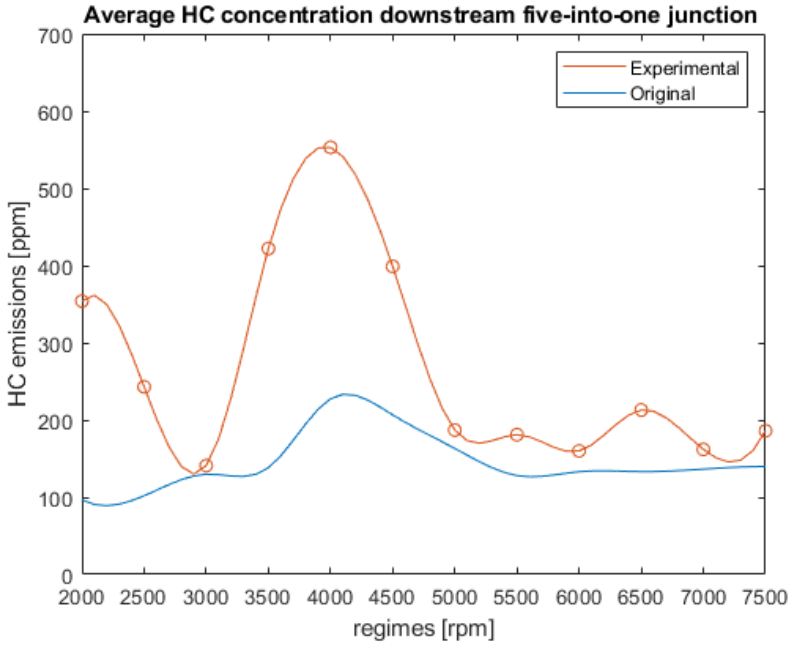

Figure 17: Average HC concentration versus engine regime

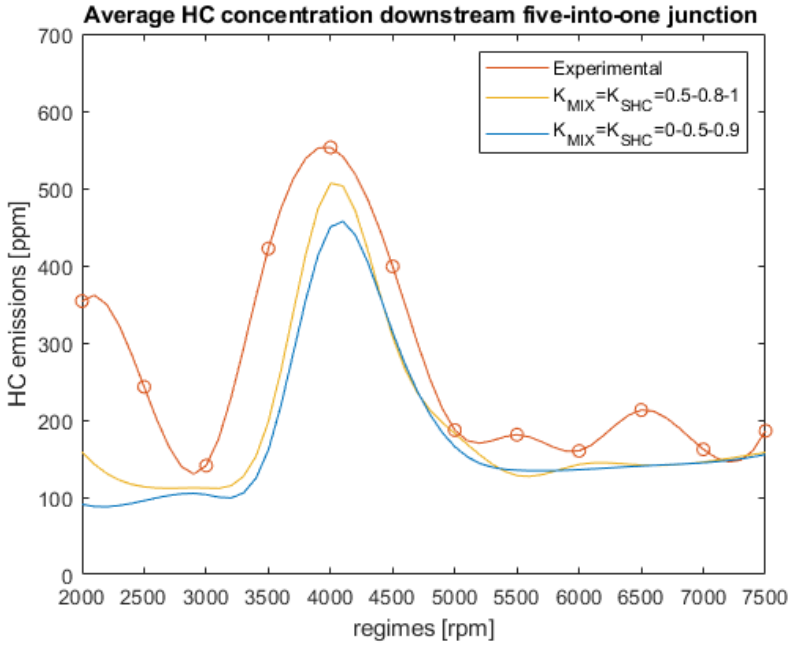

Figure 18: Average HC concentration versus engine regime

Contents

Summary

The aim of this thesis is to investigate the cylinder *scavenging* process in internal combustion SI engines, in order to predict *unburned HC* emissions. The original model implemented in *Gasdyn*, a software developed by the Energy Department of Politecnico di Milano, considers a single zone geometry for the cylinder, where perfect *mixing* of fresh charge with residuals happens. The new implemented model for scavenging, instead, is based on a four zones geometry. By tracking the mass fluxes among these regions, an improvement in the gas exchange process description is achieved: both *mixing* and *short circuit* phenomena are captured; furthermore, their magnitude is investigated as function of the cylinder *turbulence intensity*.

The results of the sensitivity analysis, performed on two simple engine architectures, as well as the experimental model validation, carried out on the Lamborghini V10 engine, allow to properly tune the calibration coefficients for *mixing* and *short circuit*.

The scavenging model improves the predictivity of *HC* emissions with respect to the original one, by keeping the same reliability in the analysis of performance parameters, such as volumetric efficiency and brake torque.

Keywords

scavenging; *unburned HC*; *mixing*; *short circuit*; *turbulence intensity*

Sommario

Lo scopo di questo elaborato di tesi è l'analisi del processo di *lavaggio* del cilindro in motori a combustione interna ad accensione comandata, in modo tale da tracciare opportunamente le emissioni di *idrocarburi incombusti*.
Il modello originale implementato in *Gasdyn*, un software sviluppato dal Dipartimento di Energia del Politecnico di Milano, considera un modello monozona per il cilindro, in cui si verifica un perfetto *miscelamento* tra carica fresca e residui di combustione.
Il nuovo modello di *lavaggio* è invece basato su un approccio multizona. L'analisi dei flussi di massa tra le quattro zone garantisce un miglioramento nella descrizione della gasdinamica durante il riempimento del cilindro: in questo modo è possibile rappresentare sia il *miscelamento*, sia il *corto circuito* della carica fresca. Inoltre, l'impatto di questi due fenomeni è quantificabile mediante un'analisi parametrica in funzione dell'*intensità di turbolenza*.
I risultati dell'analisi di sensitività, attuata su due architetture di motore semplici, insieme alla validazione sperimentale del modello, effettuata sul motore Lamborghini V10, consentono di calibrare i coefficienti di *miscelamento* e *corto circuito*.
La predittività delle emissioni di HC nei condotti di scarico migliora mediante l'utilizzo del nuovo modello di *lavaggio*, se paragonata con il modello originale; nonostante ciò, si mantiene la stessa affidabilità nell'analisi delle

performance motoristiche, quali coefficiente di riempimento e coppia.

Parole chiave

lavaggio; *idrocarburi incombusti*; *miscelamento*; *corto circuito*; *intensità di turbolenza*

Chapter 1

Gas Dynamics

1.1 Conservation Equations

Gas dynamics in internal combustion engines is characterized by three dimensionality, unsteadiness and turbulence; the flow interacts with the wall by means of frictional forces, due to fluid viscosity, and heat transfer. [1] Thus, temperature, pressure and velocity of the gas show relevant gradients inside the ducts.

The mathematical model describing the problem involves the 3D Navier Stokes equations. The analytical solution for such complex systems do not exist, while the numerical one can be achieved by means of a huge computational effort. Indeed, the intrinsic unsteadiness of the flow does not allow to solve a Reynolds Averaged Navier Stokes problem (RANS): Large Eddy Simulations (LES) are required to properly deal with the time depending 3D problem. However, this choice is viable only for single components of the system, such as catalysts, injectors and junctions, where the three-dimensionality of the flow has to be captured.

In order to deal with the whole engine simulation, a 1D model has to be

considered, with the following fundamental assumptions:

- unsteady flow;
- one-dimensional flow: the longitudinal dimension of the duct-systems is significantly greater than the transversal one;
- compressible fluid: perfect gas model, with constant specific heats, or mixture of ideal gases, with specific heats depending both on temperature and composition;
- friction and heat transfer only at the gas-wall interface;
- non-adiabatic and non-isentropic flow;
- variable cross-section with assigned law.

A 1D compressible unsteady flow into an infinitesimal duct element with variable cross-section is considered. Pressure, density and gas velocity are function both of the spatial coordinate x and the time:

$$p = p(x,t),\ \rho = \rho(x,t),\ u = u(x,t)$$

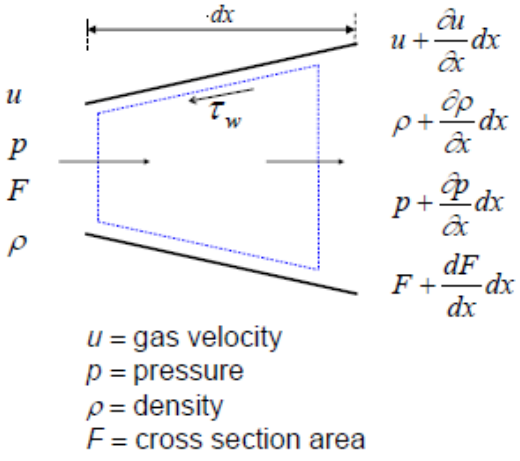

Figure 1.1: Infinitesimal duct element [8]

The conservation of mass, momentum and energy can be expressed by a system of partial differential equations.

1.1.1 Mass conservation

The variation of mass in the control volume has to be equal to the net flux through the infinitesimal element surface:

$$(\rho + \frac{\partial \rho}{\partial x}dx)(u + \frac{\partial u}{\partial x}dx)(F + \frac{dF}{dx}dx) - \rho u F = -\frac{\partial}{\partial t}(\rho F dx)$$

By considering just first order infinitesimal terms, we get:

$$\frac{\partial \rho}{\partial t} + \frac{\partial(\rho u)}{\partial x} + \frac{\rho u}{F}\frac{dF}{dx} = 0 \tag{1.1.1}$$

1.1.2 Momentum conservation

The rate of momentum increase within the control volume equals the summation of the net flux of momentum through the infinitesimal element surface and the resultant of pressure and shear forces acting on the control volume. In order to understand the different contributions to the momentum equation, it can be useful to separately analyze each term.

- Rate of change of momentum:

$$\frac{\partial(\rho u F dx)}{\partial t}$$

- Net flux of momentum through the control volume surface:

$$(\rho + \frac{\partial \rho}{\partial x}dx)(u + \frac{\partial u}{\partial x}dx)^2(F + \frac{dF}{dx}dx) - \rho F u^2 = \frac{\partial(\rho F u^2)}{\partial x}dx$$

- Pressure forces:

$$pF - (p + \frac{\partial p}{\partial x}dx)(F + \frac{dF}{dx}dx) + p\frac{dF}{dx}dx = -(\frac{\partial(pF)}{\partial x}dx + p\frac{dF}{dx}dx)$$

- Friction forces:

$$F_{friction} = -f\frac{\rho u^2}{2}(\pi D dx)$$

  f is the friction coefficient between wall and fluid: it can be evaluated as function of Reynolds number and the relative roughness of the duct wall.

Summing up the previous contribution and considering the continuity equation, we get:

$$\frac{\partial u}{\partial t} + u\frac{\partial u}{\partial x} + \frac{1}{\rho}\frac{\partial p}{\partial x} + G = 0 \tag{1.1.2}$$

where G, the dissipative contribution due to friction, can be expressed as:

$$G = f\frac{u^2}{2}\frac{u}{|u|}\frac{4}{D}$$

1.1.3 Energy conservation

By applying the first law of thermodynamic to the control volume, we can obtain:

$$\dot{Q} - \dot{W} = \frac{\partial E_0}{\partial t} + \frac{\partial H_0}{\partial x} dx \tag{1.1.3}$$

where:

- $\dot{Q}$ is the rate of heat transferred from gas to the duct walls and viceversa. It can be expressed as follows:

  $$\dot{Q} = \dot{q}\rho F dx + \Delta H_{react} F dx$$

  where $\dot{q}$ is the heat transfer per unit mass per unit time, while ΔH_{react} is the heat released (per unit volume per unit time) by chemical reactions in gas phase.

- $\dot{W}$ is the work done on or by the system, that is zero for a gas flowing in a duct of the engine.

- $\frac{\partial E_0}{\partial t}$ is the variation of stagnation internal energy, equal to:

  $$\frac{\partial E_0}{\partial t} = \frac{\partial}{\partial t}(e_0 \rho F dx)$$

  where the specific stagnation internal energy can be expressed as:

  $$e_0 = e + \frac{U^2}{2} = c_v T + \frac{U^2}{2}$$

- $\frac{\partial H_0}{\partial x}$ is the net efflux of stagnation enthalpy through the control surface:

$$\frac{\partial H_0}{\partial x} = \frac{\partial}{\partial x}(h_0 \rho F u)$$

where the specific stagnation enthalpy can be expressed as:

$$h_0 = e_0 + \frac{p}{\rho}$$

By summing up all the previous elements, assuming no work, we obtain the following form of the Energy Conservation equation:

$$\frac{\partial(\rho e_0)}{\partial t} + \frac{\partial(\rho u h_0)}{\partial x} + \frac{\rho u h_0}{F}\frac{dF}{dx} - \rho \dot{q} - \Delta H_{react} F dx = 0 \tag{1.1.4}$$

1.1.4 Strong Conservative form

In order to solve the hyperbolic system of partial derivative non linear equations, the strong conservative formulation is adopted, since it better accomplishes with the numerical methods requirements. This consideration implies to switch from momentum conservation equation to impulse conservation equation, since this latter quantity is conserved in case of shock waves, which are frequent phenomena occuring in engine ducts.

$$\begin{cases} \frac{\partial}{\partial t}(\rho F) + \frac{\partial}{\partial x}(\rho u F) = 0 & \textit{Continuity} \\ \frac{\partial}{\partial t}(\rho u F) + \frac{\partial}{\partial x}((p + \rho u^2)F) - p\frac{dF}{dx} + \rho G F = 0 & \textit{Impulse} \\ \frac{\partial}{\partial t}(\rho e_0 F) + \frac{\partial}{\partial x}(\rho u h_0 F) - \rho \dot{q} F - \Delta H_{react} F = 0 & \textit{Energy} \end{cases}$$

The second equation highlights the quantity $p + \rho u^2$, which is the impulse.
On the basis of the strong conservative form, it is convenient to express the hyperbolic problem in matricial form, in order to apply shock-capturing numerical methods.
Four vectors are introduced, each of them containing terms of continuity, impulse and energy equation.

- Vector of conserved variables

$$\vec{W} = \begin{bmatrix} \rho F \\ \rho u F \\ \rho e_0 F \end{bmatrix}$$

  It contains three groups of independent gasdynamic variables that vary with x and t.

- Vector of fluxes

$$\vec{F} = \begin{bmatrix} \rho u F \\ (\rho u^2 + p) F \\ \rho u h_0 F \end{bmatrix}$$

- Vectors of source terms

$$\vec{B} = \begin{bmatrix} 0 \\ -p\frac{dF}{dx} \\ 0 \end{bmatrix} \qquad \vec{C} = \begin{bmatrix} 0 \\ \rho G F \\ -(\rho \dot{q} + \Delta H_{react}) F \end{bmatrix}$$

The first vector $\vec{B}$ does not contain any dissipative term, since $-p\frac{dF}{dx}$ is related to the variable geometry of pipes. Vector $\vec{C}$, instead, accounts for dissipative contribution due to friction and heat transfer: these phenomena prevent the flow from being isentropic.

Thus, the hyperbolic system can be written in a more compact form:

$$\frac{\partial}{\partial t}\vec{W}(x,t) + \frac{\partial}{\partial x}\vec{F}(\vec{W}) + \vec{B}(\vec{W}) + \vec{C}(\vec{W}) = 0 \tag{1.1.5}$$

The current problem involves three equations in four unknowns (ρ, u, e, p). Therefore, a fourth equation is introduced.
A first model implemented in the code is the perfect gas one, with the fluid behaviour described by the ideal gas law:

$$pV = NRT \tag{1.1.6}$$

where R=8.314 $\frac{J}{mol \cdot K}$ is the universal gas constant.
Furthermore, the constant volume specific heat is constant, depending just on the degrees of freedom of the fluid molecules.
In this way, the specific stagnation internal energy and enthalpy may be expressed as:

$$e_0 = c_v T + \frac{u^2}{2} = \frac{p}{\rho(k-1)} + \frac{u^2}{2} \tag{1.1.7}$$

$$h_0 = c_p T + \frac{u^2}{2} = \frac{kp}{\rho(k-1)} + \frac{u^2}{2} \tag{1.1.8}$$

where k is the politropic coefficient.

However, a more general model is also implemented in the code: the fluid is considered as an ideal mixture of ideal gases and each of the species follows the ideal gas law:

$$\frac{p_j}{\rho_j} = R_j T = \frac{R}{MM_j} T \tag{1.1.9}$$

For the whole mixture, the governing equation becomes:

$$p = \frac{\rho R T}{\sum_{j=1}^{N_{species}} X_j MM_j} \tag{1.1.10}$$

where X_j is the molare fraction of the j-th species, and MM_j its molar mass; the denominator of the previous equation, instead, represents the molar mass of the whole mixture, calculated as the weigthed average of its components. The molar enthalpy and internal energy of the j-th specie of the mixture can be expressed by means of the following polynomial relationships, in which the coefficients α_{Mj} for each chemical species have been determined on the basis of the JANAF and NASA data.

$$h_j(T) = R \cdot (\alpha_{1j} T + \frac{\alpha_{2j}}{2} T^2 + \frac{\alpha_{3j}}{3} T^3 + \frac{\alpha_{4j}}{4} T^4 + \frac{\alpha_{5j}}{5} T^5 + \alpha_{6j}) \tag{1.1.11}$$

$$e_j(T) = h_j(T) - RT \tag{1.1.12}$$

The model implemented in the code is then simplified, by considering the specific internal energy as a quadratic function of temperature:

$$e_j(T) = \alpha_{1j} T + \alpha_{2j} T^2 \tag{1.1.13}$$

where the coefficients α_{1j}, α_{2j} for the j-th specie can be obtained by matching

the fifth order polynomial curve in a prefixed temperature range. As for the whole mixture, the global coefficients α_1, α_2 can be obtained as weighted average on the different species:

$$\alpha_1 = \sum_{j=1}^{N_{species}} \alpha_{1j} X_j \tag{1.1.14}$$

$$\alpha_2 = \sum_{j=1}^{N_{species}} \alpha_{2j} X_j \tag{1.1.15}$$

In this way we get:

$$e(T) = \alpha_1 T + \alpha_2 T^2 \tag{1.1.16}$$

1.1.5 Transport of chemical spiecies

Ad additional set of equation of species conservation is required in order to investigate some problems, such as emissions prediction, chemical reactions inside the pipes and simulation of catalyst and EGR performance.
The following assumptions are considered:

- negligible diffusion in the flow, mass transfer by advection only;
- reactions take place in the engine ducts, species concentration can vary with the linear coordinate.

The chemical species transport equation can be expressed as:

$$\frac{\partial}{\partial t}(\rho F Y_j) + \frac{\partial}{\partial x}(\rho u F Y_j) + \rho F \dot{Y}_j = 0 \tag{1.1.17}$$

The latter equation holds for $j = 1, 2, ..., N_{species}-1$, since for the N-th species the continuity equation is valid:

$$Y_N = 1 - \sum_{j=1}^{N_{species}-1} Y_j \tag{1.1.18}$$

The first two terms of equation (1.1.17) represent respectively the rate of change of species j-th within the control volume in time and the advective flux of species j-th; the last term, instead, is a source contribution related to the production or consumption rate of species, due to the reactions in the gas and solid phase.
The complete form of the hyperbolic system of PDE's becomes:

$$\begin{cases} \frac{\partial}{\partial t}(\rho F) + \frac{\partial}{\partial x}(\rho u F) = 0 & \textit{Continuity} \\ \frac{\partial}{\partial t}(\rho u F) + \frac{\partial}{\partial x}((\rho u^2 F + pF) - p\frac{dF}{dx} + \rho G F = 0 & \textit{Impulse} \\ \frac{\partial}{\partial t}(\rho e_0 F) + \frac{\partial}{\partial x}(\rho u h_0 F) - \rho \dot{q} F - \Delta H_{react} F = 0 & \textit{Energy} \\ \frac{\partial}{\partial x}(\rho u F Y_j) + \rho F \dot{Y}_j = 0 & \textit{Species transport} \end{cases}$$

The matricial form can be exploited also in this case:

$$\frac{\partial}{\partial t}\vec{W}(x,t) + \frac{\partial}{\partial x}\vec{F}(\vec{W}) + \vec{B}(\vec{W}) + \vec{C}(\vec{W}) = 0$$

The vectors are extended with respect to the case without species transport.

- Vector of conserved variables

$$\vec{W} = \begin{bmatrix} \rho F \\ \rho u F \\ \rho e_0 F \\ \rho \vec{Y} F \end{bmatrix}$$

- Vector of fluxes

$$\vec{F} = \begin{bmatrix} \rho u F \\ (\rho u^2 + p) F \\ \rho u h_0 F \\ \rho u \vec{Y} F \end{bmatrix}$$

- Vectors of source terms

$$\vec{B} = \begin{bmatrix} 0 \\ -p\frac{dF}{dx} \\ 0 \\ 0 \end{bmatrix} \qquad \vec{C} = \begin{bmatrix} 0 \\ \rho G F \\ -(\rho \dot{q} + \Delta H_{react}) F \\ \rho \dot{Y} F \end{bmatrix}$$

Chapter 2

Spark Ignition Engine Pollutant Emissions

As the other thermal machines, internal combustion engines take air from the atmosphere and, after a thermodynamic cycle involving compression, combustion and expansion processes, they release the burnt gases back to the enviroment. In this way, they modify the natural air composition.
In order to reduce the environmental impact of cars, governments decided to regulate the amount of emissions of the main pollutant compounds, such as:

- Carbon monoxide (CO): it is one of the major products of the combustion process. It could cause poisoning and cardiovascular disease;
- Unburned hydrocarbons (HC): they are the result of an incomplete combustion;
- Particulate matter (PM) or soot: solid material dissolved into the gases;
- Nitrogen oxides (NO_x): they come from the air nitrogen and their formation is mainly due to high temperature. The main compound

produced inside the cylinder is NO, with around 98% of all the nitrogen oxides emitted.

- Carbon dioxide (CO_2): it is the main product of the combustion process. Although it is not considered as polluting, since it does not result in direct consequences on human health, it is recognized as the main cause of global warming and climate changes.

All these pollutants are currently measured over a test cycle called *World harmonized Light duty Test Procedure* ($WLTP$), which tries to simulate the use of the car both in the city and in the highways. Another test called *Real Driving Emission* (RDE) is going be extensively adopted in order to further verify ICE emissions. This test does not take place in a lab like the previous one, but directly on the road, trying to replicate more severe and real driving conditions: increased acceleration, both in number and in magnitude, higher average and maximum speed and longer measurement cycle duration. This test is going to be complementary to the WLTP and will be used to confirm or deny the results of the lab test.
In the following table, the limits for the pollutants, according to different regulations, are shown.

TIER	DATE	CO	HC	NOx	HC+NOx	PM	PN [N/km]
EURO 1	JUL 1992	-	-	-	0.97	-	-
EURO 2	JAN 1996	-	-	-	0.5	-	-
EURO 3	JAN 2000	0.2	-	0.15	-	-	-
EURO 4	JAN 2005	0.1	-	0.08	-	-	-
EURO 5	SEP 2009	0.1	0.068	0.06	-	0.005	-
EURO 6	SEP 2014	0.1	0.068	0.06	-	0.005	$6x10^{11}$

As shown from the data above, the limits have become progressively stricter,

according to the aim to reduce as much as possible engines emissions.
Thus, modern ICE cars designed under the EURO 6 regulation have comparable PM emission to electric ones, since the major sources are brakes and tires, as we can see in figure 2.1.

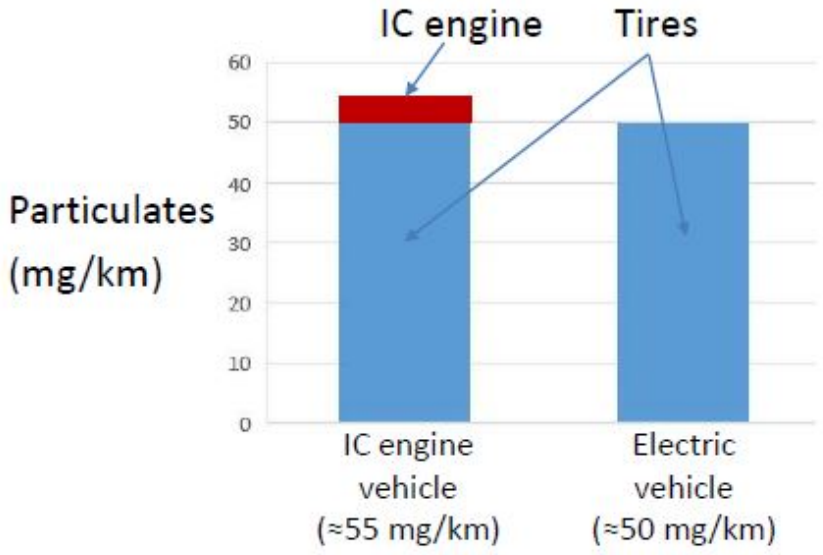

Figure 2.1: [8] PM emissions from an IC engine car versus an electric vehicle: brakes PM emission is not included, only tires are considered.

Being this topic so crucial in modern engine design, the *Gasdyn* code developed by Politecnico di Milano ICE Group can predict the formation of all the previously mentioned pollutants.
Before focusing on each emitted compound, a brief discussion about the combustion model is reported: indeed, combustion has a strong influence in the composition of the exhaust gases.

2.1 Combustion model

A multi-zone predictive model for the combustion process is necessary to achieve a good prediction of cylinder temperature, pressure and composition, since these quantities strongly influence the formation of pollutants. The concept behind the multi-zone approach can be easily understood by considering, at first, a two-zone model.

2.1.1 Two-zone model

The mass in the cylinder is divided into two zones, fresh mixture and burned gases, both of them subjected to mass and energy balance.

$$\begin{cases} \frac{dm_{uz}}{dt} = \frac{dm_{in}}{dt} - \frac{dm_b}{dt} & Mass\ Unburned \\ \frac{dm_{uz}e_{uz}}{dt} = \frac{dm_{in}h_{in}}{dt} - \frac{dm_b h_{uz}}{dt} - \frac{dQ_{wuz}}{dt} - p\frac{dV_{uz}}{dt} & Energy\ Unburned \\ \frac{dm_{bz}}{dt} = -\frac{dm_{ex}}{dt} + \frac{dm_b}{dt} & Mass\ Burned \\ \frac{dm_{bz}e_{bz}}{dt} = -\frac{dm_{ex}h_{ex}}{dt} + \frac{dm_b h_{uz}}{dt} - \frac{dQ_{wbz}}{dt} - p\frac{dV_{bz}}{dt} & Energy\ Burned \end{cases}$$

The main assumption is ideal gas behaviour for both zones. This approach allows to predict the local temperature inside the cylinder. Moreover, it can be coupled with kinetic models in order to predict knock in the unburned zone or pollutant emissions in the burned one.
In the following, picture 2.2 shows all the fluxes.

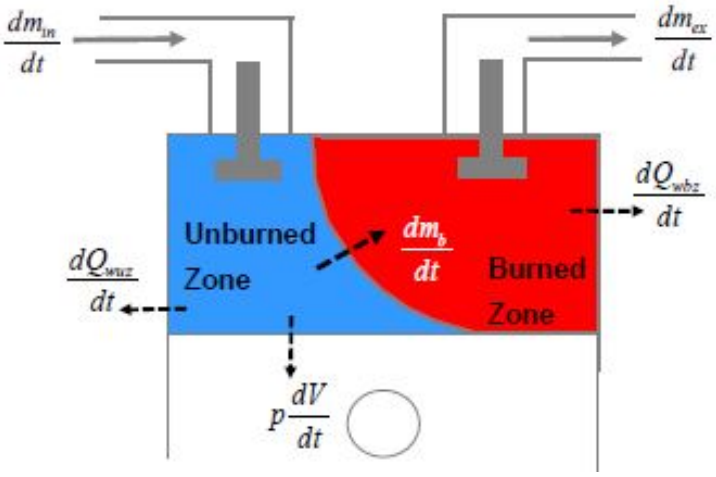

Figure 2.2: [8] Two-zone model fluxes

2.1.2 Multizone model

By further dividing the burned gas zone into subelements of equal mass, we can track the propagation of the flame front. Once a subelement burns it suddenly expands, thus compressing the remaining mixture. Thus, we can distinguish T_{be} from T_{bl} as in figure 2.3, representing respectively the temperature of earlier burning elements and later burning ones.

The elements closer to the spark plug are indeed compressed after their combustion, while the mixture close to the piston, which burns later, is compressed before its combustion: this mechanism results in a temperature stratification inside the cylinder (figure 2.4).

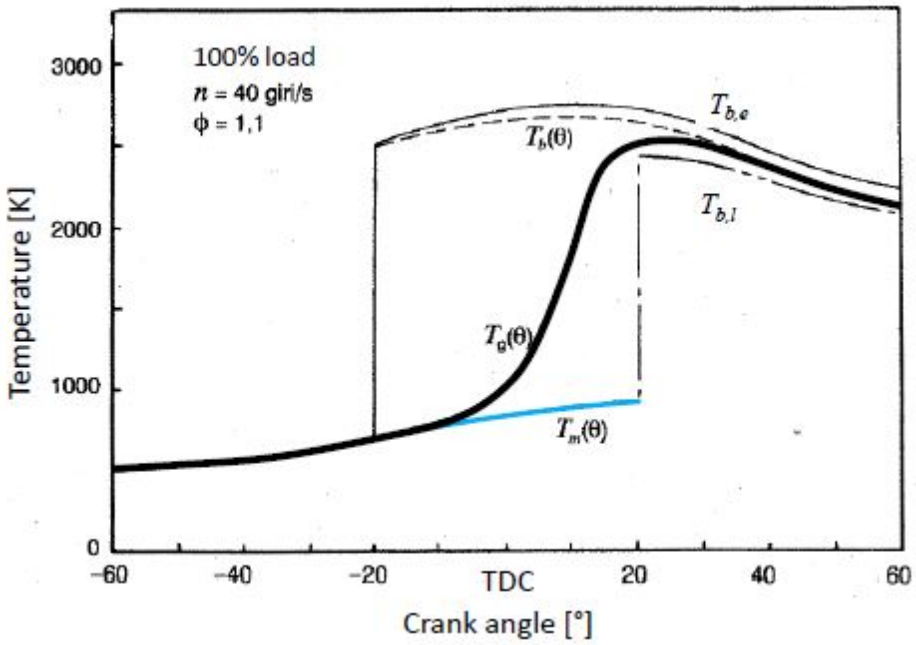

Figure 2.3: [1] Temperature variation during combustion versus crank angle

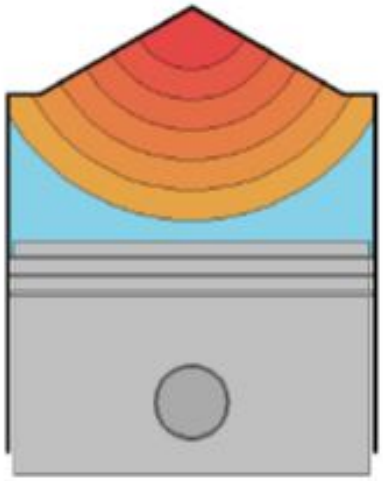

Figure 2.4: Stratified temperature inside the cylinder [1]

The temperature difference between earlier and later burning zones can reach 300-400 K, with strong influence in the pollutants formation.

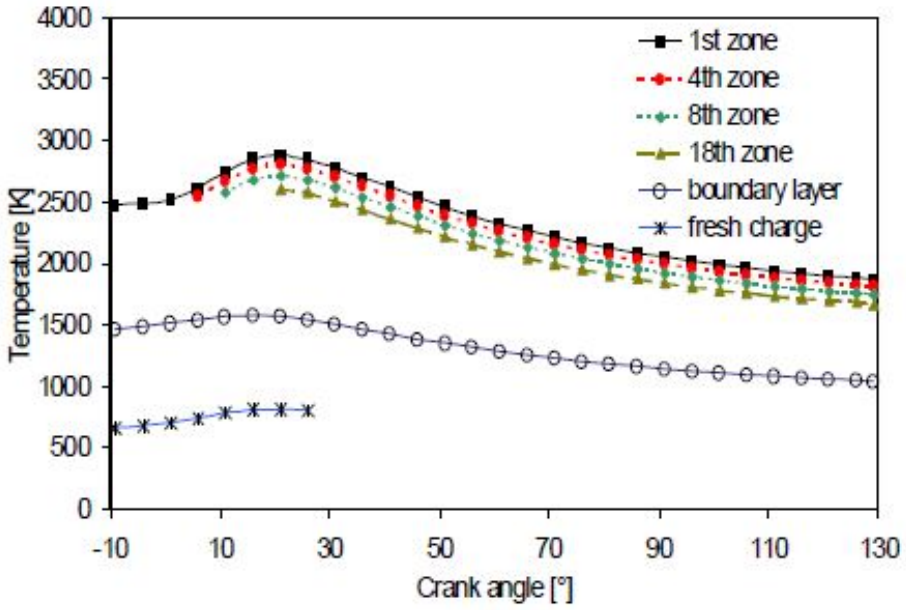

Figure 2.5: Temperature variation in multizone model during combustion versus crank angle [8]

In the following paragraphs we are going to discuss the formation and the prediction model used for CO, HC and NO_x.

2.2 Carbon Monoxide

2.2.1 Formation

Carbon monoxide (CO) is the major pollutant product from combustion, representing about 90% of the overall pollutant emissions. Its formation occurs in the reaction zone of the flame, as an intermediate product of the hydrocarbon oxidation process. This latter may be summarized as:

hydrocarbon → radicals → peroxides → aldehydes → ketons → CO

Then, CO is oxidized to CO_2 and this process is controlled by the following reactions:

$$CO \ + \ OH \rightleftharpoons CO_2 \ + \ H \tag{2.2.1}$$

$$CO \ + \ O_2 \rightleftharpoons CO_2 \ + \ O \tag{2.2.2}$$

However, these reactions are much slower than the CO formation, thus equilibrium composition cannot be reached. Indeed, CO concentration in the exhaust gases is kinetically controlled: due to the rapid temperature decrease during expansion stroke, the oxidation process is frozen and part of the CO produced during combustion is emitted.

The most important engine parameter that influences the formation of CO is the Air Fuel Ratio A/F, which is the ratio between the air mass and the fuel mass introduced in the cylinder in a single thermodynamic cycle. CO formation is enhanced in a rich mixture, since the lack of oxygen prevents the hydrocarbons from being completely oxidized to CO_2, while in a lean mixture it is hindered thanks to O_2 abundance.

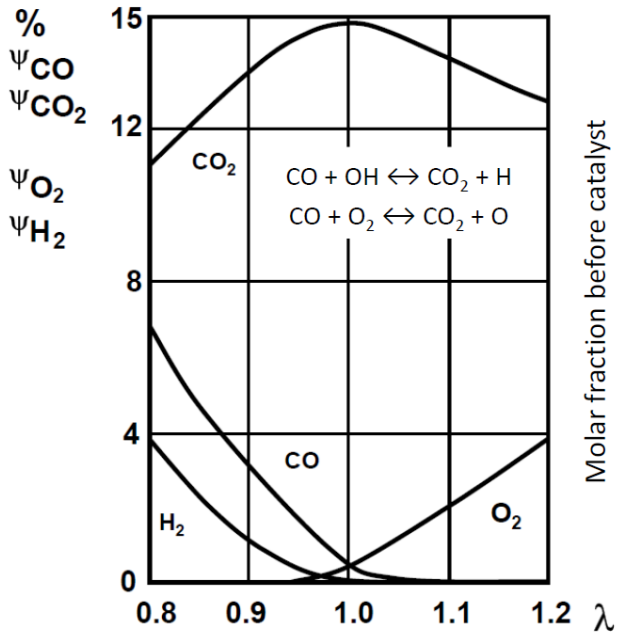

Figure 2.6: [8] CO concentration against relative Air/Fuel ratio coefficient

Since Spark Ignition engines at partial load usually operate in stoichiometric conditions, CO emissions must be controlled by an after treatment process. This latter is even more important at full load, as the mixture becomes richer.

2.2.2 Prediction Model

CO concentration can be computed by solving a differential equation based on the *Heywood and Ramos* reactions 2.2.1 and 2.2.2.

$$\frac{d[CO]}{dt} = -k_1^+ \cdot [CO] \cdot [OH] + k_1^- \cdot [CO_2] \cdot [H] - k_2^+ \cdot [CO] \cdot [O_2] + k_2^- \cdot [CO_2] \cdot [O]$$

At equilibrium:

$$k_1^+ \cdot [CO]_e \cdot [OH]_e = k_1^- \cdot [CO_2]_e \cdot [H]_e$$

$$k_2^+ \cdot [CO]_e \cdot [O_2]_e = k_2^- \cdot [CO_2]_e \cdot [O]_e$$

Assuming that $[OH]$, $[CO_2]$, $[H]$ and $[O]$ are always at equilibrium, the CO reaction rate can be expressed as follows:

$$\frac{d[CO]}{dt} = (R_1 + R_2) \cdot (1 - \frac{[CO]}{[CO]_e}) \tag{2.2.3}$$

where R_1, R_2 are given by:

$$R_1 = k_1^+ \cdot [CO]_e \cdot [OH]_e$$
$$R_2 = k_2^- \cdot [CO]_e \cdot [O_2]_e$$

Thanks to the kinetic approach, a better prediction of the CO emission can be obtained. The difference with respect to quilibrium based approach is highlighted in figure 2.7: this gap enlarges as the engine regime increases.

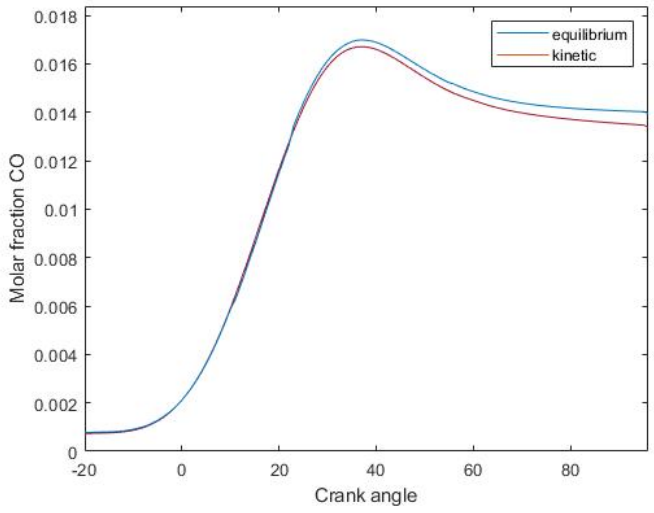

Figure 2.7: Predicted in-cylinder CO molar fraction versus crank angle in a syngle cylinder SI engine. A/F: 13.0; regime: 10000 rpm

The approach explained so far is more complex to apply, thus a semi-empirical method has been developed in order to simplify the problem. The *Baruah* method states that the actual concentration of CO is lower than the maximum value in the cylinder and higher than the equilibrium one. Starting from that, the following expression has been proposed:

$$CO = CO_{eq} + f_{CO} \cdot (CO_{max} - CO_{eq}) \tag{2.2.4}$$

The term f_{CO} is a calibration factor that varies from 0 to 1: if $f_{CO} = 0$ the CO emissions are equal to the equilibrium value; if $f_{CO} = 1$ they are equal to the peak.

2.3 Nitrogen oxides

2.3.1 Formation

Three main mechanisms cause the nitrogen oxides formation in thermal machines:

- Thermal NO_x: high temperature promotes the dissociation of N_2 from air, followed by its oxidation;
- Fuel NO_x: nitrogen embedded into the fuel, bounded to other compounds, dissociates and oxydates;
- Prompt NO_x: in the flame region, nitrogen reacts directly with hydrocarbon radicals.

All of these mechanisms are based on kinetics of reactions, since equilibrium condition cannot be assumed. The last two sources of NO_x are negligible in intenal combustion engines: nitrogen is not contained into the fuel exploited in such machines; the prompt mechanism is instead relevant just at low temperature, as the thermal dissociation is hindered.
To conclude, thermal dissociation and oxidation represent the main cause of NO_x formation in IC engines.

The most widely accepted mechanism to describe NO formation in IC engines is the Zeldovich model:

$$N_2 + O \rightleftharpoons NO + N \tag{2.3.1}$$

$$N + O_2 \rightleftharpoons NO + O \tag{2.3.2}$$

$$N + OH \rightleftharpoons NO + H \tag{2.3.3}$$

The driving force of these reactions is the high temperature in the flame region. If the temperature exceeds 2000 K, dissociation of nitrogen molecules occurs, thus activating Zeldovich mechanism reactions. Earlier burning elements are those that reach the highest temperature, since they are further compressed by later burning ones: a NO_x concentration gradient headed towards the spark plug is formed inside the combustion chamber.
The rate of reaction of NO is given by [16]:

$$\begin{aligned}\frac{d[NO]}{dt} = &+ k_1^+[O][N_2] + k_2^+[N][O_2] + k_3^+[N][OH] \\ &- k_1^-[NO][N] - k_2^-[NO][O] - k_3^-[NO][H]\end{aligned} \tag{2.3.4}$$

A simplifying assumption adopted states that the change in atomic nitrogen concentration is a quasi-steady process:

$$\frac{d[N]}{dt} = 0$$

This assumption is true for most combustion cases, except in extremely fuel rich environment [20].
Thus, equation 2.3.4 can be reduced to:

$$\frac{d[NO]}{dt} = 2k_1^+[O][N_2]\frac{(1 - \frac{k_1^- k_2^-[NO]^2}{k_1^+ k_2^+[N_2][O_2]})}{(1 + \frac{k_1^-[NO]}{k_2^+ k_3^+[O_2][OH]})} \tag{2.3.5}$$

The resulting equation highlights the two parameters influencing NO emissions: NO formation rate increases with oxygen concentration, as well as with temperature: beyond 2200 K, for every 90 K temperature increase, NO

production rate doubles [20]. In particular, temperature plays the most important role, since below 1800-2000 K the reaction rate of N_2 dissociation becomes negligible.
Thus, the main engine specifics affecting NO_x emissions are [1]:

- Air/Fuel ratio;
- Spark advance versus TDC;
- Exhaust Gases Recirculation (EGR);
- Engine rotational speed and load;
- Compression ratio and supercharging.

Focusing on the first item, the in-cylinder maximum NO_x concentration occurs for a slightly lean mixture, with equivalence ratio $\Phi = \frac{\alpha}{\alpha_s} = 0.9$. Indeed, despite the temperature peak is achieved with slightly rich mixture, with complete fuel consumption, oxygen availabilty is important to produce nitrogen oxydes.
By increasing the spark advance, instead, the combustion process happens closer to TDC, with consequent higher pressure and temperature peak, thus higher NO_x emissions.
Finally, a brief explaination of EGR influence on this pollutant is provided. At partial load, as EGR percentage increases up to 15-20%, we get two positive contributions: the mixture is cooled down, and oxygen availability decreases, thus NO_x emissions are reduced.

2.3.2 Prediction Model

Zeldovich extended 6 reactions model

The Zeldovich extended 6 reactions model is the simplest NO_x predictive approach implemented in *Gasdyn*.
The involved reactions are:

$$N_2 + O \rightleftharpoons NO + N \tag{2.3.6}$$

$$N + O_2 \rightleftharpoons NO + O \tag{2.3.7}$$

$$N + OH \rightleftharpoons NO + H \tag{2.3.8}$$

$$N_2O + O \rightleftharpoons 2NO \tag{2.3.9}$$

$$N_2O + O \rightleftharpoons N_2 + O_2 \tag{2.3.10}$$

$$N_2O + H \rightleftharpoons N_2 + OH \tag{2.3.11}$$

The substantial difference with respect to the simpler three reactions Zeldovich model is the presence of the intermediate N_2O.
N_2O rate of reaction can be expressed as:

$$\begin{aligned}\frac{d[N_2O]}{dt} = &+ k_4^-[NO]^2 + k_5^-[N_2][O_2] + k_6^-[N_2][OH] \\ &- k_4^+[N_2O][O] - k_5^+[N_2O][O] - k_6^+[N_2O][H]\end{aligned} \tag{2.3.12}$$

Since the characteristic formation and destruction time scales of N_2O are lower than NO, quasi-steady state for N_2O can be assumed [20]:

$$\frac{d[N_2O]}{dt} = 0$$

Thus, N_2O can be expressed as:

$$[N_2O] = \frac{k_4^-[NO]^2 + k_5^-[N_2][O_2] + k_6^-[N_2][OH]}{k_4^+[O] + k_5^+[O] + k_6^+[H]} \tag{2.3.13}$$

Finally, we can express the NO reaction rate in the 6 reactions model:

$$\begin{aligned}\frac{d[NO]}{dt} = &+ k_1^+[O][N_2] + k_2^+[N][O_2] + k_3^+[N][OH] - k_1^-[NO][N] \\ &- k_2^-[NO][O] - k_3^-[NO][H] + k_4^+[N_2O][O] - k_4^-[NO]^2\end{aligned} \tag{2.3.14}$$

where $[N_2O]$ can be computed from 2.3.13.

Zeldovich super-extended 67 reactions model

This approach includes a variety of additional species with respect to the default simulation model.

In particular, the following 22 species are considered: N_2, O, N, O_2, OH, H, N_2O, HO_2, NO, NO_2, O_3, NO_3, HNO, NH, H_2, H_2O, Ar, H_2O_2, NH_3, NH_2, N_2H_3, N_2H_2.

It is experimentally observed that the production and destruction time scales for N, NH, NH_3, NH_2, N_2O, HNO are lower than NO ones, but higher than N_2, O, O_2 and OH. Therefore, a system of 7 reaction rate equations has to be solved, in order to get [NO], as stated by [8].

The model intrinsic complexity limits its use to extreme conditions, such as to calibrate the simpler scheme.

2.4 Unburned hydrocarbons

2.4.1 Formation

The emission of unburned hydrocarbons is the result of an incomplete combustion. Several engine design parameters influence the HC level in the exhaust, such as [1]:

- Air/Fuel ratio;
- Spark advance with respect to TDC;
- Surface/Volume ratio and combustion chamber shape;
- Amounts of deposit on the walls;
- Engine rotational speed and load;
- Cooling system efficiency;
- Overlap angle;
- Pressure drop due to the exhaust system.

The first two parameters affecting HC emissions have a stronger influence than the others.
Focusing on Air/Fuel ratio, it has an important effect on the level of HC emissions, since it controls the oxygen availability. The minimum value, as we can see in figure 2.8, is reached for a slightly lean mixture. Rich mixtures result in lack of oxygen, while very lean ones in poor combustion quality.

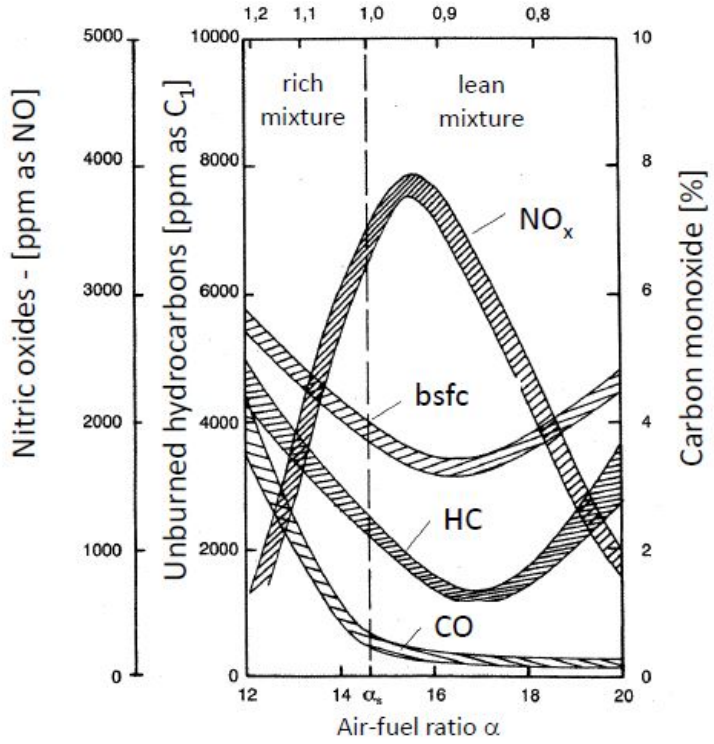

Figure 2.8: [1] Pollutants concentration against relative Air/Fuel ratio coefficient

As for the spark advance, instead, it influences the amount of HC that can be post-oxidized. If the spark advance decreases, the combustion process is delayed and it continues during the expansion stroke. The HC that have escaped from the primary combustion are mixed with the burned gases and oxidized. Even if a small reduction of the spark advance may be beneficial in terms of HC emissions, it is detrimental for engine performance as well.

Picture 2.8 shows another important concept: HC emissions have to be reduced not only because they cause environmental pollution, but also to increase engine efficiency: the profile of Brake Specific Fuel Consumption (BSFC) has the same trend as HC one.

Several mechanisms bring to the formation of HC: in this section it is provided a brief explaination of the main causes, while in the next chapter the focus is entirely on scavenging.

- **HC from scavenging**

  During the valve overlap period, as the scavenging of the combustion chamber takes place, part of the fresh mixture could directly flow from the intake to the exhaust valve, so that the embedded unburned fuel is emitted. This is the most important phenomenon that causes HC emissions.

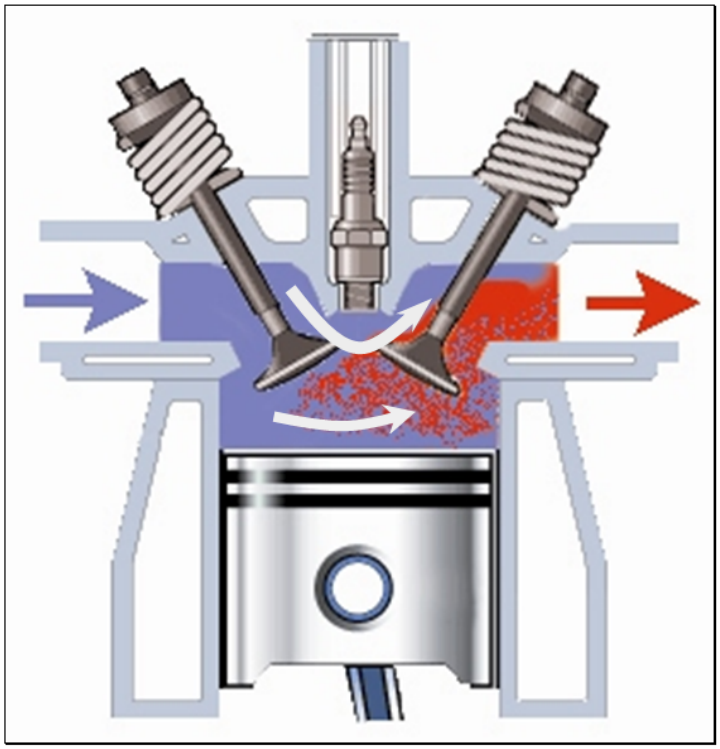

Figure 2.9: Short circuit durign overlap period

- **HC from crevices**

  Fuel mass stored inside cylinder crevices causes HC formation, since the flame cannot reach it. After the flame has passed, only part of the fuel is post-oxidized during the expansion stroke.

- **HC from oil film**

  The oil film on the cylinder wall can absorb the fuel hydrocarbons when the HC partial pressure is high, then release them during expansion stroke, as pressure decreases.

- **HC from quenching**

  Quenching is a term that describes the flame extinction close to the cylinder walls or on the piston crown. The temperature on these surfaces is much lower than inside the combustion zone: when the flame approaches them, if the temperature is too low, the combustion may not occur. This phenomenon is particularly frequent after a cold start of the engine.

- **HC from blow-by flux**

  A small portion of the cylinder mixture may flow through the rings and go into the engine basement. Then it is directly dispersed into the environment, causing HC emissions.

2.4.2 Prediction Model

In this section we are going to discuss the approaches to predict the HC emissions from crevices and oil film, while in the next chapter we will focus on the analysis of the scavenging model and the evaluation of HC due to short circuit, mixing and inlet backflow.

HC from crevices

Gasdyn code evaluates per each step the flame front radius and the distance between spark-plug and crevices: by comparing them, it can be understood whether the unburned fuel is going to be oxidized or not. The mass inside the crevices is evaluated by means of the following equation:

$$m_c = \frac{pV_cM}{RT_p} \tag{2.4.1}$$

where:

p: combustion chamber pressure $[Pa]$;

V_c: cervices volume $[m^3]$;

M: fresh mixture molar mass $[g/mol]$;

R: universal gas constant $[J/molK]$;

T_p: piston temperature $[K]$.

The mass variation in time is:

$$\frac{dm_c}{dt} = \frac{V_cM}{RT_p} \cdot \frac{dp}{dt} \tag{2.4.2}$$

The main assumptions are:

- mass temperature is equal to piston temperature (contact thermal boundary condition);
- the spark-plug is in the cylinder head, in the center;
- the flame front has a spherical shape with its center in the spark-plug.

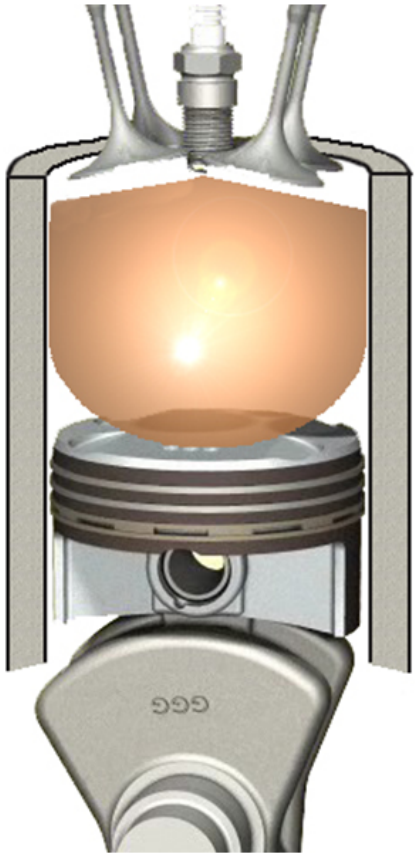

Figure 2.10: Flame front propagation

HC from oil film

In order to evaluate the emission of unburned hydrocarbon from the oil film, since mass transfer is diffusion controlled, a 1D differential equation for mass conservation has to be solved:

$$\frac{\partial Y_{HC}}{\partial t} - D\frac{\partial^2 Y_{HC}}{\partial x^2} = 0 \tag{2.4.3}$$

where:

Y_{HC}: fuel mass fraction in the oil film $[kg_f/kg_o]$;

x: distance from cylinder wall $[cm]$;

D: coefficient of diffusion in the solvent $[cm^2/s]$.

Cylinder 2D space has to be divided into a number of small elements in both radial and vertical direction. This approach allows the code to solve the equation and to evaluate the emission of HC.

Chapter 3

Scavenging model

3.1 Introduction

In the previous chapter, pollutants emission modelling has been described. As for unburned hydrocarbons sources, three main phenomena have been mentioned: crevices, oil film and scavenging. The first two contributions have been properly analyzed so far, while scavenging is dealt with in this chapter.

Scavenging model is capable to capture the emissions of HC during the valve overlap period, mainly due to the following phenomena:

- *short circuiting* of the unburned mixture directly through the exhaust port;
- *mixing* between unburned and burned mixtures;
- *inlet backflow*.

The main aim of this thesis is to highlight the magnitude of the scavenging process on the overall HC emissions of spark ignition engines. Indeed, the

original version of the *Gasdyn* code is not able to capture all the complex fluid dynamic phenomena contributing to HC emissions during the valve overlap period.

Thus, in the follow-up of this dissertation the focus will be on the model description and implementation, as well as on the comparison of the calculated results with the experimental ones.

3.2 Cylinder scavenging process

As the crank angle varies, the mixture contained into the engine cylinders changes both its mass and its composition.

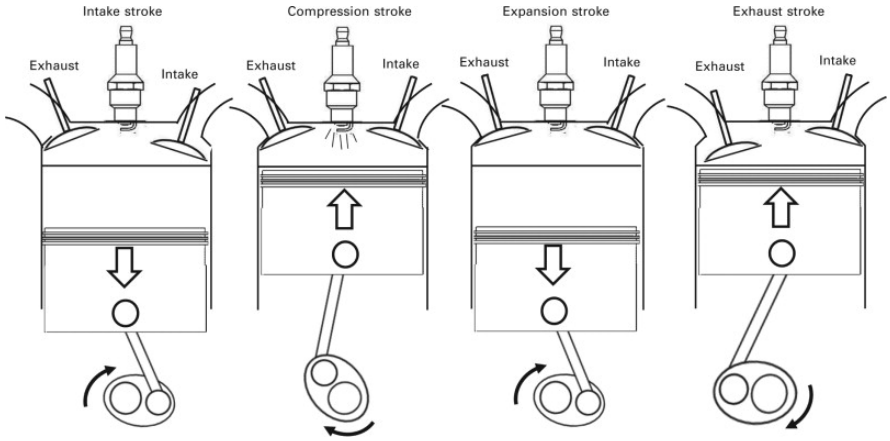

Figure 3.1: Four strokes engine gas exchange process [9]

At the exhaust valve opening (EVO) , typically 40°- 60° before BDC depending on the specific engine, the burned gases flow through the exhaust duct, decreasing the in-cylinder pressure and temperature. This process occurs during the last part of the expansion stroke and the whole exhaust stroke, since exhaust valve closing (EVC) happens at around 370-400 crank angle degrees, i.e. the beginning of intake stroke.

Nearly at the end of the exhaust stroke, around 10°- 40° before TDC, the intake valve opens (IVO). The fresh charge from the environment is delivered to the cylinder, flowing through the intake port during the whole intake stroke and the beginning of the compression stroke. In-cylinder pressure increases, as long as the overall mass contained. Intake valve closing (IVC) typically takes place 40°- 80° after BDC.
As shown in picture 3.2, valve overlap period may occur in common engines. During this crank angle interval, which can vary as function of the engine regime and load, intake and exhaust systems may interact:

- If the fluid inertia is strong enough, fresh charge may short circuit the cylinder, flowing directly through the exhaust port.

- Burned gases from exhaust ducts can backflow through the intake port, if pressure pulses are favourable: a sort of internal exhaust gases recirculation (EGR) occurs, with positive consequence on NO_x emissions, as discussed in the previous chapter.

The short circuit does not have any impact on unburned hydrocarbons emissions in direct injection engines, such as Diesel and modern spark ignition (GDI) ones, since only air is lost. However, in indirect injection engines a relevant amount of HC is emitted during valve overlap period due to short circuit.

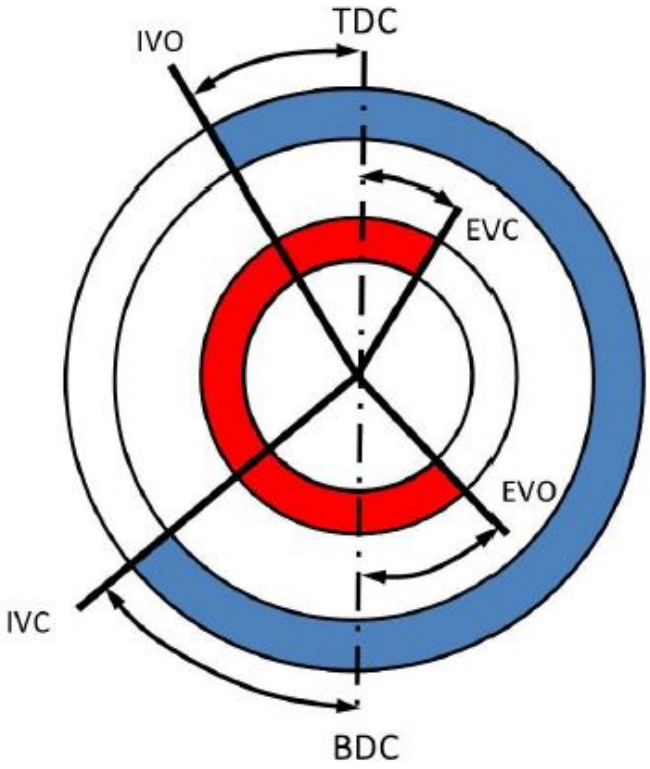

Figure 3.2: Circular diagram with opening and closing time of intake and exhaust valves [9]

3.2.1 Original cylinder model

The original model for the gas exchange process implemented in the *Gasdyn* code describes the engine cylinder by means of a single zone approach. There is no distinction between residuals and unburned, since perfect mixing is assumed: in this way both the inlet and the outlet fluxes contribute directly to the variation of the cylinder mass and composition. This model is quite well predictive of CO and NO_x emissions, as well as HC from crevices and oil film. Its weakest point concerns the HC emitted during the valve overlap period, since the short circuit of the fresh charge cannot be captured.

3.2.2 Scavenging submodels

Three different submodels can be adopted to properly describe the scavenging process:

1. perfect displacement;
2. homogeneous mixing;
3. pure short circuit;

Picture 3.3 shows their application on a two stroks engine, where the magnitude of scavenging is much higher.

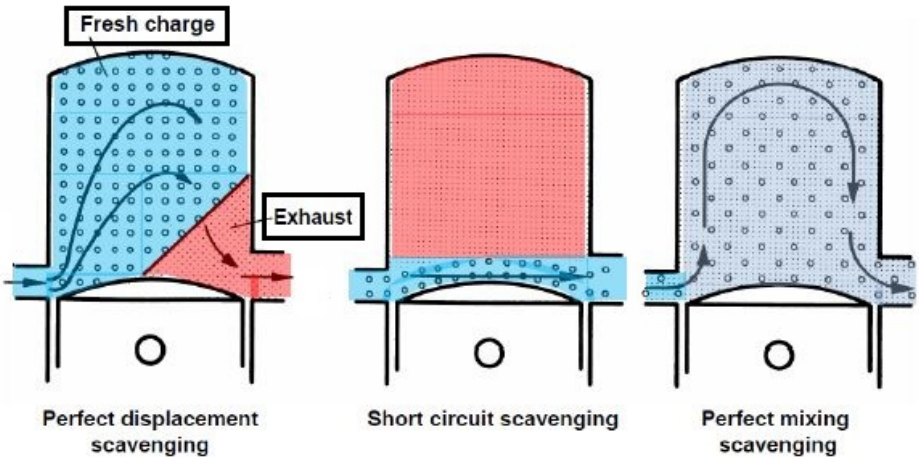

Figure 3.3: Scavenging submodels [9]

All of these models will be discussed in the following, starting from the first, which represents an ideal process.
In order to describe scavenging process, three coeffiecients are introduced:

- volumetric efficiency $\lambda_v = \frac{mass\ of\ air\ trapped\ per\ cycle}{displaced\ volume \cdot ambient\ density} = \frac{m_a}{m_t}$
- trapping efficiency $\lambda_{tr} = \frac{mass\ of\ air\ trapped\ per\ cycle}{mass\ of\ air\ delivered\ to\ the\ cylinder} = \frac{m_a}{m_s}$

- scavenging coefficient $\lambda_s = \frac{mass\ of\ air\ delivered\ to\ the\ cylinder}{displaced\ volume \cdot ambient\ density} = \frac{m_s}{m_t}$

where m_t is the reference mass.

Despite the last two indexes are typically adopted in two strokes engines, they can be exploited also in four stokes to properly describe the phenomenon.

Perfect displacement

Perfect displacement represents an ideal situation: fresh charge entering from the intake port would displace the combustion products without any mixing. If the incoming mass m_s does not exceed the reference one m_t, the mass flux leaving the cylinder through the exhaust port is entirely composed by burned gases: all the mass entering is trapped inside the cylinder for the combustion process. If instead the mass m_s exceeds the reference value m_t, the surplus is discharged through the exhaust port, causing HC emissions.

Picture 3.4 shows the trend of λ_v versus λ_s.

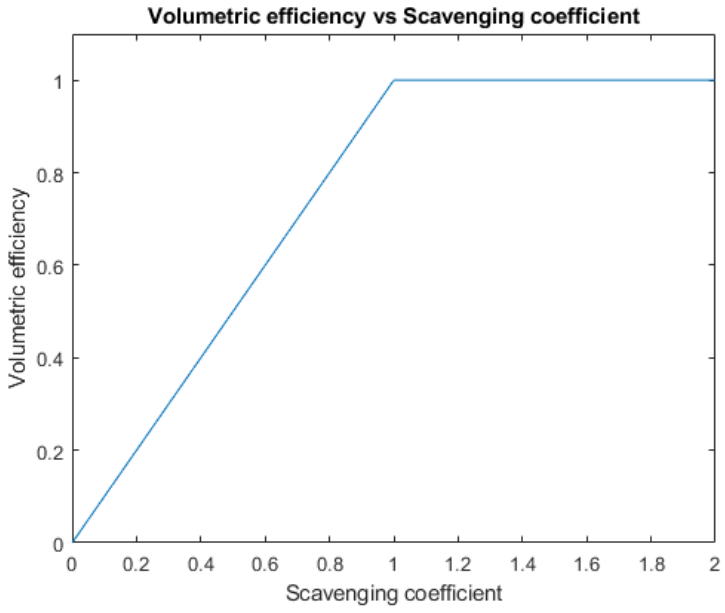

Figure 3.4: Perfect displacement volumetric efficiency trend

These concepts may be summarized as:

$$\lambda_s \leq 1 \ \rightarrow \ \lambda_v = \lambda_s \ and \ \lambda_{tr} = 1 \tag{3.2.1}$$

$$\lambda_s > 1 \ \rightarrow \ \lambda_v = 1 \ and \ \lambda_{tr} = \frac{1}{\lambda_s} \tag{3.2.2}$$

Homogeneous mixing

According to [1], homogeneous mixing is "a quite pessimistic model of the real behaviour". In order to describe this assumption, the following terms are introduced:

- m_a: fresh charge retained into the cylinder;
- m_r: residual mass retained into the cylinder;
- m_m: overall cylinder mixture mass;
- dm_s: scavenging mass element;
- dm_m: outgoing mass element of mixture;
- $dm_{a,out}$: outgoing mass element of fresh charge.

In a generic time instant t, the overall cylinder mass m_m is equal to the summation of the first two terms:

$$m_m = m_a + m_r \tag{3.2.3}$$

As gas exchange process goes on, the mixture mass m_m vary both its quantity and composition. Focusing on an infinitesimal interval dt, the mass of fresh charge retained in that time step in the cylinder can be expressed as:

$$dm_a = dm_s - dm_{a,out} \tag{3.2.4}$$

Since homogeneous mixing is assumed, the composition of the mixture leaving the cylinder in the infinitesimal time step is the same as the overall control volume:

$$\frac{dm_{a,out}}{dm_m} = \frac{m_a}{m_m} \tag{3.2.5}$$

Thus, combining (3.2.4) and (3.2.5) we get:

$$dm_a = dm_s - \frac{m_a}{m_m} dm_m \tag{3.2.6}$$

The model can be visualized in picture 3.5

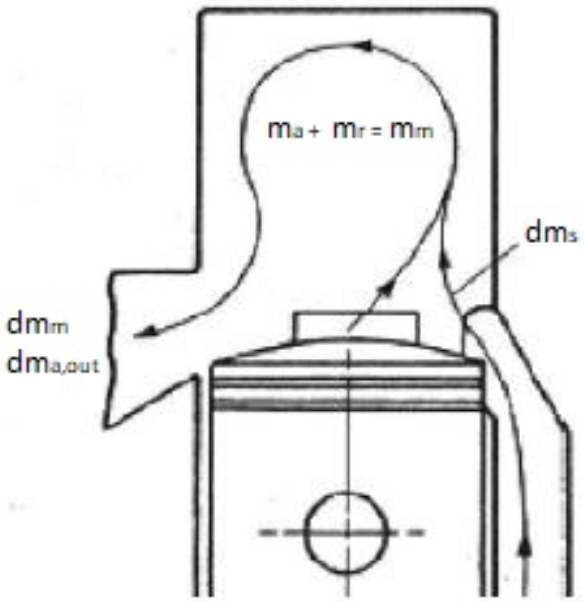

Figure 3.5: Homogeneous mixing scavenging model in two strokes engine [1]

At this point, two more assumptions are introduced:

1. the cylinder pressure variations during valve overlap period when scavenging process occurs are so low that gas compressibility may be neglected;

2. the piston motion around BDC is small, so that the cylinder volume can be considered constant in time, equal to its mean value $V_{m,cyl}$.

Starting from this latter hypothesis, we can express $V_{m,cyl}$ as:

$$V_{m,cyl} = \frac{m_m}{\rho_m}$$

Therefore, the volume of gas entering in interval dt equals the leaving one:

$$\frac{dm_s}{\rho_s} = \frac{dm_m}{\rho_m}$$

Equation (3.2.4) becomes:

$$\begin{aligned} dm_a &= dm_s[1 - (\frac{\rho_m}{\rho_s})(\frac{m_a}{m_m})] \\ &= dm_s[1 - \frac{m_a}{\rho_s \ V_{m,cyl}}] \end{aligned} \tag{3.2.7}$$

The ordinary differential equation obtained can be solved by means of variables separation. Finally we get to the following form:

$$m_a = \rho_s \ V_{m,cyl}[1 - exp(-\frac{m_s}{\rho_s \ V_{m,cyl}})] \tag{3.2.8}$$

This result states that, in case of perfect mixing, the mass of fresh charge

contained into the cylinder undergoes and exponential increase, tending to the limiting value $\rho_s V_{m,cyl}$. Therefore, this model represents the most unfavourable situation to remove all the residuals from the cylinder, since a theoretical infinite mass of fresh charge would be required to accomplish the full scavenging of the combustion chamber. Moreover the incomplete scavenging causes a worsening of the combustion process, since part of the mixture partecipating to the new thermodynamic cycle has already been burned.

This situation can be represented by rearranging equation (3.2.8). In particular, by dividing both sides by the reference mass m_t=ρ_aV and expressing m_s as m_s=λ_s m_t, we get:

$$\frac{m_a}{m_t} = (\frac{\rho_s \ V_{m,cyl}}{\rho_a V})[1 - exp(-\lambda_s \frac{\rho_a V}{\rho_s \ V_{m,cyl}})] \tag{3.2.9}$$

By introducing the non-dimensional coefficient $\Psi = \frac{\rho_s \ V_{m,cyl}}{\rho_a V}$, we get the dimensionless form of the cylinder filling law:

$$\lambda_v = \Psi[1 - exp(-\frac{\lambda_s}{\Psi})] \tag{3.2.10}$$

Ψ is typically close to 1, according to [1]: in that special case, we can represent the trend of the function $\lambda_v = 1 - exp(-\lambda_s)$ in figure 3.6:

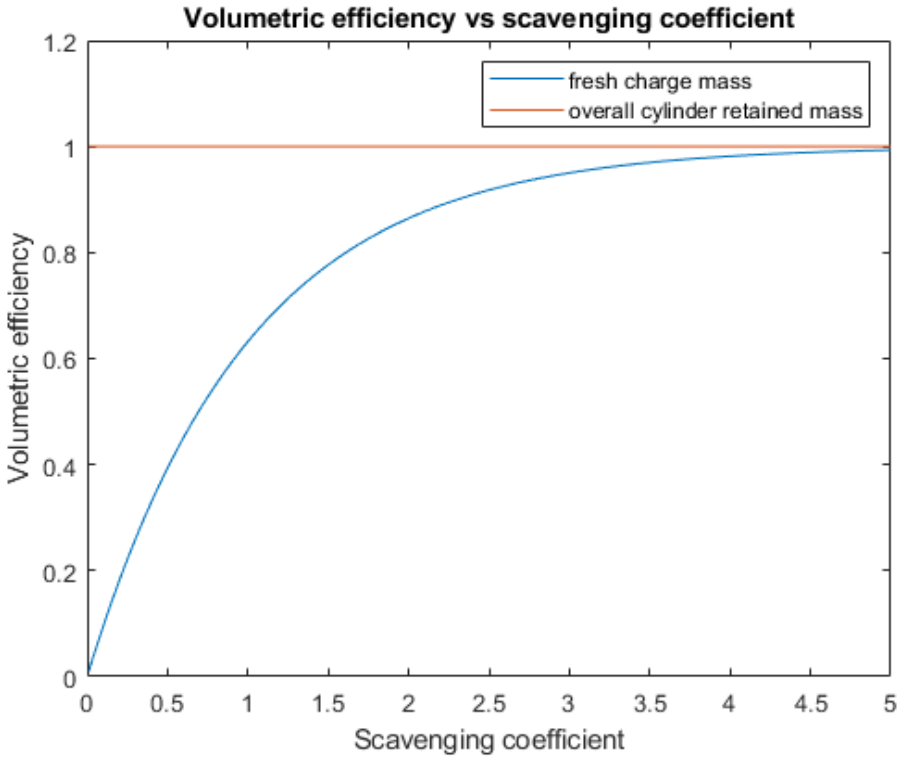

Figure 3.6: Cylinder filling in homogeneous mixing scavenging model

To complete the analysis, the trapping efficiency λ_{tr} can be expressed by substituting equation (3.2.10) into λ_{tr} definition:

$$\lambda_{tr} = \frac{\lambda_v}{\lambda_s} = (\frac{\Psi}{\lambda_s})[1 - exp(-\frac{\lambda_s}{\Psi})] \tag{3.2.11}$$

In the end, we can identify the working area where real cases stay into, as shown in green in figure 3.7.

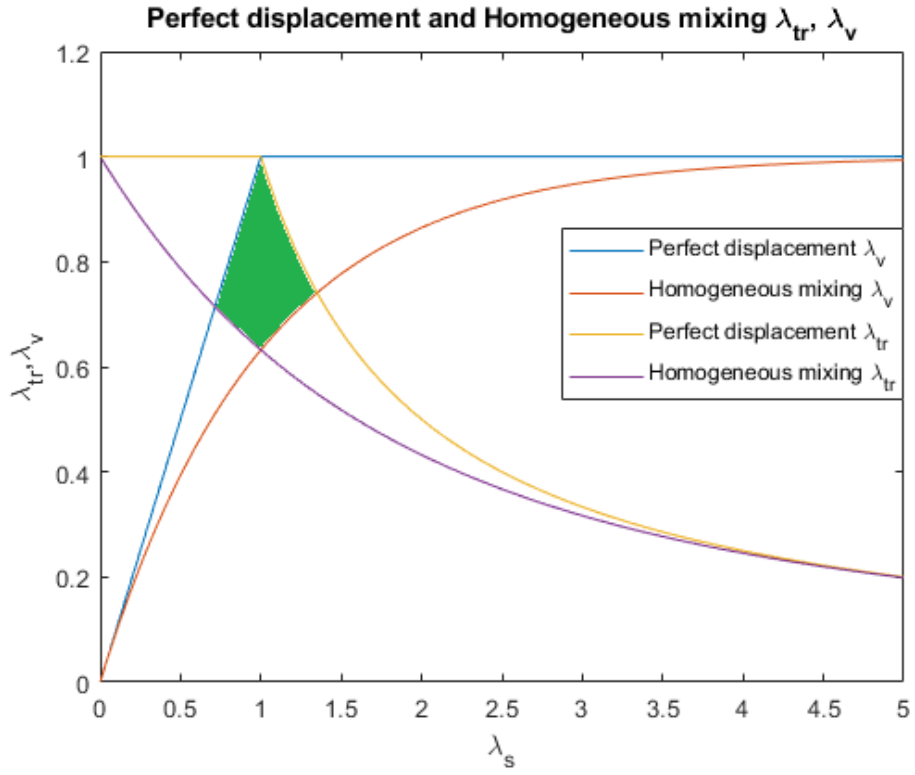

Figure 3.7: Volumetric and trapping efficiency versus scavenging coefficient

Pure short circuit

Pure short circuit represents the worst situation of scavenging process. Fresh mixture, after displacing all the combustion products on its pathway, flows directly through the exhaust port, without any mixing with the burned gases. A schematic of this phenomenon is shown in figure 3.8.
There are two main consequences of this situation:

1. high emission of unburned HC;
2. low volumetric efficiency.

Despite short circuit does not occur alone, it can participate together with mixing to the overall scavenging process, causing an increase of HC emissions.

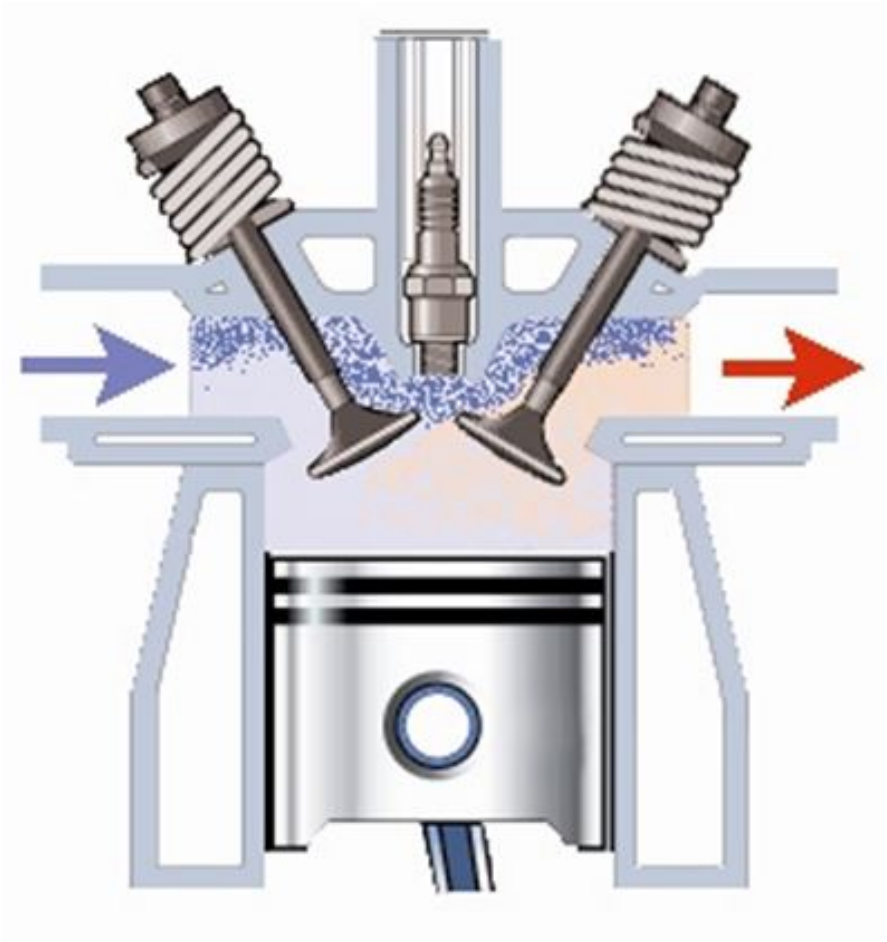

Figure 3.8: Short circuit mass flux

3.3 Scavenging model

3.3.1 Fundamental assumptions

In order to investigate the gas exchange process, a four zones model is adopted to describe the cylinder-ducts system: each control volume has variable mass and composition as function of the crank angle. As shown in picture 3.9, we can distinguish the following zones:

1. cylinder unburned zone;
2. cylinder burned zone;
3. inlet duct;
4. exhaust duct;

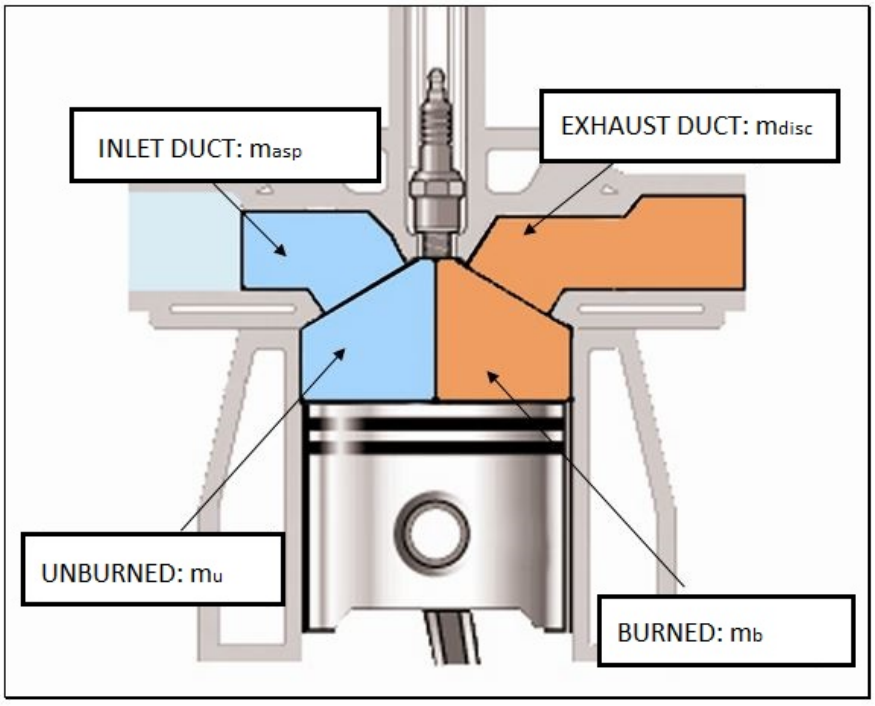

Figure 3.9: Cylinder-ducts system four zones model

We can associate to each control volume its mass:

1. m_{ASP}, cumulative mass in the intake duct due to the inlet backflow;
2. m_{DIS}, cumulative mass in the exhaust duct, due to the regular exhaust port discharge;
3. m_U, cylinder unburned region mass;
4. m_B, cylinder burned region mass.

As for the fluid modelling, the simplest assumption is the perfect gas, with constant specific heats. However, each zone is considered as composed by an ideal mixture of ideal gases. This choice is dictated by the requirement of emission tracking in the exhaust system: in order to assess a crank angle dependent analysis of both concentration and mass flow rate of the species in the pipes, the transport of species has to be implemented. A further benefit of this assumption is that the specific heat at constant pressure is function of both temperature and composition, so that thermodynamic calculations are more precise.
14 species are tracked inside the pipes by the code:

- 11 reacting species: N_2, O_2, CO_2, H_2O, CO, H_2, H, O, OH, NO and FUEL. This latter can be arbitrary chosen as an input;
- Argon as inert species;
- 2 unburned hydrocarbons species: C_3H_6, C_3H_8

Their concentration vary with the crank angle, according to gas exchange phenomena and combustion process.
Finally, a brief mention to the sign convention of flows through the cylinder ports is provided. For each angular step, the inlet and exhaust mass flow

rates are computed by proper functions already implemented in the code. In the following picture, their sign convention is shown.

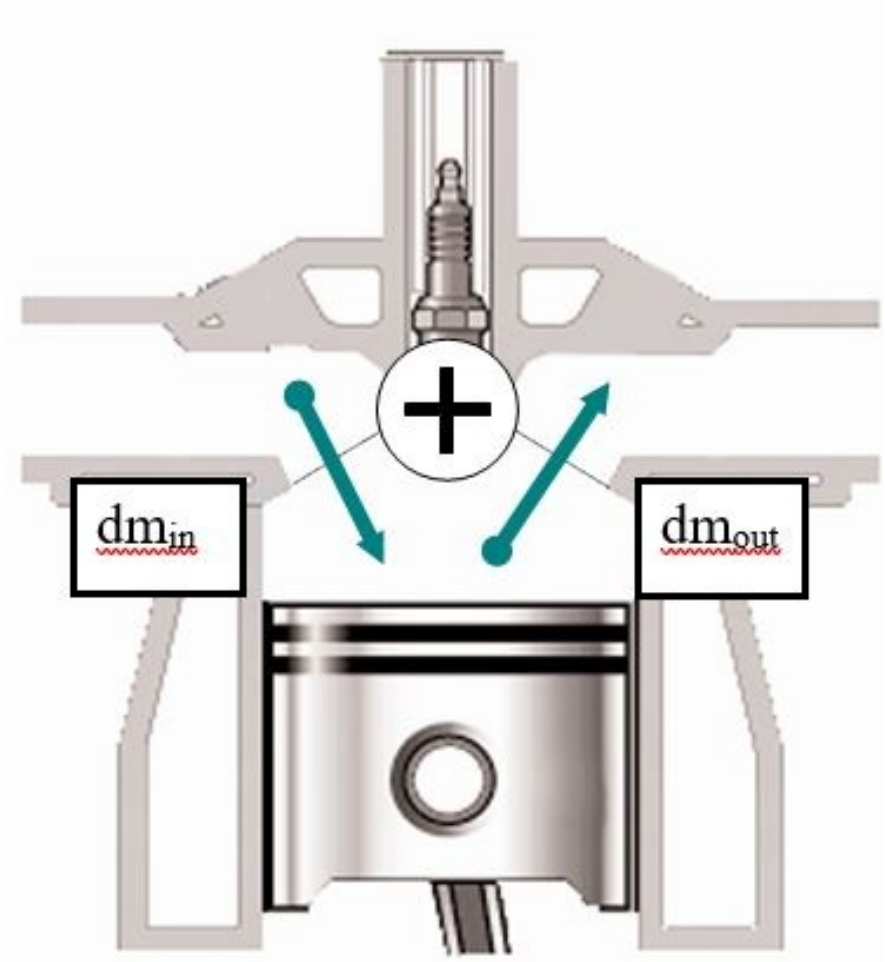

Figure 3.10: Inlet and exhaust mass flow rate

We can identify four primary fluxes among the zones:

1. Intake → Unburned;
2. Burned → Exhaust;
3. Unburned → Burned: *mixing* flux;
4. Unburned → Exhaust: *short circuit* flux.

The first three fluxes happen between adjacent control volumes. Specifically, the first two link the cylinder volume with ducts, representing gas exchange through the valves, while the third one occurs entirely inside the cylinder. The short circuit flux, instead, accounts for the fresh mixture bypassing the cylinder volume, by flowing directly through the exhaust port.
Furthermore, two secondary fluxes can be modelled:

1. Intake → Burned;
2. Unburned → Exhaust.

The last contribution, despite being directed as the short circuit one, has a different meaning: it represents the mass flow rate discharged to the exhaust duct directly from the unburned zone when the burned mass is null.
This complex framework can be visualized in the picture below (3.11).

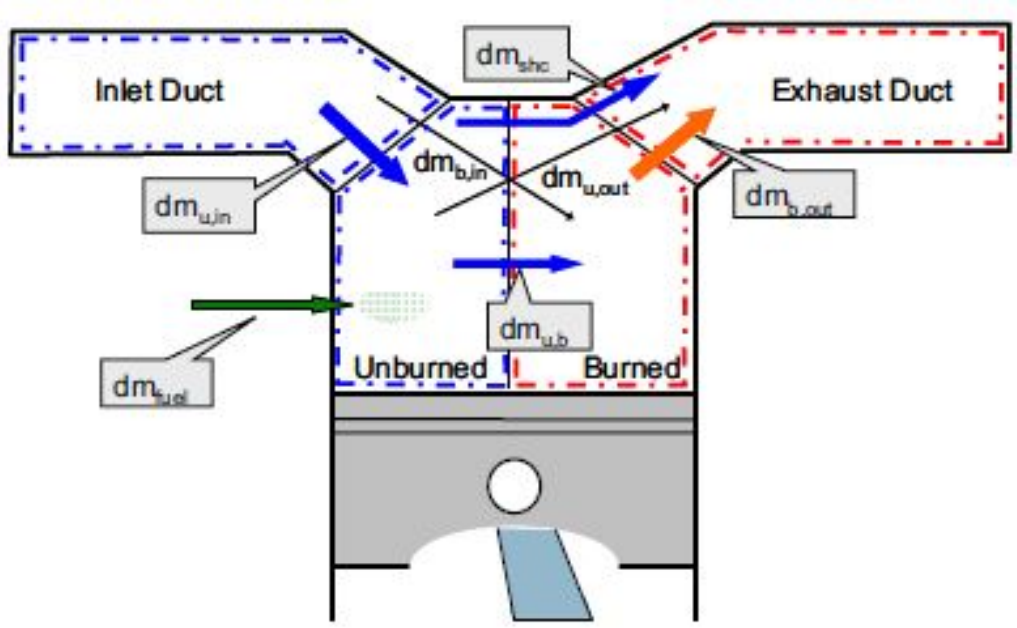

Figure 3.11: Four zone model fluxes [11]

Picture 3.11 distinguish four kind of fluxes, represented by arrows:

- Primary fluxes of fresh mixture are portrayed in blue;
- The only primary flux of burned gases is in orange;
- The two secondary fluxes are represented in black;
- The fuel injected is in green.

Focusing on the last item, even if fuel injection is indirect, the *Gasdyn* code models it as if it was direct. Indeed, fuel does not pass through the intake valve, but it is directly submitted to the cylinder. The difference with respect to direct injection consists in the timing: direct injection occurs when the exhaust ports are closed, while *Gasdyn* injection starts when the inlet air flux begins at IVO.

3.3.2 Mass fluxes

The new model implemented in the *Gasdyn* code takes into account both mixing and short circuit of the fresh charge. Inside the cylinder, three macro species are modelled: air, fuel and residuals.
The starting point consists in assuming that, if the calculation angle α is lower than IVO, the cylinder mass is entirely made of residuals, located in the burned zone. Both fuel and air are not present inside the cylinder so far, since the combustion has taken place. Moreover, the mass of the unburned region is null.
As the calculation angle α exceeds IVO, the scavenging process is modelled. Firstly, all mass fluxes are computed, starting from primary ones; then mass balances are revised.

- **Short circuit**

  Short circuit is represented as a flux from *unburned* to *exhaust* zone. In order to have this phenomenon, the following conditions have to be respected simultaneously:

$$\begin{cases} dm_{IN} > 0 \\ dm_{OUT} > 0 \\ m_U > 0 \end{cases}$$

  The first two statements highlight that the overall flux must be headed from the intake pipe to the exhaust one, without backflow effects; the last one, instead, means that no short circuit happens if only burned gases are present within the cylinder.
  The short circuit mass flux in the time step is expressed as:

$$dm_{SHC} = K_{SHC} \cdot min\ [dm_{IN}; dm_{OUT}] \tag{3.3.1}$$

The through-flow mass flow rate is function of ports fluxes and a coefficient depending on the flow turbulence intensity, whose calibration will be properly discussed in the next sections.

- **Mixing**

  Mixing is represented as a flux from *unburned* to *burned* zone. It can be modelled as:

$$dm_{MIX} = K_{MIX} \cdot (dm_{IN} - dm_{SHC}) \tag{3.3.2}$$

  The following conditions have to be respected:

$$\begin{cases} dm_{IN} > 0 \\ m_U > 0 \\ m_B > 0 \end{cases}$$

  In order to properly understand them, it has to be noticed that mixing is irreversible: dm_{MIX} must be positive, so $dm_{IN} > 0$. The last two conditions are strictly related to the nature of this phenomenon: $m_U > 0$ is required to provide fresh charge to the burned zone; m_B has to be positive, otherwise unburned mass would self-mix.

  Equation 3.3.2 states that mixing flux is limited by short circuit one: being both K_{MIX} and K_{SHC} at most equal to unity, the following inequality is verified at any time step, during valve overlap period:

$$dm_{SHC} + dm_{MIX} \leq dm_{IN} \tag{3.3.3}$$

  Thus, the excess of mass entering with respect to the one leaving the unburned region contributes to increase m_U.

Furthermore, for both mixing and short circuit, if one of the conditions is not satisfied, then the correspondent mass flow rate is set equal to zero.
Short circuit and mixing fluxes are then partitioned among air, fuel and residuals, depending on the mass fractions in the unburned control volume:

$$dm_{SHC}^{(j)} = \frac{m_U^{(j)}}{m_U} \cdot dm_{SHC}$$

$$dm_{MIX}^{(j)} = \frac{m_U^{(j)}}{m_U} \cdot dm_{MIX}$$

where apex j represents the j-th macro-specie.
To conclude the calculation of primary fluxes, the contributions at the ports have to be discussed.

- **Inlet flux**

  In order to calculate inlet flux, different situations have to be examined.

  - Firstly, we consider the case when the incoming mass flow rate dm_{IN} is negative, which represents *backflow* from the cylinder to the intake pipe. Due to this phenomenon, the composition of the leaving stream is detemined by the unburned zone. Obviously, the flux is non null if the unburned mass is greater than zero. This case can be summarized as:

$$\begin{cases} dm_{IN} < 0 \\ m_U > 0 \end{cases}$$

$$dm_{U,IN}^{(j)} = \frac{m_U^{(j)}}{m_U} \cdot dm_{IN} \tag{3.3.4}$$

    where the apex j in the previous equation represents the j-th macro

species: air, fuel or residual. In this case, also, the mass flow rate of injected fuel represented in figure 3.11 is null: $dm_{FUEL} = 0$.

– When there is cumulative mass in the intake pipe, due to backflow in previous time steps, it is preferentially sent to the cylinder, rather than environmental air. This means that, as the inlet mass flow rate becomes positive, the accumulate in the first zone decreases until complete depletion. This assumption is reasonable, since the backflow volume behaves as a buffer. The composition of the incoming flux is dictated by the one of the intake zone.
The following conditions summarize this situation:

$$\begin{cases} dm_{IN} > 0 \\ m_{ASP} > 0 \end{cases}$$

$$dm_{U,IN}^{(j)} = \frac{m_{ASP}^{(j)}}{m_{ASP}} \cdot dm_{IN} \tag{3.3.5}$$

Furthermore, as in the previous case, $dm_{FUEL} = 0$: this statement satisfies the requirement to keep the Air-Fuel Ratio constant to the fresh charge input value.

– The other possible situation concerning the intake flux to examine is consequential to the previous one: if the mass flows from inlet pipe to cylinder without any buffer to deplete, the composition is fixed by the intake system. In that case, the fuel is injected to satisfy the A/F requirement. These concepts can be expressed as:

$$\begin{cases} dm_{IN} > 0 \\ m_{ASP} = 0 \end{cases} \rightarrow \begin{cases} dm_{IN} = dm_{A,IN} \\ dm_{FUEL} = dm_{IN} \cdot \frac{1}{A/F} \end{cases}$$

- **Outlet flux**

  The primary flux at the outlet port, named $dm_{B,EX}$, occurs from *burned* zone to *exhaust* one. Two possible situations may happen, with the following relation in common:

$$dm_{B,EX} = dm_{OUT} - dm_{SHC} \tag{3.3.6}$$

  – If both the outlet mass flow rate and the overall mass inside the burned zone are positive, then the composition is dictated by the cylinder burned zone:

$$\begin{cases} dm_{OUT} > 0 \\ m_B > 0 \end{cases}$$

$$dm_{B,EX}^{(j)} = \frac{m_B^{(j)}}{m_B} \cdot (dm_{OUT} - dm_{SHC}) \tag{3.3.7}$$

  Thus, the model assumes that a portion of dm_{OUT} is due to short circuit, if present, while the rest is given by $dm_{B,EX}$.

  – If there is $backflow$, dm_{OUT} is negative; the composition is fixed by the exhaust duct, provided that an accumulate is available:

$$\begin{cases} dm_{OUT} < 0 \\ m_{DIS} > 0 \end{cases}$$

$$dm_{B,EX}^{(j)} = \frac{m_{DIS}^{(j)}}{m_{DIS}} \cdot dm_{OUT} \tag{3.3.8}$$

As anticipated so far, two secondary fluxes are modelled to guarantee the closure of the balances in every cases: they are thought to represent quite unusual but possible situations.

- **Inlet secondary flux**

  By considering inlet port, in case of backflow from cylinder to intake system, the mass flow rate of the j-th macro species has been computed in equation (3.3.4). However, if there is no mass in the unburned region, an alternative has to be proposed. In particular, provided that m_B is positive, which is trivial since either unburned or burned have to occupy the cylinder, the inlet secondary flux moves from *burned* to *intake* zone. Its composition depends on the burned region one:

$$\begin{cases} dm_{IN} < 0 \\ m_U = 0 \\ m_B > 0 \end{cases}$$

$$dm_{B,IN}^{(j)} = \frac{m_B^{(j)}}{m_B} \cdot dm_{IN} \tag{3.3.9}$$

- **Outlet secondary flux**

  The secondary flux at the discharge port moves from *unburned* to *exhaust* zone: its pathway is the same as short circuit one, but the background is different. Indeed, this flow rate appears as an alternative to normal discharge $dm_{B,EX}$. If there is no mass to discharge in the burned region, as for example close to EVC, then the regular flow at the exhaust port is guaranteed by this unburned gas flux:

$$\begin{cases} dm_{OUT} > 0 \\ m_B = 0 \\ m_U > 0 \end{cases}$$

$$dm_{U,EX}^{(j)} = \frac{m_U^{(j)}}{m_U} \cdot (dm_{OUT} - dm_{SHC}) \tag{3.3.10}$$

3.3.3 Mass balances

Once all the fluxes have been computed, mass balances are performed:

$$dm_{IN} = dm_{U,IN} + dm_{B,IN} \qquad Intake \tag{3.3.11}$$

$$dm_{EX} = dm_{B,EX} + dm_{U,EX} + dm_{SHC} \qquad Exhaust \tag{3.3.12}$$

$$dm_U = dm_{U,IN} + dm_{U,B} + dm_{SHC} + dm_{U,EX} \qquad Unburned \tag{3.3.13}$$

$$dm_B = dm_{U,B} + dm_{B,EX} + dm_{B,IN} \qquad Burned \tag{3.3.14}$$

It has to be noticed that all the previous equations are in algebraic form, meaning that their terms may become negative.
Focusing on fuel macro species in the unburned region, a further contribution due to injection modelling, named dm_{FUEL}, has to be accounted.
The four above mentioned balances are representative of the whole zones. In the code, however, the implementation is different, since equations 3.3.11 to 3.3.14 are applied to the macro species inside the zone. Considering the unburned zone:

$$m_{FUEL,U}^{(t+dt)} = m_{FUEL,U}^{(t)} + dm_{U,IN}^{(FUEL)} + dm_{U,B}^{(FUEL)} + dm_{SHC}^{(FUEL)} + dm_{U,EX}^{(FUEL)} + dm_{FUEL}$$

$$m_{AIR,U}^{(t+dt)} = m_{AIR,U}^{(t)} + dm_{U,IN}^{(AIR)} + dm_{U,B}^{(AIR)} + dm_{SHC}^{(AIR)} + dm_{U,EX}^{(AIR)}$$

$$m_{RES,U}^{(t+dt)} = m_{RES,U}^{(t)} + dm_{U,IN}^{(RES)} + dm_{U,B}^{(RES)} + dm_{SHC}^{(RES)} + dm_{U,EX}^{(RES)}$$

Then, the three contributions are joined, to get the whole unburned zone mass:

$$m_{U}^{(t+dt)} = m_{FUEL,U}^{(t+dt)} + m_{AIR,U}^{(t+dt)} + m_{RES,U}^{(t+dt)}$$

The same procedure is carried out for other control volumes.
No mention to chemical species has been done so far. Since macro species and control volumes mass balances have been performed, the amount of each chemical species inside the cylinder can be obtained. It is important to notice that at this point no further distinction among unburned and burned region is done, since the aim is to calculate the overall mass of the j-th spcies inside the cylinder at the generic time step.

- Air is assumed to be composed by 79% nytrogen and 21% oxygen, on molar basis. Therefore, the correspondent percentage of the all $m_{AIR,U}^{(t+dt)}$, on mass basis, is allocated on them.
- Residuals are divided among all the species according to the combustion chamber composition calculated at EVO.
- Fuel is entirely allocated on its correpondent species.

As for example, is it shown the calculation of nytrogen mass:

$$m_{N_2}^{(t+dt)} = m_{AIR}^{(t+dt)} \cdot 0.79 \cdot \frac{MM_{N_2}}{MM_{MIX}} \cdot (1 - EGR_{\%}) + m_{RES}^{(t+dt)} * y_{N_2,\ RES}$$

In table 3.3.3, a recap of the fluxes specifications is provided.

PRIMARY FLUXES		
	Conditions	Value
SHC	$dm_{IN} > 0$ $dm_{OUT} > 0$ $m_U > 0$	$dm_{SHC} = K_{SHC} \cdot min[dm_{IN}; dm_{OUT}]$ $dm_{SHC}^{(j)} = \frac{m_U^{(j)}}{m_U} \cdot dm_{SHC}$
MIX	$dmIN > 0$ $m_U > 0$ $m_B > 0$	$dm_{MIX} = K_{MIX} \cdot (dm_{IN} - dm_{SHC})$ $dm_{MIX}^{(j)} = \frac{m_U^{(j)}}{m_U} \cdot dm_{MIX}$
INLET	$dm_{IN} < 0$ $m_U > 0$	$dm_{U,IN}^{(j)} = \frac{m_U^{(j)}}{m_U} \cdot dm_{IN}$
	$dm_{IN} > 0$ $m_{ASP} > 0$	$dm_{U,IN}^{(j)} = \frac{m_{ASP}^{(j)}}{m_{ASP}} \cdot dm_{IN}$
	$dm_{IN} > 0$ $m_{ASP} = 0$	$dm_{A,IN} = dm_{IN}$ $dm_{FUEL} = dm_{IN} \cdot \frac{1}{A/F}$
OUTLET	$dm_{OUT} > 0$ $m_B > 0$	$dm_{B,EX}^{(j)} = \frac{m_B^{(j)}}{m_B} \cdot (dm_{OUT} - dm_{SHC})$
	$dm_{OUT} < 0$ $m_{DIS} > 0$	$dm_{B,EX}^{(j)} = \frac{m_{DIS}^{(j)}}{m_{DIS}} \cdot dm_{OUT}$
SECONDARY FLUXES		
INLET	$dm_{IN} < 0$ $m_U = 0$ $m_B > 0$	$dm_{B,IN}^{(j)} = \frac{m_B^{(j)}}{m_B} \cdot dm_{IN}$
OUTLET	$dm_{OUT} > 0$ $m_B = 0$ $m_U > 0$	$dm_{U,EX}^{(j)} = \frac{m_U^{(j)}}{m_U} \cdot (dm_{OUT} - dm_{SHC})$

3.4 Turbulence

In the previous sections we introduced the coefficients K_{SHC} and K_{MIX}, saying that their values depend on the fluid *turbulence intensity* u' inside the cylinder. The aim of the former paragraph is to briefly explain how the gas motions into the cylinder work, highlighting the bond with our target parameter. Also, an explaination of the K-k model to determine u' is given.

3.4.1 Turbulence in SI engines

The gas motion in the cylinder is very important for the mixing of air and fuel, as well as for the development of combustion process. The flow inside the engine cylinders is always turbulent and characterized by vortexes of different size. For this reason, a statistical approach has to be used. Firstly, we can consider a generic velocity $U_{(t)}$ that changes every cycle since the flow patterns are not perfectly periodic. For this velocity we can define two quantities: $U^c_{(t)}$, the average value of $U_{(t)}$ in a cycle, and $U^e_{(t)}$ the ensemble average, i.e. the average value based on many cycles. In order to correctly characterize the flow field, instantaneous fluctuations $u_{(t)}$ have to be considered:

$$u_{(t)} = U_{(t)} - U^e_{(t)}$$

The fluctuations are referred to the ensemble average in order to avoid cyclic variations. To neglect $u_{(t)}$ sign, its root mean square value is considered, so the turbulence intensity is defined as:

$$u' = \sqrt{\frac{1}{T} \cdot \int_0^T u^2_{(t)} dt} \tag{3.4.1}$$

In order to properly study the turbulent flow and the size distribution of the random vortexes, the following length scales are defined:

- the integral scale L_l, correspondent to the largest vortex size;
- the Taylor microscale L_T, the largest length scale where viscosity affects the dynamics of the turbulent eddies in the flow;
- the Kolmogorov scale L_K, the smallest length scale where the flow kinetic energy is dissipated by the fluid molecular diffusion.

Moreover, different scales vortexes are characterized by different lifetime: the larger the scale, the longer the lifetime.
As consequence of the intake and compression processes, large scale motions are formed in the engine cylinder. Their characteristic lengths are of the order of magnitude of the cylinder bore, thus larger than the Kolmogorov one, and they are the effective source of turbulence motions inside the cylinder. An energy cascade from larger to smaller eddies takes place, supplying these latter of the kinetic energy required by turbulence.
In Spark Ignition Engines the structured large scale gas motions are useful because:

- they enhance the mixing between air, fuel and residuals;
- they generate turbulence that increases the flame propagation speed, resulting in a better combustion;
- they guarantee to achieve stratified mixture distribution.

The most important phenomena concerning large scale gas motions are presented in the following.

Swirl

Swirl is a structured rotational flow on a plane that is normal with respect to the cylinder axis. It is formed during the intake stroke and imposed by the geometry of the intake duct or by the shape of the combustion chamber. Some examples of geometries are proposed in figure 3.12.
In direct injection engines, *Swirl* enhances the fuel/air mixing, while in indirect injection ones it is useful to increase the turbulent flame speed.

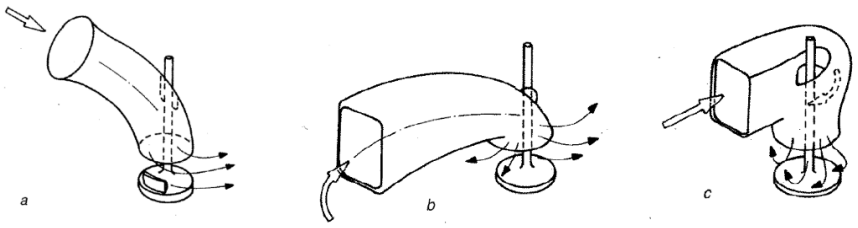

Figure 3.12: Different geometries used to obtain swirl: a) Shrouded valve; b) Directed port; c) Helical port [1].

Tumble

Tumble is a structured rotational flow on a cylinder axial plane. As swirl, it is generated during the intake stroke but it is enhanced in the compression one. It was studied to be applied in four valves pent-roof combustion chambers: in this kind of engine cylinders, swirl cannot be generated during the intake stroke, due to the symmetry of the combustion chamber. One way to achieve tumble is by means of directed intake ports: the entering air is mainly oriented towards the area underneath the exhaust valves. There, interacting with the cylinder walls and piston head, the flow reverses its movement direction, forming a structured vortex on an axial plane. As we said before, tumble is enhanced during compression stroke: when the piston

moves towards TDC, the vortex radius is decreased and, as a consequence, also the momentum of inertia. Neglecting the effects of fluid friction, the angular momentum of the system is conserved, thus the angular velocity of the vortex must increase.

In figure 3.13, different tumble intensities during intake and compression stroke are shown.

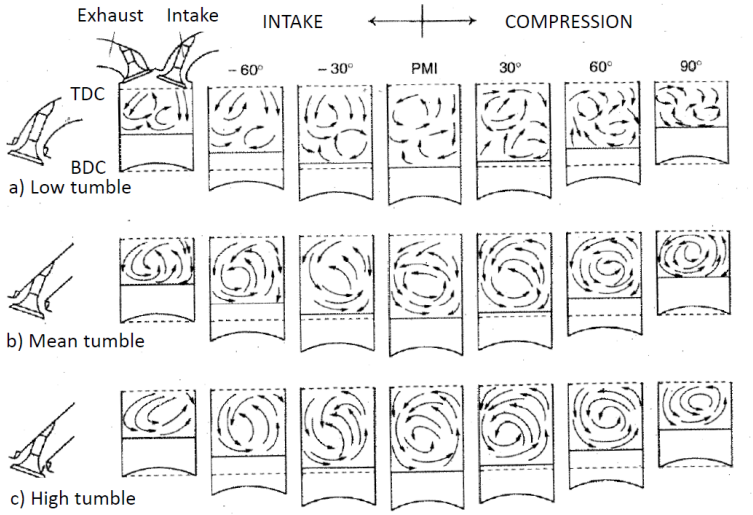

Figure 3.13: Tumble during intake and compression stroke [1].

Squish

Squish is a structured rotational flow on a cylinder axial plane, generated towards the end of the compression stroke. It is due to the non-uniform decrease in time of the volume in different zones ot the combustion chamber. Indeed, the peculiar shape of the cylinder head in SI engines, as well as the geometry of the piston head in Diesel engines, cause structured vortexes inside these volumes, as shown in figure 3.14.

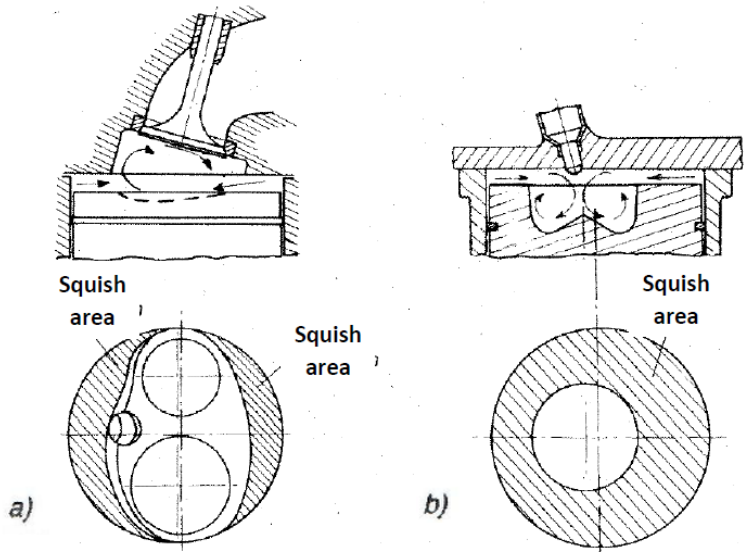

Figure 3.14: Squish generation in SI engines (a) and in Diesel engines (b) [1].

During compression, density varies in time but it is quite uniform in space, thus the mass is proportional to the volume of the zone in which it is contained. As the piston approaches the TDC, the volume of the squish area is reduced faster than the rest of the combustion chamber. For this reason, a squish structured vortex is generated by the cup shape mainly in an axial plane.

3.4.2 K-k model for turbulence intensity

The phenomenological model used to predict turbulence characteristic into the cylinder is indicated with the acronym K-k, referring to the mean motion kinetic energy K and the turbulent kinetic energy k, the main variables occurring in the two balance equations which characterize the model.
The basic assumption states that turbulent motions inside cylinders can be considered as generated by a zero-dimensional energy cascade. In particular, kinetic energy is supplied to the fluid inside the cylinder through the intake

valves, increasing its mean motion kinetic energy; K is converted into turbulent kinetic energy k and then to fluid internal energy, through viscous dissipation. On the other side, when some fluid flows out of the cylinder through exhaust valves, it carries with it both mean and turbulent kinetic energy. These concepts are represented in picture 3.15.

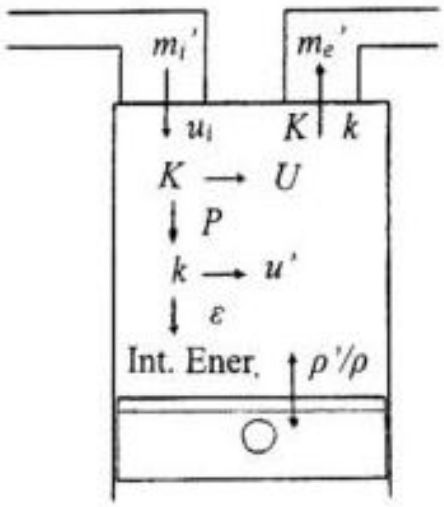

Figure 3.15: Schematic of the zero-dimensional energy cascade able to approximate the generation of turbulent motions inside cylinders [1]

Two balance equations for production and dissipation of K and k are written:

$$\begin{cases} \frac{dK}{dt} = \frac{1}{2}\dot{m}_i u_i^2 - \frac{1}{2}\dot{m}_e u_e^2 - P - K(\frac{\dot{m}_e}{m}) + K(\frac{\rho'}{\rho}) \\ \frac{dk}{dt} = P - \epsilon - k(\frac{\dot{m}_e}{m}) + k(\frac{\rho'}{\rho}) \end{cases}$$

In the following, a brief description of all the terms is provided.

- $\frac{dK}{dt}$ and $\frac{dk}{dt}$ represent the time variation of mean flow and turbulent kinetic energy;
- $\frac{1}{2}\dot{m}_i u_i^2$ and $\frac{1}{2}\dot{m}_e u_e^2$ are the contributions of kinetic energy carried inside

and outside the cylinder, due to the mass flowing through the valves with velocities u_i and u_e;

- P is the production rate of turbulent kinetic energy:

$$P = c_p \, (\frac{K}{\tau_I})$$

where c_p is a model constant, while τ_I is the integral time scale of large eddies.

- ϵ is the dissipation rate of k:

$$P = c_\epsilon \, (\frac{k}{\tau'})$$

where c_ϵ is a model constant, while τ' is the time scale of turbulent eddies.

- K $(\frac{\dot{m}_e}{m})$ and k $(\frac{\dot{m}_e}{m})$ are the fraction of mean flow kinetic energy K and turbulent kinetic energy k carried out by mass flow rate $\dot{m}_e$, related to the mass m inside the cylinder;

- K $(\frac{\rho'}{\rho})$ and k $(\frac{\rho'}{\rho})$ account the effect of density variation $\frac{\rho'}{\rho}$, both on mean flow kinetic energy K and turbulent kinetic energy k, due to piston motion and combustion progress.

Assuming that turbulence is homogeneous and isotropic, meaning that it does not have preferential direction, at any time step the mean flow velocity U and the turbulent intensity u' are related to their relative kinetic energies by the following equations:

$$K = \frac{1}{2} m U^2 \tag{3.4.2}$$

$$k = \frac{1}{2} m (u_x'^2 + u_y'^2 + u_z'^2) = \frac{3}{2} m u'^2 \tag{3.4.3}$$

Introducing the macro scale of turbulence, calculated as a fraction of the representative geometric length scale l, the time scales of large and turbulent eddies are then computed:

$$l_I = c_{LI} l = c_{LI} \frac{4V}{\pi D^2} \tag{3.4.4}$$

$$\tau_I = \frac{l_I}{U} \tag{3.4.5}$$

$$\tau' = \frac{l_I}{u'} \tag{3.4.6}$$

Thus, the K-k model, starting from two balance equations for production and dissipation of kinetic energies, computes the two main quantities of turbulence field: the *turbulence intensity u'* and the *integral length scale* l_I.

In the following chapter, by validating the scavenging model discussed so far, we will highlight the relevance of *turbulence intensity u'* on the calibration coefficients K_{SHC} and K_{MIX}.

Chapter 4

Theoretical model validation

In this chapter we will analyze the effect of the scavenging model on simple architectures, in order to understand if it behaves as we expect from theory; then a sensitivity analysis is carried out.

4.1 Single cylinder engine

In this section we will investigate quantities affecting both cycle average and instantaneous HC emissions at the exhaust port: K_{MIX} and K_{SHC}, which are model parameters, and valve overlap period, which is instead an operating parameter. The model, if properly designed, should show significant changes in the results, as either calibration coefficients or valve overlap angle vary.
The sample exploited is a single cylinder, 2 valves, spark ignition engine, whose schematic is represented in picture 4.1. It has to be noticed that outputs are evaluated at the exhaust port.

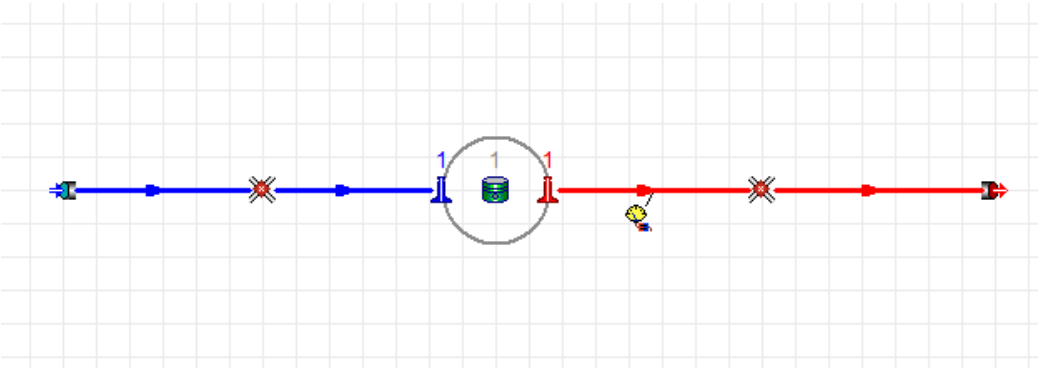

Figure 4.1: single cylinder, 2 valve, 373 cm^3 displacement, spark ignition engine

4.1.1 K_{MIX} and K_{SHC} sensitivity analysis

K_{MIX} and K_{SHC} range from 0 to 1. Their variation is related to the cylinder turbulence intensity u', which has been discussed in the previous chapter. In particular, three situations are considered: the first two are limiting cases; the last one represents the general situation.

- perfect mixing, i.e. K_{MIX}=1, K_{SHC}=0;
- pure short circuit, i.e. K_{MIX}=0, K_{SHC}=1;
- turbulence intensity dependence, i.e. $K_{MIX} = K_{SHC} = f(u')$

Perfect mixing

In case of perfect mixing, the scavenging model is expected to provide results extremely close to the original cylinder model. This latter is indeed based on a single zone approach, with perfect mixing occurring without any short circuit.

The comparison is carried out for two different quantities: the average emitted mass of HC during a cycle, plotted for each rotational speed, and the HC instantaneous outgoing flux at a fixed regime.

As shown in the charts 4.2 and 4.3, the discrepancy between the two models is negligible, and it is due just to the different approach to the problem: single zone in the original model, four zone in the through-flow one.

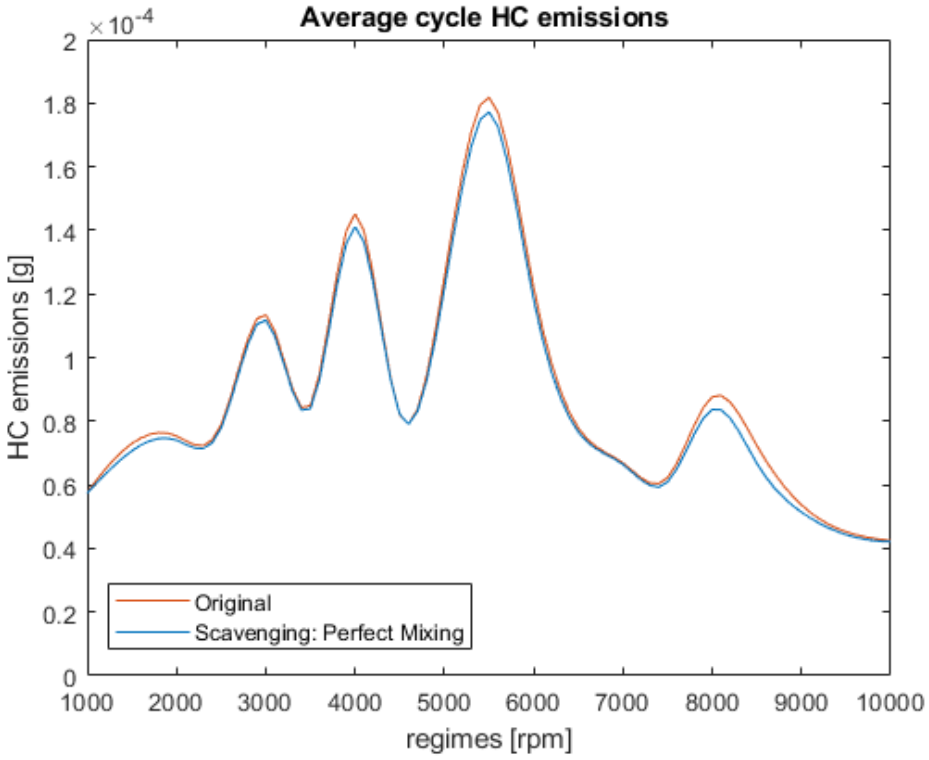

Figure 4.2: Average cycle HC emissions versus regime

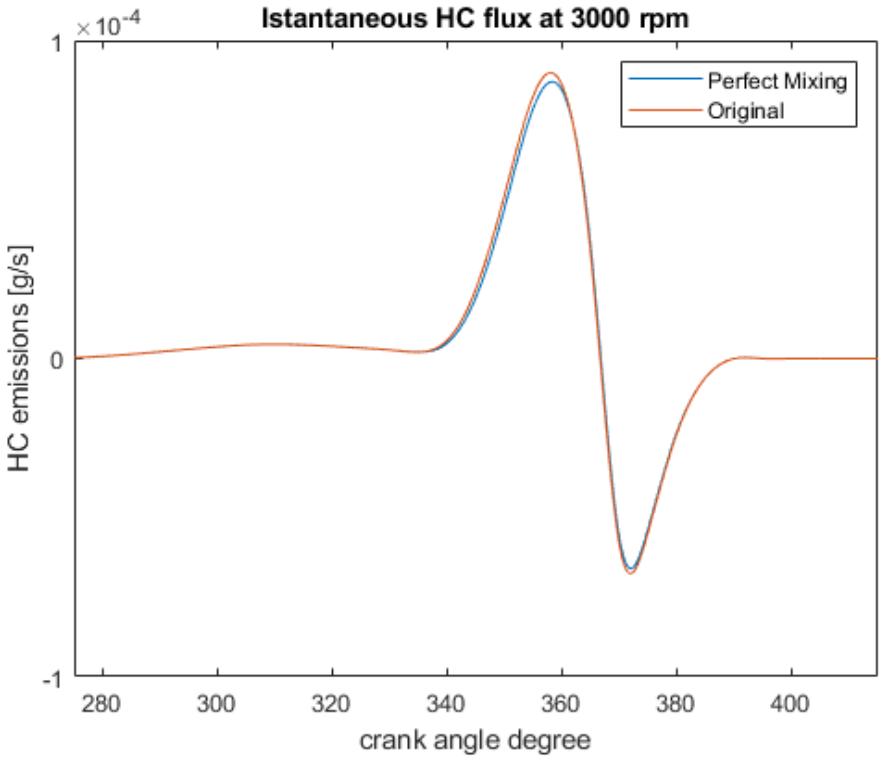

Figure 4.3: Istantaneous HC flux emitted at 3000 rpm

Pure short circuit

The same quantities plotted for the perfect mixing case can be considered also to analyze the short circuit effect. In particular, in this paragraph pure through-flow is investigated, meaning K_{SHC}=1 and K_{MIX}=0.
Since the fresh charge by-passes the cylinder without any mixing with the burned volume, we expect an increase of both the cycle average and the instantaneous HC emissions. Thus, the outgoing mass flow rate has a higher concentration of unburned fuel than in any other case. The following charts highlight this forecast.

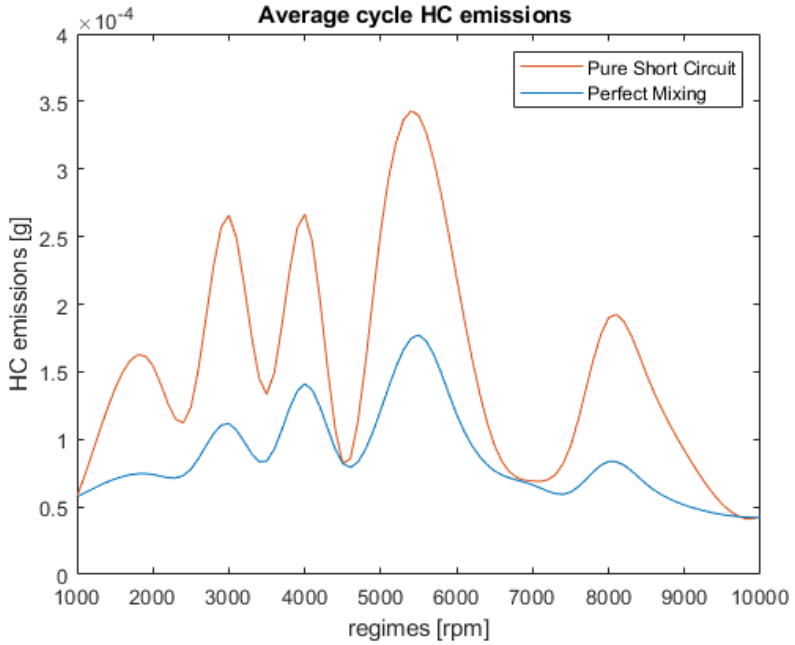

Figure 4.4: Average cycle HC emissions versus regime

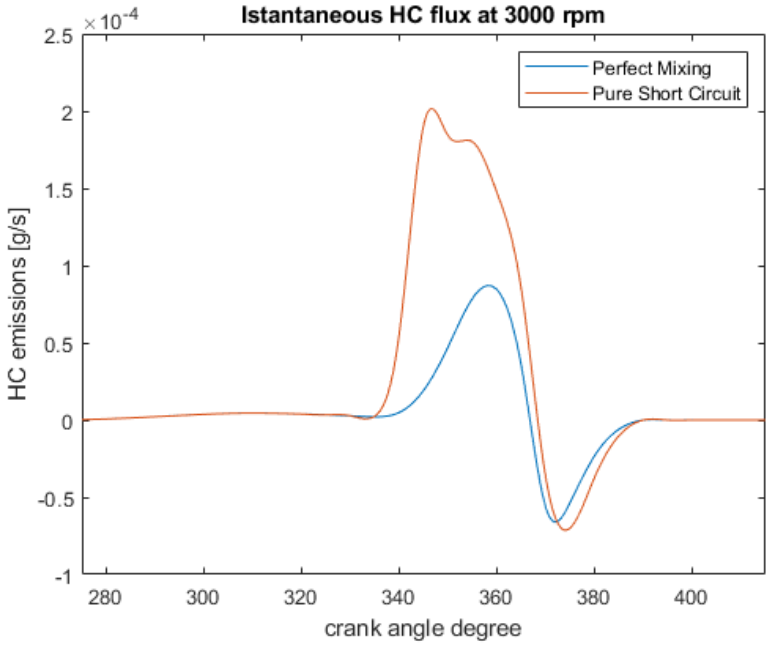

Figure 4.5: Istantaneous HC flux emitted at 3000 rpm

The model behaves as expected also in this situation: the average emissions are not only higher than in perfect mixing case, as expected, but they have also the same profile. Indeed, chart 4.4 shows that the two models are characterized by correspondent peaks, which are related to the same fluid dynamic phenomena, such as pressure pulses in the manifolds.

Turbulence intensity effect

According to [11], we can identify a correlation between the cylinder *turbulence intensity u'* and the calibration coefficients K_{MIX} *and* K_{SHC}. This choice allows to avoid the definition of a further parameter to be tuned.
In particular, the proposed values are shown in table 4.1.

Interval	Value
$0 < u' < 3$	$K_{MIX} = K_{SHC} = 0$
$3 < u' < 4$	$K_{MIX} = K_{SHC} = 0.5$
$u' > 4$	$K_{MIX} = K_{SHC} = 0.9$

Table 4.1: Calibration coefficients as function of the turbulence intensity

If we still consider the single cylinder engine, turbulence intensity is always lower than 3, resulting in null mixing and short circuit. Thus, we cannot perform a sensitivity analysis on the calibration coefficients under these conditions. Two possibilities are viable:

1. to keep the same correlation proposed by [11], by changing the engine sample;

2. to exploit different values of K_{MIX} and K_{SHC} on the same architecture, by assuming them always higher than zero.

In the former analysis, the second option is chosen, despite the first one is a good chance as well. The proposed correlation is shown in table 4.2: the experimental validation will proof the goodness of these values.

Interval	Value
$0 < u' < 3$	$K_{MIX} = K_{SHC} = 0.5$
$3 < u' < 4$	$K_{MIX} = K_{SHC} = 0.8$
$u' > 4$	$K_{MIX} = K_{SHC} = 1$

Table 4.2: Calibration coefficients as function of the turbulence intensity

Since the engine under investigation is the same as before, being u' always lower than 3, only the first value is exploited: $K_{MIX} = K_{SHC} = 0.5$.
HC emissions are compared both to perfect mixing and pure short circuit.

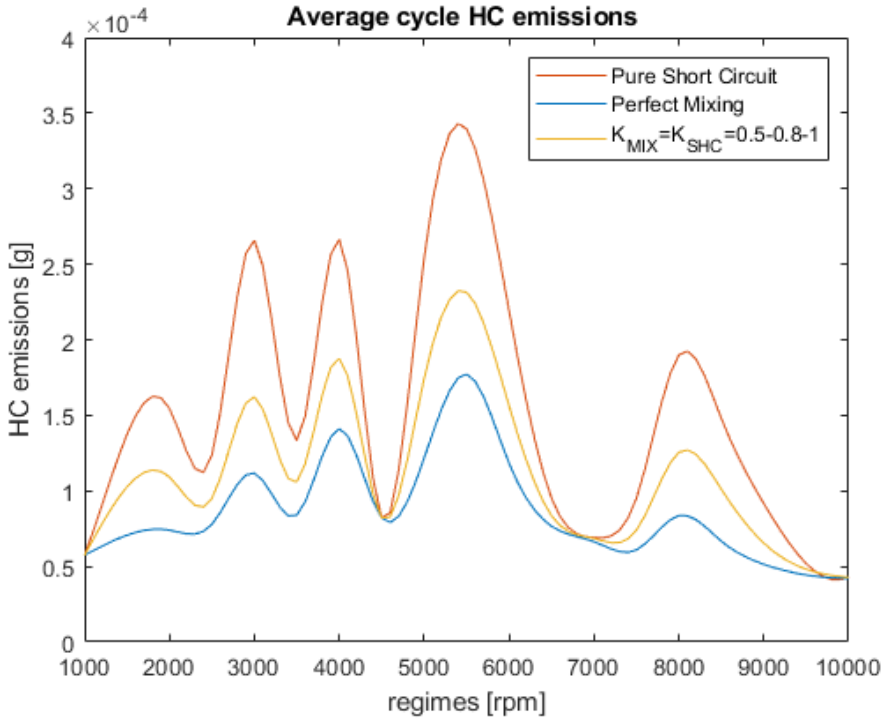

Figure 4.6: Average cycle HC emissions versus regime

As we expect, the current HC emissions are in between the perfect mixing and the pure short circuit cases. This consideration highlights the relevance of the calibration coefficients in capturing the HC emissions and, more in general, the goodness of the model to describe the scavenging phenomenon. However, in the following sections, we will investigate more complex engines in order to satisfy the validation of the model in case of higher turbulence.

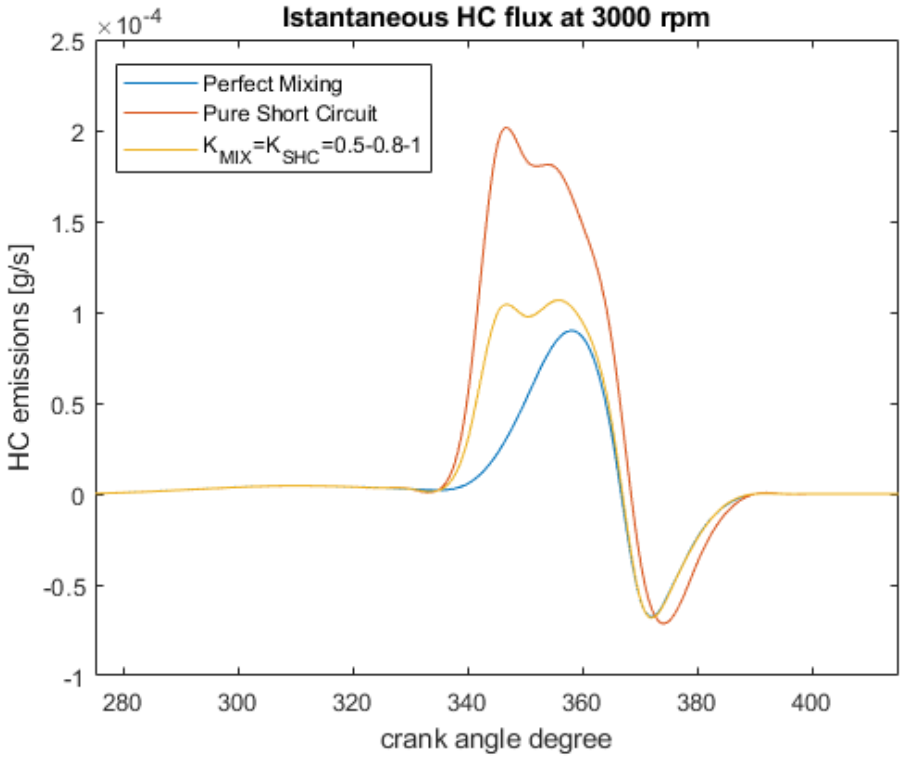

Figure 4.7: Istantaneous HC flux emitted at 3000 rpm

4.1.2 Valve overlap period: sensitivity analysis

An operating parameter that strongly influences the HC emissions is the valve overlap angle: the longer the two valves are contemporarily open, the larger the amount of fresh charge escaping through the exhaust port.
A sensitivity analysis on this parameter is carried out, by increasing it from 30° to 70°. In picture 4.8 the istantaneous HC emissions versus crank angle are represented, for a fixed rotational speed equal to 3000 rpm. The evaluation of K_{MIX} and K_{SHC} is done by means of the correlation proposed in table 4.4. We can clearly notice that, by increasing the overlap period, both the peak and the integral emissions over the crank angle increase.

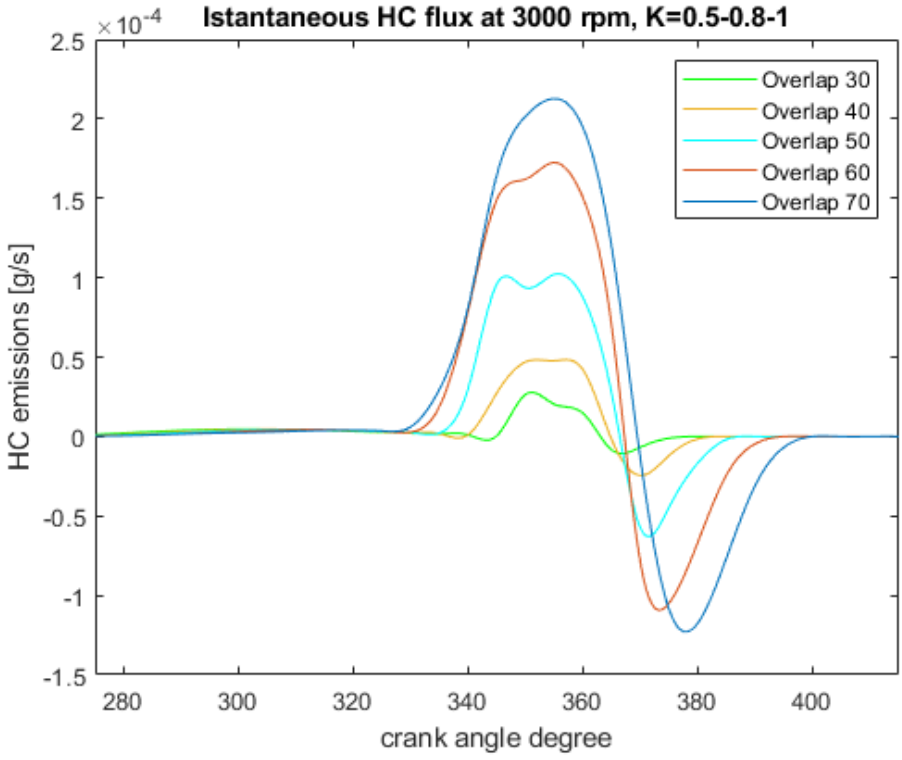

Figure 4.8: Istantaneous HC flux at 3000 rpm, $K_{MIX} = K_{SHC}$=0.5-0.8-1

The same analysis can be realized by considering either perfect mixing or pure short circuit. In the following, the pure through-flow case is reported in chart 4.9:

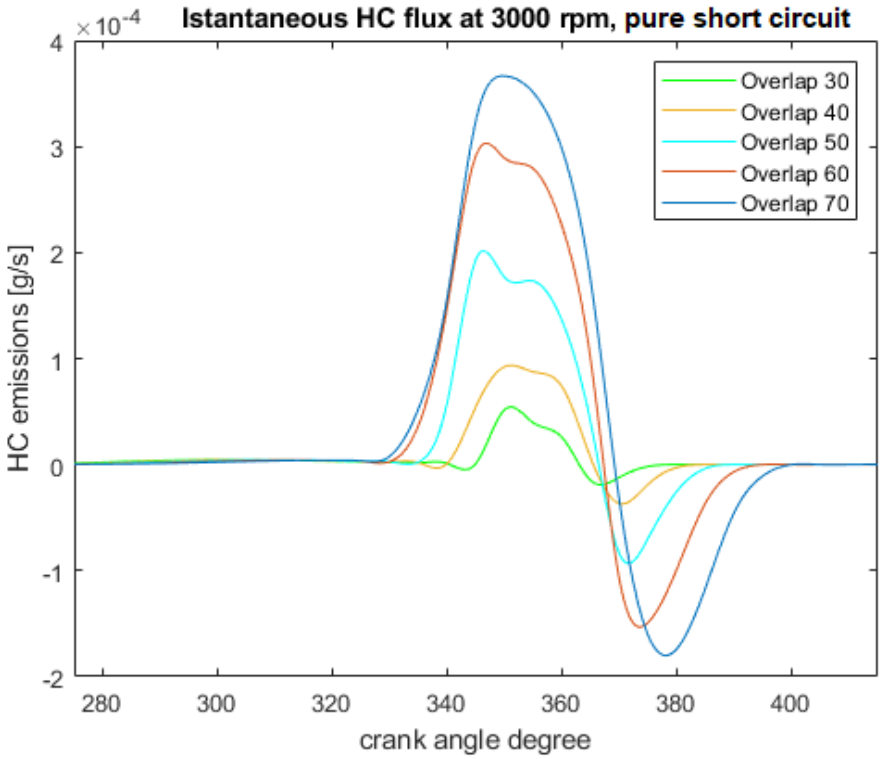

Figure 4.9: Istantaneous HC flux at 3000 rpm, pure short circuit

The chart above shows that the effect of the valve overlap period is relevant, also in case of pure short circuit.

Therefore, we can further investigate this aspect by comparing the peak HC emissions versus overlap angle for the pure short circuit and the turbulence intensity dependent cases.

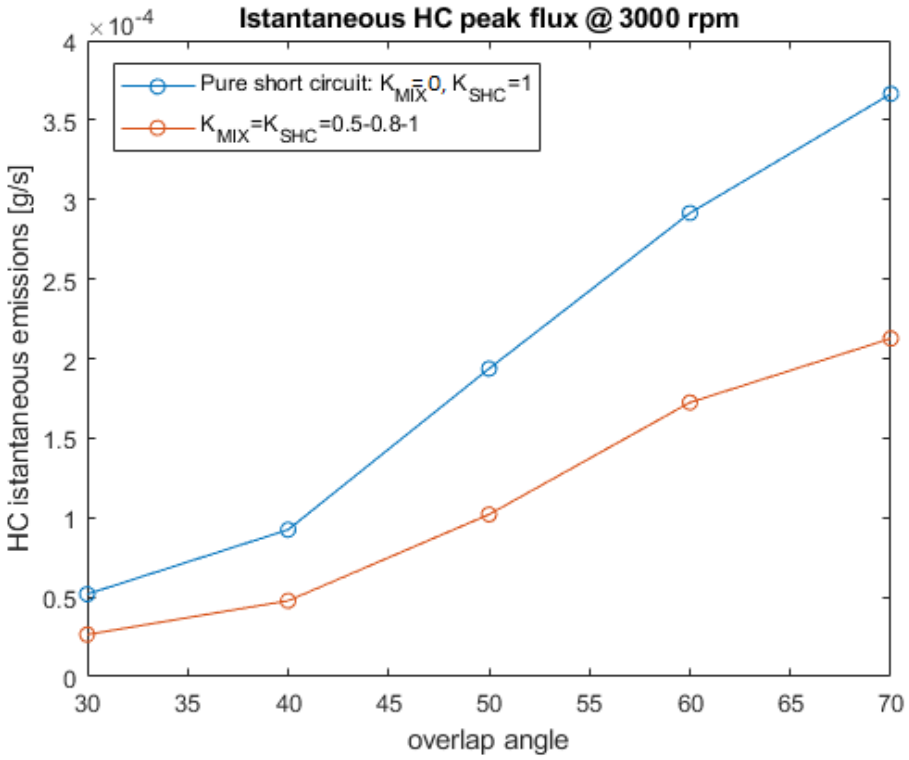

Figure 4.10: Istantaneous HC peak flux emitted at 3000 rpm, comparison

It is evident that, for every overlap angle, the pure short circuit peak flux is higher than the turbulence intensity dependent one. Moreover, both their trend is approximately linear, with similar slope: this means that the overlap angle variation have a similar effect for every value of K_{MIX} and K_{SHC}, so that a parametric analysis on the calibration coefficients is enough to calibrate the model.

4.1.3 NO_x and CO emissions

The scavenging model does not have a relevant influence on the other pollutants, i.e. NO_x and CO. Indeed, the controlling parameters are the temperature level inside the combustion chamber, which is not affected by the scavenging phenomenon, the compression ratio and the air fuel ratio.
In the following charts, we report the CO and NO_x emission trend for the single cylinder engine introduced so far.

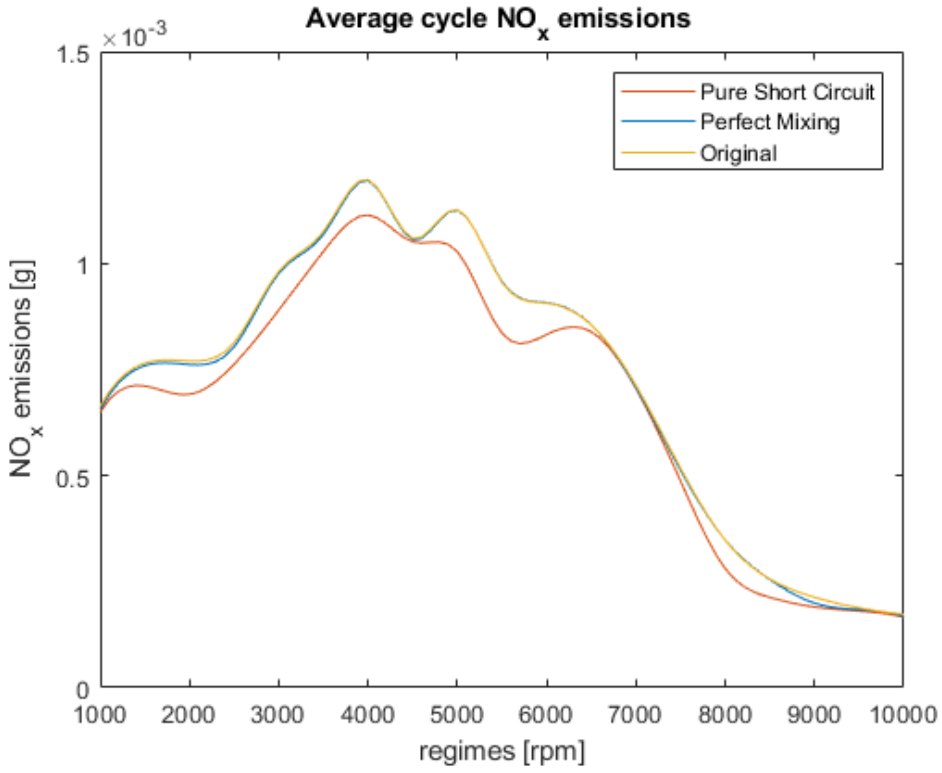

Figure 4.11: Average NO_x emissions versus engine rotational speed

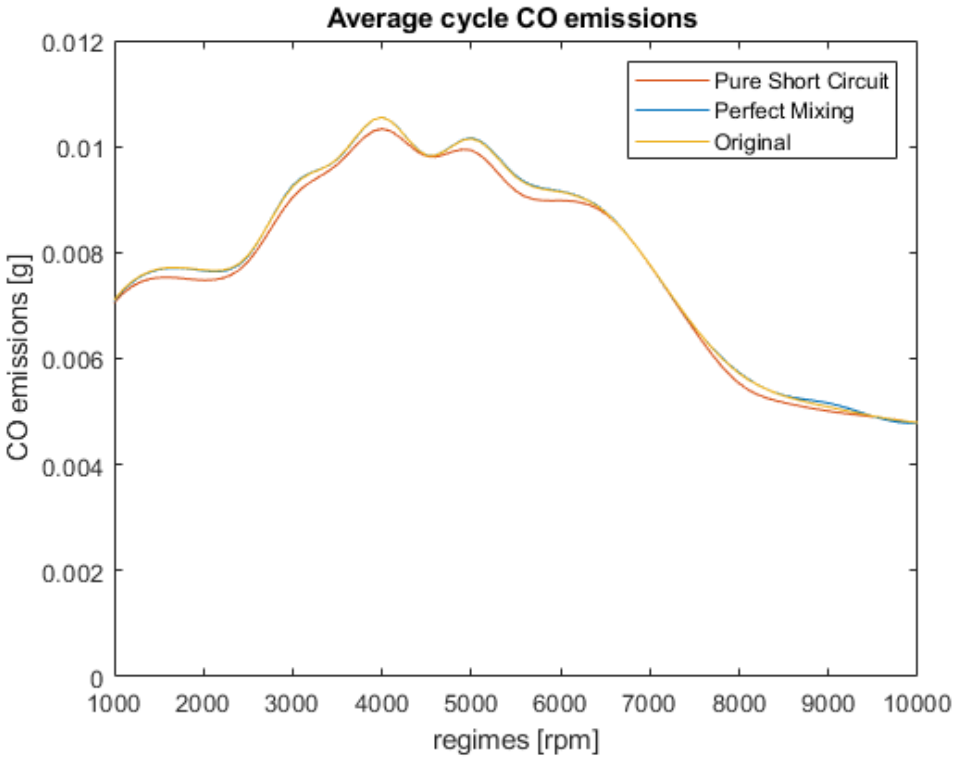

Figure 4.12: Average CO emissions versus engine rotational speed

We can clearly appreciate that the perfect mixing scavenging model emulates the original one, for both CO and NO_x. Furthermore, the pure through-flow emissions are quite closed to the others, since they are not affected too much by the gas exchange process.

The reason why the NO_x emissions are slightly lower for the pure short circuit is that part of the fresh charge is lost into the exhaust duct, by-passing the cylinder. Thus, a lower amount of air is available to form NO_x during combustion process.

The same happens also for CO, but with lower magnitude, since carbon atoms embedded in fuel molecules escape together with air, thus reducing their amount inside the cylinder.

4.2 Alfa Romeo 4 cylinders engine

In this section we will analyze the performance of the scavenging model on a more complex sample with respect to the previous one. The Alfa Romeo 4 cylinders, 16 valves, spark ignition engine is shown in figure 4.3.

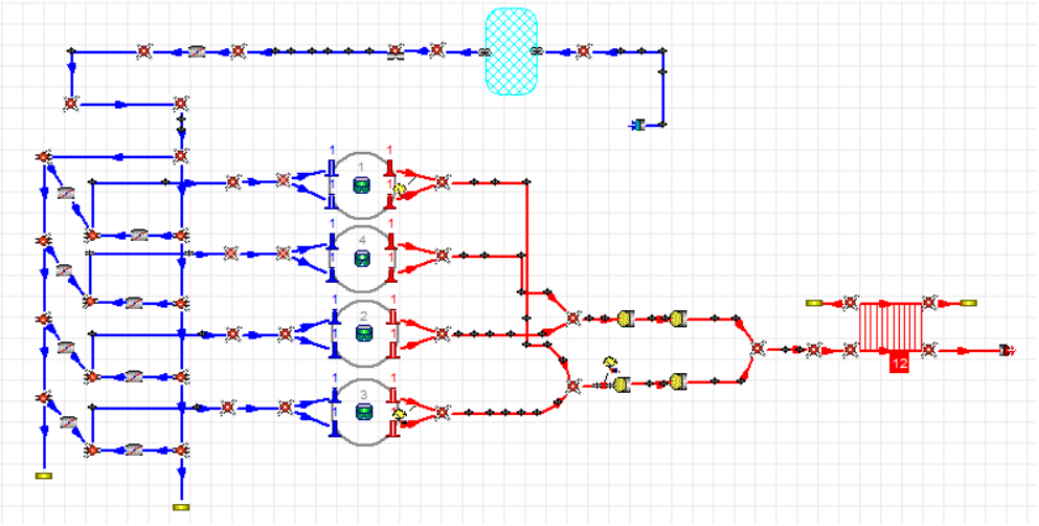

Figure 4.13: four cylinders, 16 valves, 2000 cm^3 displacement, spark ignition engine

The technical specification are reported in table 4.3.
This architecture is characterized by a higher turbulence intensity than the single cylinder, so that we may consider the laws for K_{MIX} and K_{SHC} proposed by [11]. The correlation for the calibration coefficient discussed so far is recalled in table 4.4.

Architecture	4 cylinders in line
Stroke	91.0 [mm]
Bore	83.0 [mm]
Rod length	145 [mm]
Surface ratio	1.12
Stroke to bore ratio	1.13
Cylinder displacement	493 [cm^3]
Total engine displacement	1970 [cm^3]
Compression ratio	10.0
Cylinder intake valves	2
Cylinder exhaust valves	2
Maximum torque	180 [Nm] at 3800 [rpm]
Maximum power	150 [CV] at 6300 [rpm]

Table 4.3: Alfa Romeo four cylinders technical data

Interval	$f_1(u')$	$f_2(u')$
$0 < u' < 3$	$K_{MIX} = K_{SHC} = 0$	$K_{MIX} = K_{SHC} = 0.5$
$3 < u' < 4$	$K_{MIX} = K_{SHC} = 0.5$	$K_{MIX} = K_{SHC} = 0.8$
$u' > 4$	$K_{MIX} = K_{SHC} = 0.9$	$K_{MIX} = K_{SHC} = 1$

Table 4.4: Calibration coefficients as function of the turbulence intensity

The focus is on both the average emitted mass of HC during a cycle, plotted for each rotational speed, and the HC instantaneous outgoing flux at a fixed regime. Thanks to the more complex scheme, we can investigate fluid dynamic quantities in different sections of the exhaust manifold. In particular, we will consider the first node of the duct downstream cylinder 1 and last node of the pipe upstream first catalyst (downstream the Y-junction).

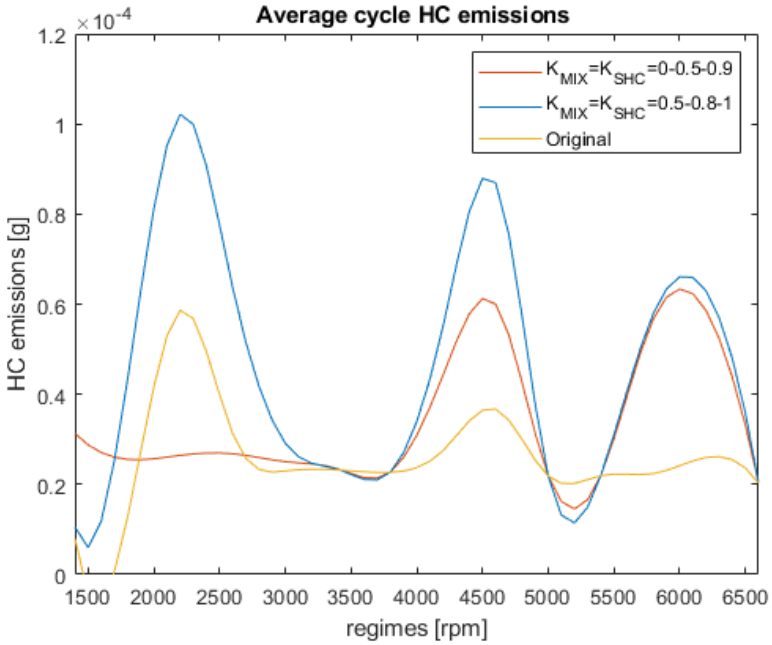

Figure 4.14: Average emitted mass of HC after cylinder 1.

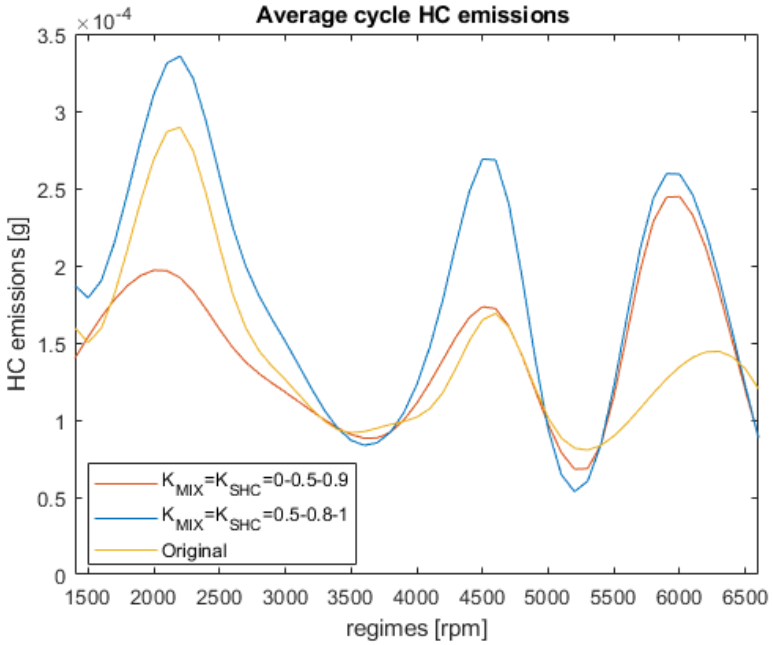

Figure 4.15: Average emitted mass of HC before the first catalyst.

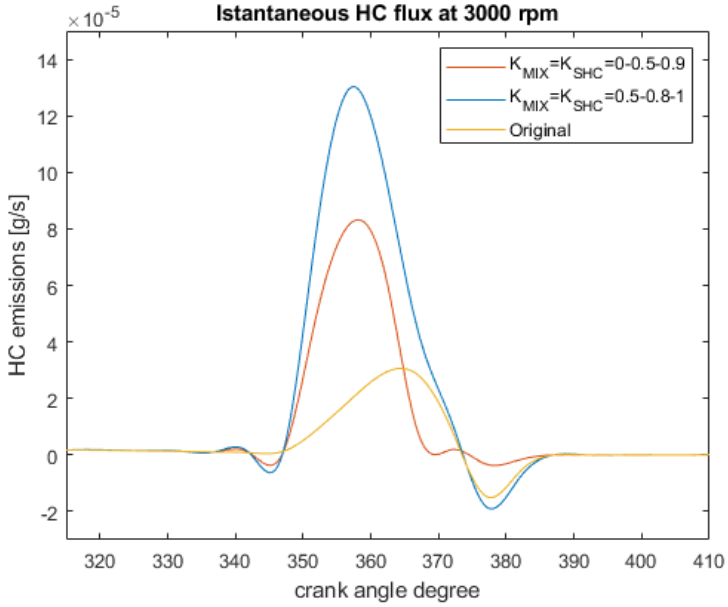

Figure 4.16: HC fluxes during overlap across the exhaust valve of cylinder 1.

The two correlations are both reliable, but the average HC emission charts reported above highlight some differences. Indeed, the first law considers neither mixing nor short circuit occuring in case of low turbulence intensity ($u' < 3$), resulting in a flat trend at low regimes, as we can appreciate in figure 4.14.

The second correlation, instead, shows correspondent peaks of HC emission to the original model, whichever the regime; also, the magnitude of these emissions is always clearly higher than the original model, as expected.

Furthermore, charts 4.14 and 4.15 give a clear idea of the relative impact of short circuit and mixing: the difference between $f_2(u')$ and the original model increases with the engine regime. Being the original model strictly closed to the scavenging one with perfect mixing, it is evident that short circuit magnitude over mixing increases with rotational speed as well.

The result obtained so far is that, for simple engine architectures, $f_2(u')$ seems to behave better along the whole rotational speed range. However, an experimental investigation on a more complicated engine will be proposed in the next chapter, in such a way to conclude which correlation is the best.

Chapter 5

Experimental model validation

In this chapter the scavenging model proposed so far will be validated, by comparing the values predicted by *Gasdyn* to the experimental ones. In particular, we will further investigate the proposed laws for K_{MIX} and K_{SHC}, in order to conclude which one describes the reality in the best way possible. We will focus on the Lamborghini V10, 5.0 litres, spark ignition engine. This architecture is more complex that the two analyzed so far: the number of cylinders, ducts and junctions is much higher than before; the geometries are more refined, with the aim to achieve the best tuning possible.

5.1 Lamborghini V10: technical description

The schematic of the Lamborghini V10 is reported in the figure 5.1.

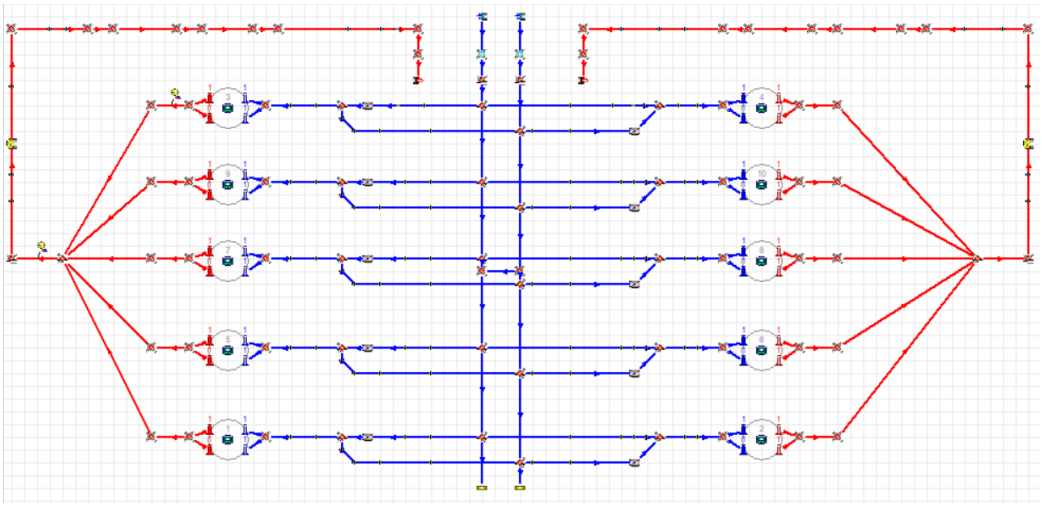

Figure 5.1: 10 cylinders, V of 90°, 40 valves, 4960 cm^3 displacement, spark ignition engine

A technical description of the engine is reported in table 5.1. The engine is equipped with a variable valve timing system, which regulates both the intake valve opening (IVO) and the exhaust valve opening (EVO): depending on the engine regime, a different crank angle is set. This system allows to optimize the volumetric efficiency, thus to maximize the torque at each rotational speed.

Another difference with respect to the simpler Alfa Romeo engine previously analyzed concerns the exhaust manifold collector junction: instead of using a simple boundary condition, where negligible pressure losses are considered, a multi-pipe junction is adopted. This assumption, according to [11], is more reliable, since it allows to account for pressure pulses coming from the neighbouring ducts, resulting in a more dissipative but realistic behaviour.

The scheme of this kind of junction is represented in figure 5.2.

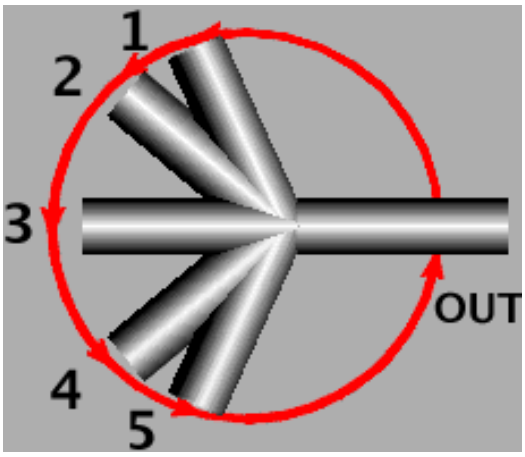

Figure 5.2: Multi-pipe, five-into-one junction scheme

Architecture	10 cylinders, 90° V shaped
Stroke	92.8 [mm]
Bore	82.5 [mm]
Rod length	154 [mm]
Surface ratio	1.03
Stroke to bore ratio	1.13
Cylinder displacement	496 [cm^3]
Total engine displacement	4960 [cm^3]
Compression ratio	11.3
Cylinder intake valves	2
Cylinder exhaust valves	2
Maximum torque	510 [Nm] at 4500 [rpm]
Maximum power	460 [CV] at 7500 [rpm]

Table 5.1: Lamborghini V10 technical data

5.2 Engine performance validation

Before going through the analysis of the scavenging model, it is required to validate the engine under investigation. In order to do that, the predicted profiles of pressure distribution in ducts, volumetric efficiency and brake torque have to be as close as possible to the experimental ones.
Starting from pressure distribution, the comparison to experimental result is carried out in different points, whose location is shown in chart 5.3.

- intake plenums (black);
- intake duct (yellow);
- exhaust duct (brown);
- cylinder (green).

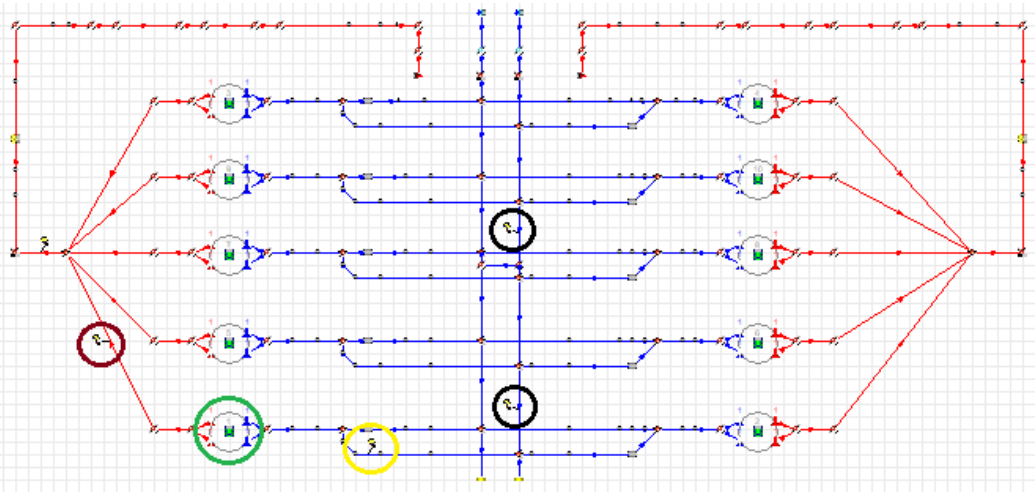

Figure 5.3: Output location

For all of these items, the comparison of the calculated pressure to the experimental one is done at 4000 and 7000 rpm.

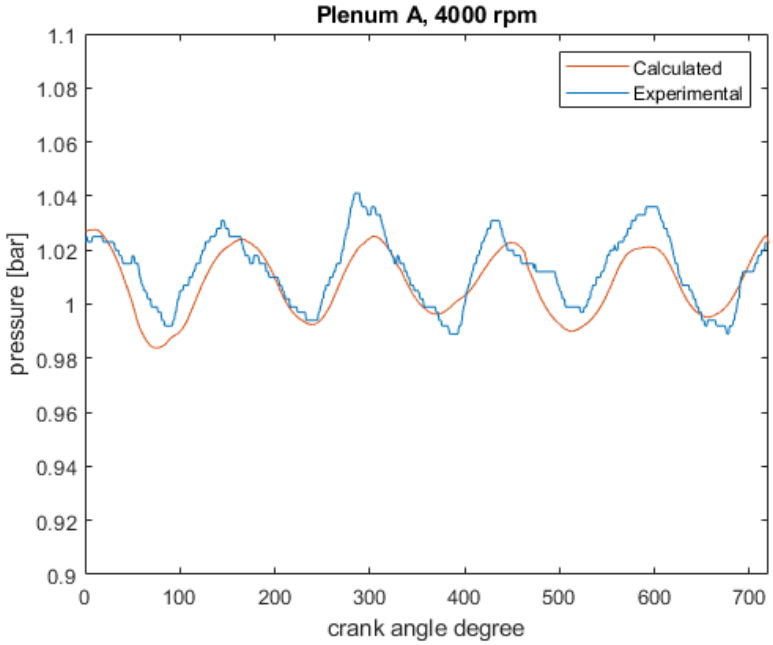

Figure 5.4: Pressure profile plenum A, 4000 rpm

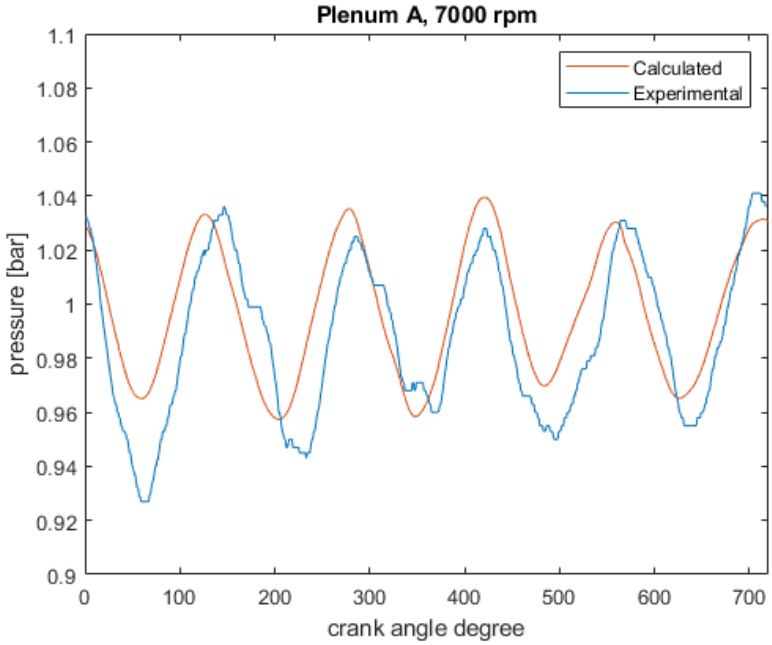

Figure 5.5: Pressure profile plenum A, 7000 rpm

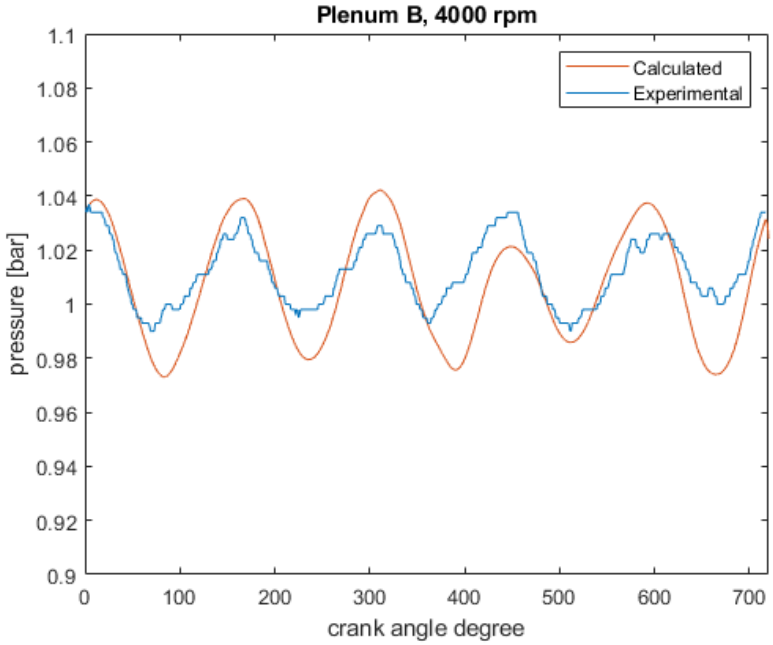

Figure 5.6: Pressure profile plenum B, 4000 rpm

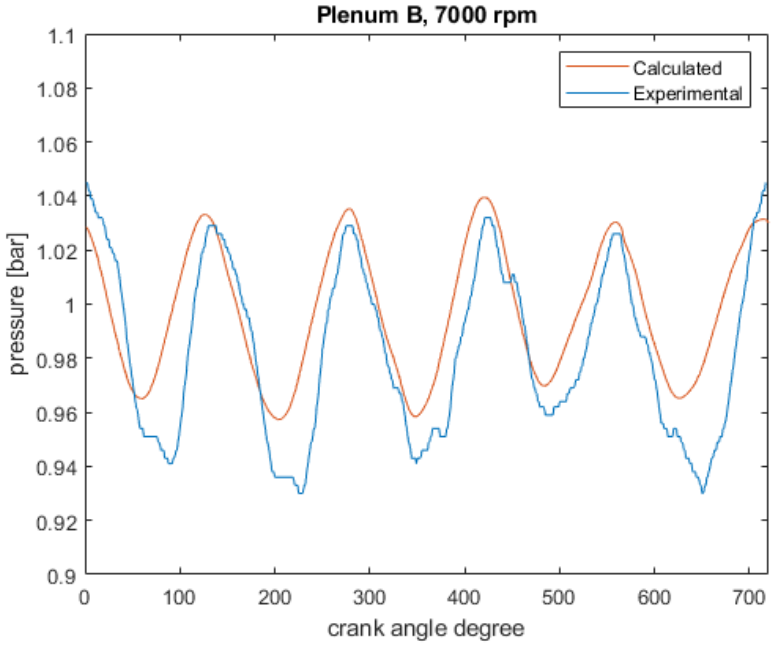

Figure 5.7: Pressure profile plenum B, 7000 rpm

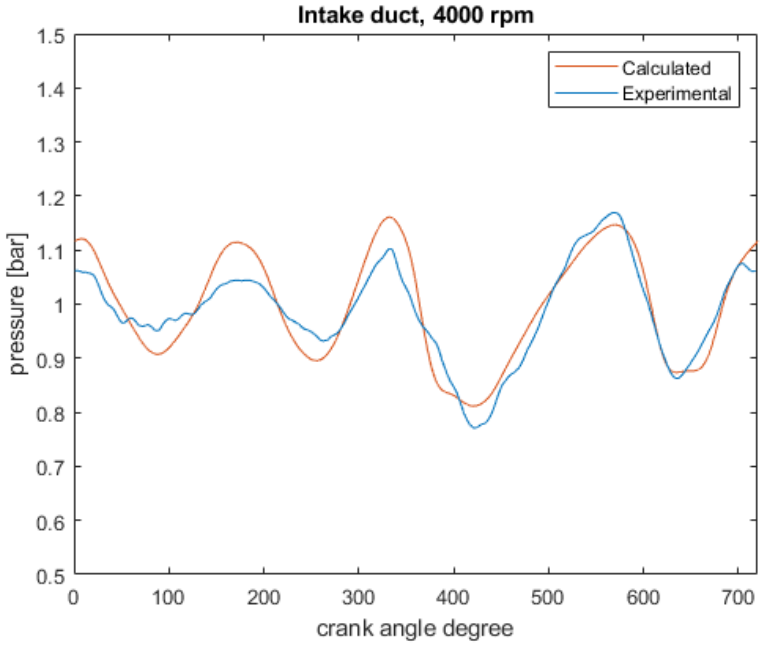

Figure 5.8: Pressure profile intake duct, 4000 rpm

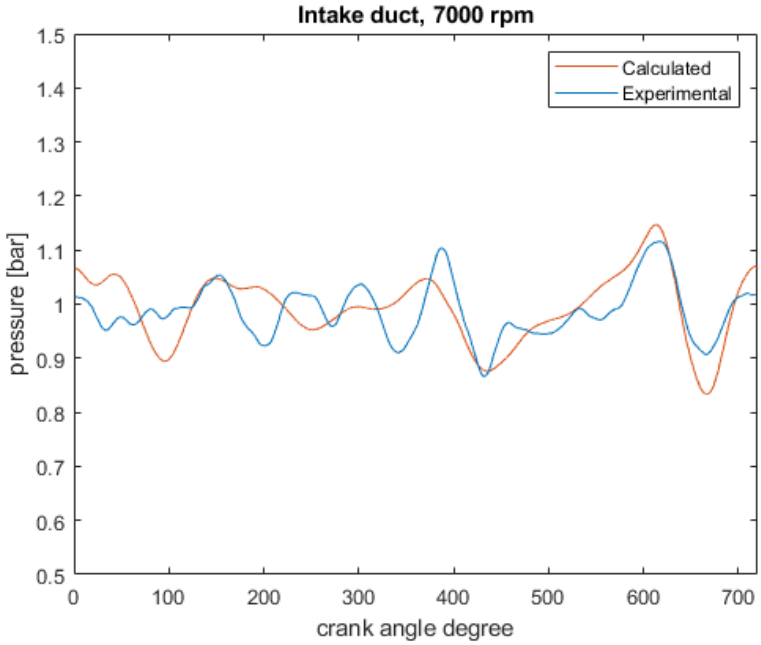

Figure 5.9: Pressure profile intake duct, 7000 rpm

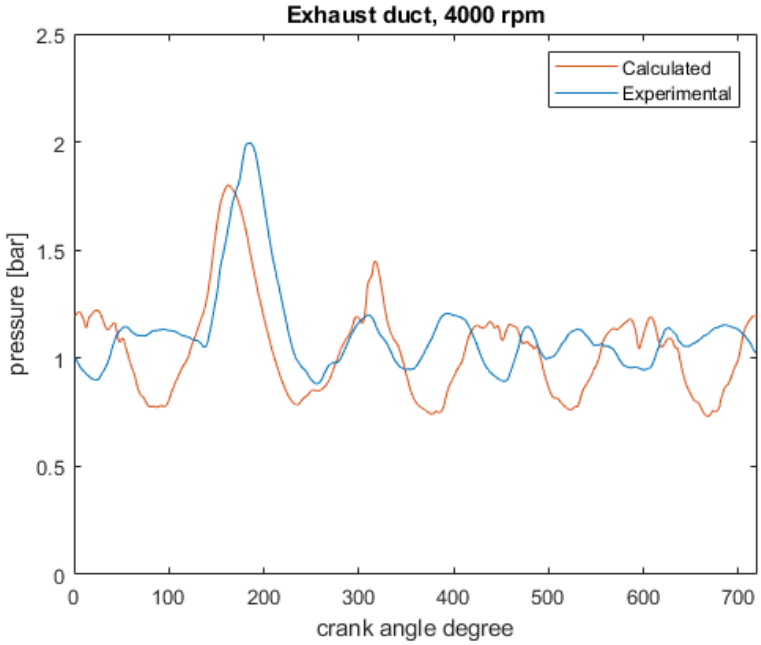

Figure 5.10: Pressure profile exhaust duct, 4000 rpm

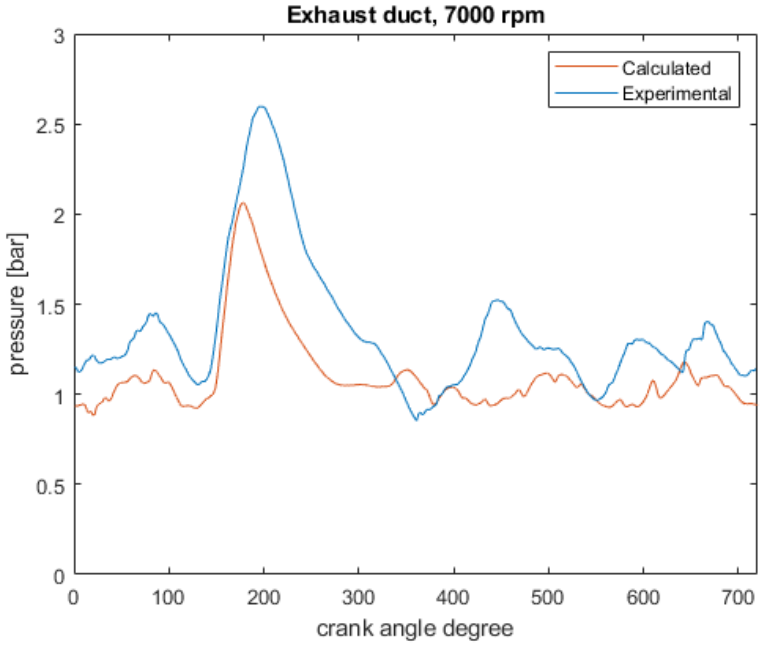

Figure 5.11: Pressure profile exhaust duct, 7000 rpm

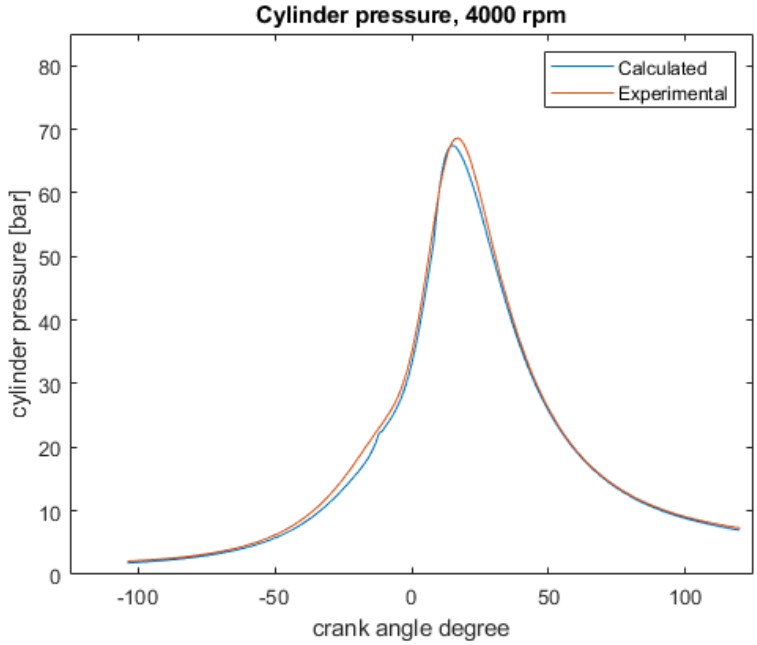

Figure 5.12: Cylinder pressure, 4000 rpm

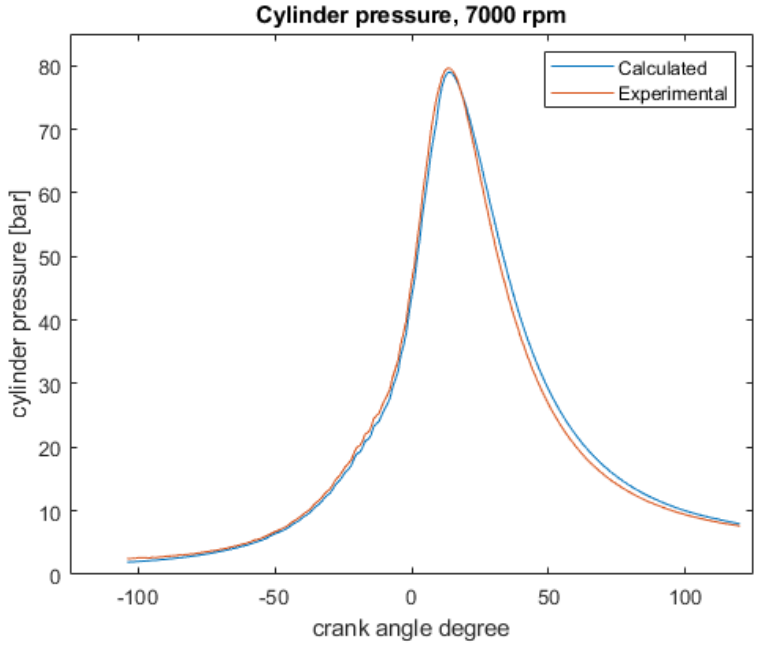

Figure 5.13: Cylinder pressure, 7000 rpm

The pressure profiles inside plenums are always well representative of the experimental results, with correspondent pressure peaks and good agreement to their absolute values. The same happens to the in-cylinder pressure. Focusing on intake and exhaust duct, instead, the predicitivity of the model is limited to the trend, with pressure variations in correspondence of experimental data peaks: similar trends were proposed by [11].

Once pressure profiles have been validated, the focus switches to volumetric efficiency and brake torque. In particular, in the following we will plot experimental data versus calculated ones, these latter both with original and scavenging model.

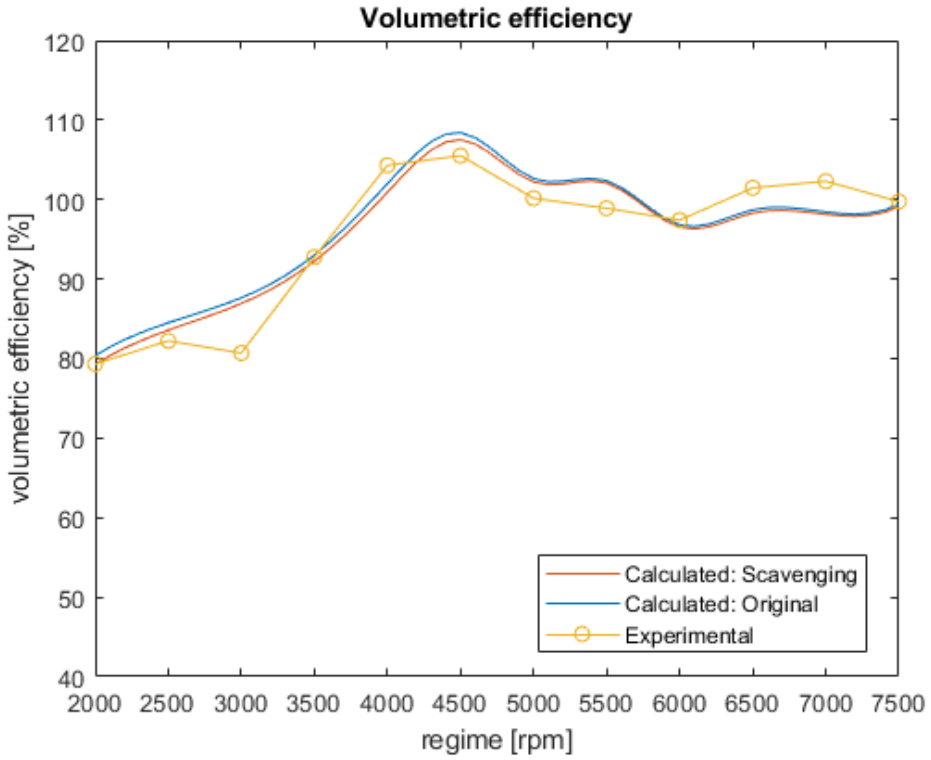

Figure 5.14: Volumetric efficiency versus engine rotational speed

Starting from volumetric efficiency, figure 5.14 shows that the trends predicted by the two models are quite closed one to the other. They are both weak in capturing the real trend at 3000 rpm, where experimental data show a slight decrease; for the other engine rotational speeds, the trend is well represented. Moreover, the regimes with upper and lower peak of the volumetric efficiency, i.e. 2000 and 4500 rpm, correspond to the real ones, with just a slight overestimation of the experimental results.
Switching to torque, the predictivity of the models is improved especially at low engine speed, as shown in chart 5.15.

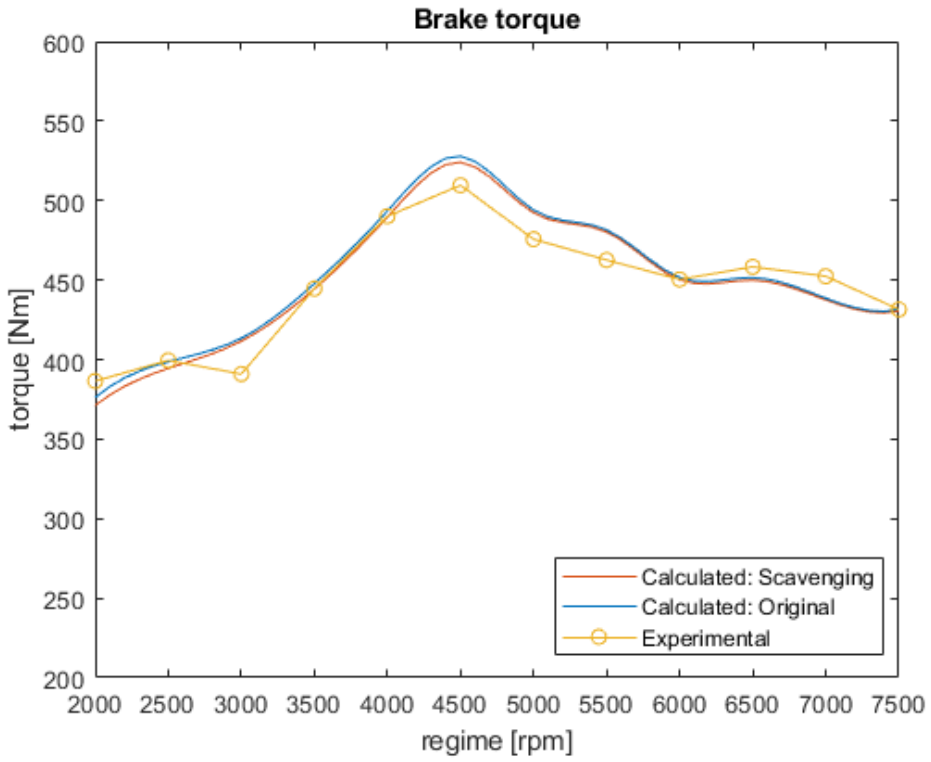

Figure 5.15: Torque versus engine rotational speed

As for volumetric efficiency, we can appreciate a little discrepancy between original and scavenging models, with this latter providing slightly lower val-

ues. This fact can be explained by thinking to the throughflow phenomenon: if we assume that the overall mass inside the cylinder is the same with and without throughflow, the percentage of residuals is higher in the first case, since a part of fresh charge escapes through the exhaust port.
Finally, figure 5.16 shows that the trend of the predicted power is really close to the real one.

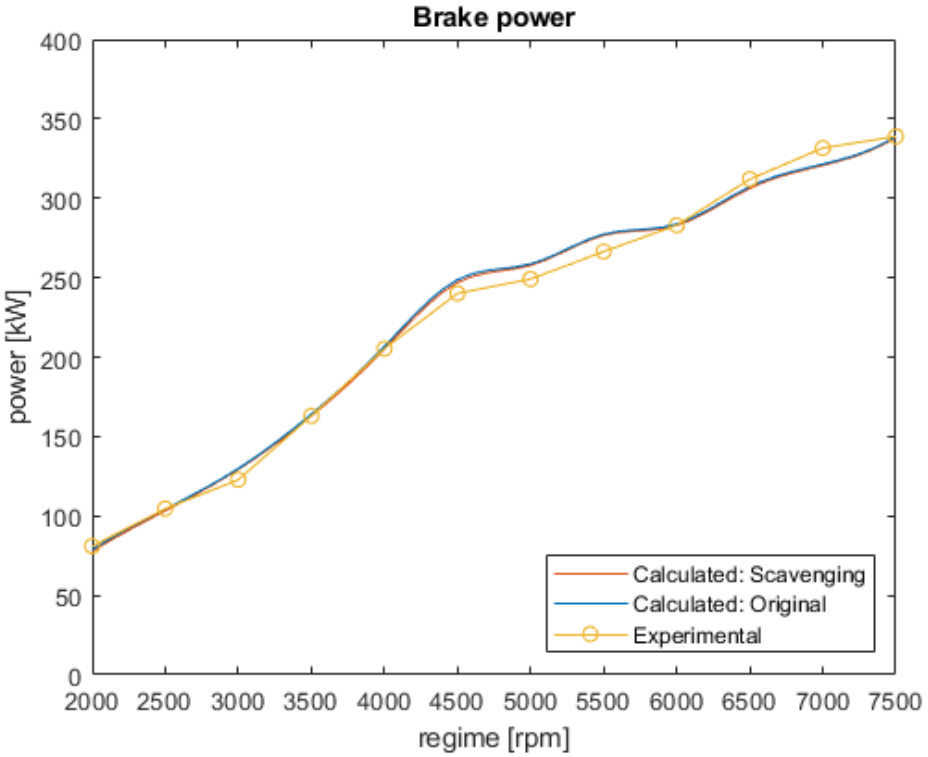

Figure 5.16: Power versus engine rotational speed

5.3 Pollutant emissions

The experimental analysis of pollutant emissions is performed downstream the five-into-one junction of the left engine bank, thus upstream the precat.

5.3.1 NO_x and CO emissions

As previously discussed, we expect that scavenging and original models have a similar behaviour in predicting NO_x and CO emissions, while they are clearly different in the description of HC.

To begin with, NO_x and CO predicted emissions are plotted together with experimental results.

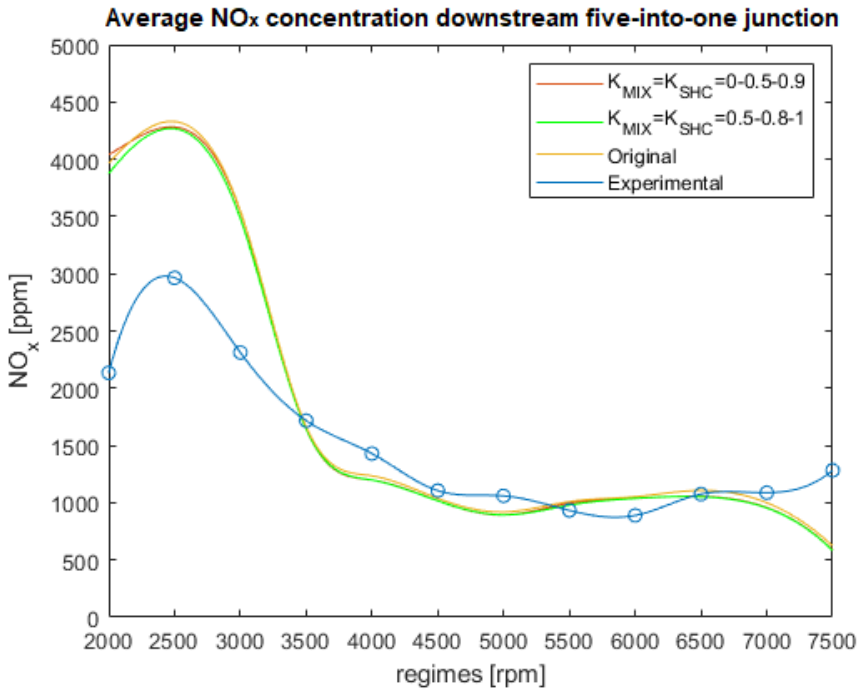

Figure 5.17: Average NO_x concentration versus engine rotational speed

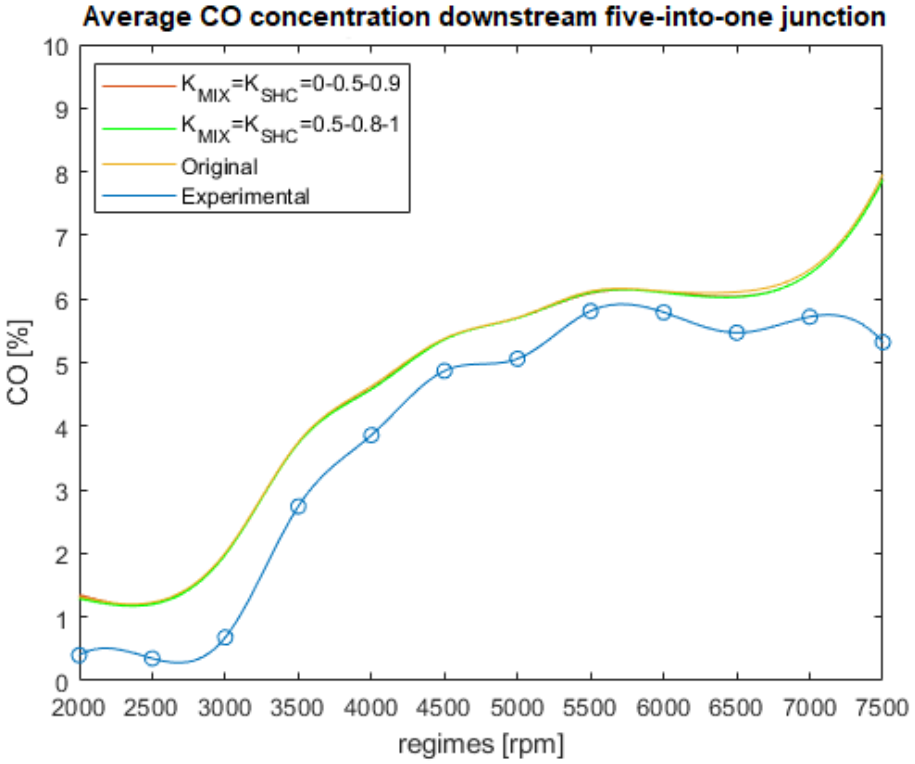

Figure 5.18: Average CO concentration versus engine rotational speed

From NO_x and CO trend, it is evident that scavenging model, with both correlations, behaves about in the same way as the original model.

Focusing on NO_x, the predictivity is quite good in the whole engine rotational speed range, with correspondent raise and decrease of the modelled concentration to the experimental one. For the lower engine regimes, the absolute value of the concentration is overestimated, despite the trend is correct; for n=7500 rpm, instead, the trend is opposite to the real one.

The CO predicted profile is good for all the regimes, except from the highest one, with opposite trend with respect to the experimental one, as it happens for NO_x.

Despite CO_2 is not a local pollutant, its concentration provides another example of the similarity between scavenging and original model results, as reported in chart 5.19.

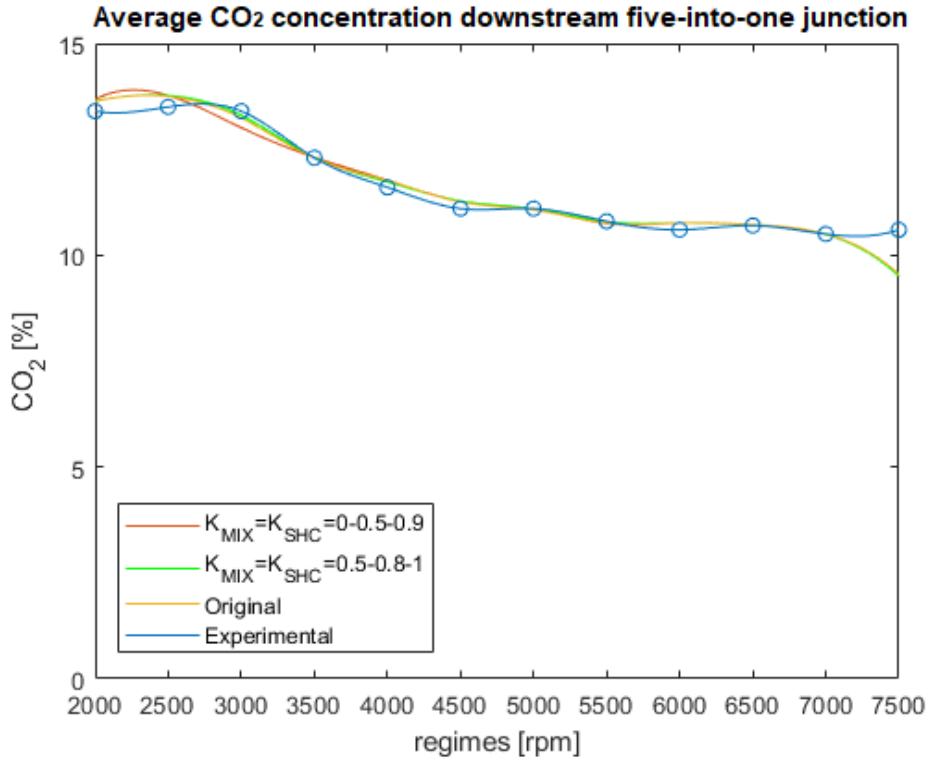

Figure 5.19: Average CO_2 concentration versus engine rotational speed

5.3.2 Unburned HC emissions

Unburned hydrocarbon emission is the main area of investigation of this thesis: in particular, we aim to establish an improved model with respect to the original one, able to capture peak emissions at mean engine regime. In this scenario, at first we compare the experimental average HC mass fraction downstream the junction to the result obtained with of the original model (figure 5.20).

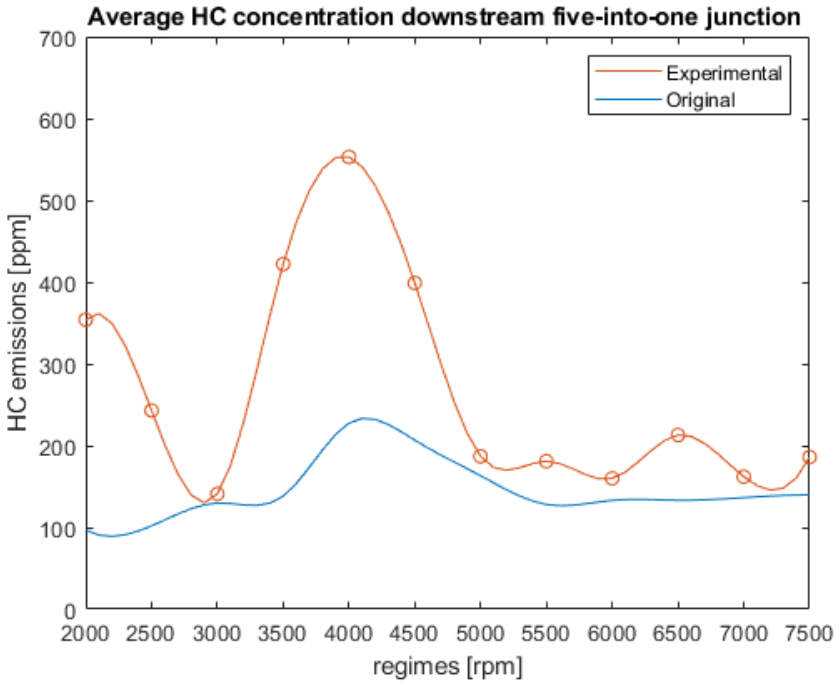

Figure 5.20: Average HC concentration versus engine regime

The profile is almost flat, far from the real HC concentration: it is evident that the original code is not able to significantly capture the peak emissions at 4000 rpm, as well as the decreasing trend at low regimes.
An improvement in the HC concentration description is provided by the scavenging model introduced so far.

The analysis is carried out with two different correlations for the calibration coefficients, as shown in table 5.2

Interval	$f_1(u')$	$f_2(u')$
$0 < u' < 3$	$K_{MIX} = K_{SHC} = 0$	$K_{MIX} = K_{SHC} = 0.5$
$3 < u' < 4$	$K_{MIX} = K_{SHC} = 0.5$	$K_{MIX} = K_{SHC} = 0.8$
$u' > 4$	$K_{MIX} = K_{SHC} = 0.9$	$K_{MIX} = K_{SHC} = 1$

Table 5.2: Calibration coefficients as function of the turbulence intensity

Chart 5.21 compares HC concentration predicted by the two laws to the experimental results.

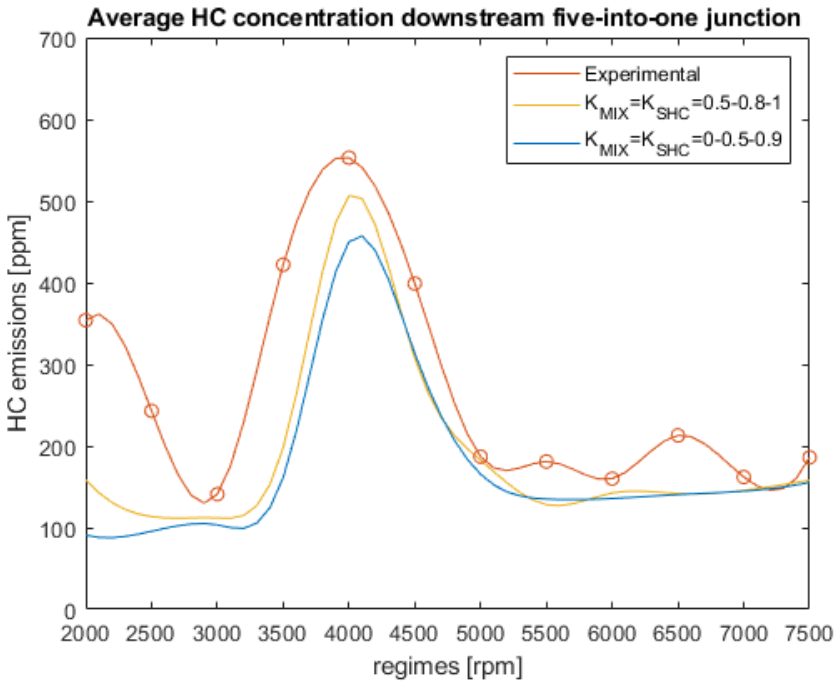

Figure 5.21: Average HC concentration versus engine regime

Chart 5.21 shows that both the correlations introduced so far are good in

predicting the peak HC emissions at 4000 rpm.

However, $f_2(u')$ is better because of the following reasons:

1. higher HC peak emissions at 4000 rpm, closer to the experimental trend;

2. capability to capture the decreasing trend from 2000 to 3000 rpm.

The results obtained by means of $f_2(u')$ applied to scavenging model are then compared to those of the original one, as shown in figure 5.22.

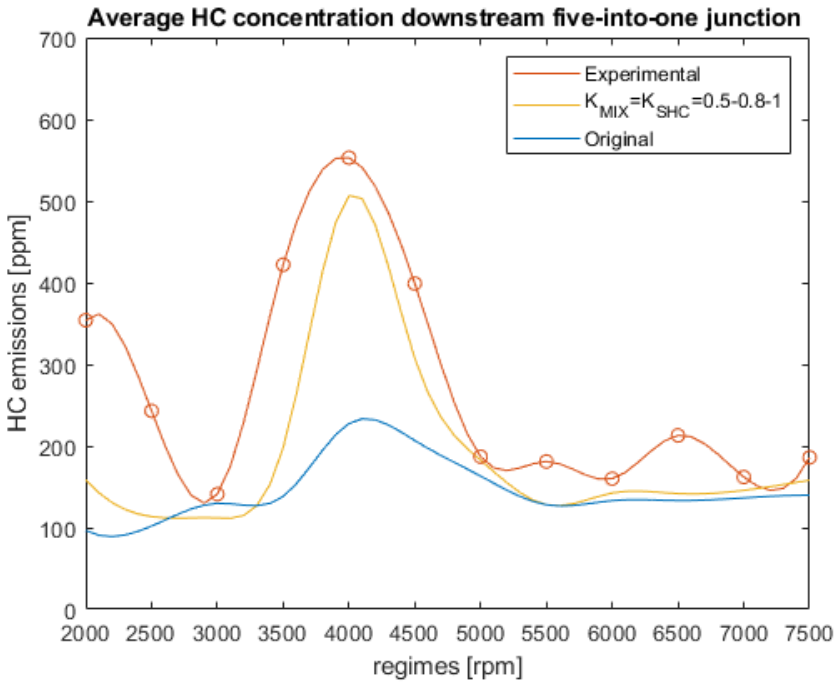

Figure 5.22: Average HC concentration versus engine regime

It is evident from chart 5.22 that the scavenging model guarantees an improvement of the simulation concerning HC emissions, with respect to the original one.

Conclusions

This thesis is a research on the thermo-fluid-dynamic simulation of internal combustion engines, based on the *Gasdyn* code, developed by the Energy Department of Politecnico di Milano.
The focus of this work has been the validation of the scavenging model in four stroke, naturally aspirated, spark ignition engines: the aim is to improve the predictivity of unburned HC emissions with respect to the original one.

Results

In order to assess the goodness of the model, a sensitivity analysis is performed on two simple engine architectures:

- single cylinder, 0.4 dm^3 displacement, 2 valves, naturally aspirated, SI engine;
- Alfa Romeo four cylinders in line, 2.0 dm^3 displacement, 16 valves, naturally aspirated, SI engine.

The parameters under investigation are calibration coefficients K_{MIX} and K_{SHC}, which are exploited by the new model, and the valve overlap period, which is a technical specification of the engine.
The main results are summarized below:

- the new scavenging four zone model emulates, in case of perfect mixing, the original single zone;
- pure through-flow is the situation with the highest HC emissions;
- different correlations for the calibration coefficients K_{MIX} and K_{SHC} allow to find a number of intermediate solutions between perfect mixing and pure short circuit;
- the larger the valve overlap angle, the higher the HC concentration in the exhaust manifold.

The model behaves as expected from theory. The correlation that better performs is represented in table 5.3: the main advantage is that it guarantees a good predictivity of HC peak emissions also for low values of the turbulence intensity, such as at low regimes and for simple engine architectures.

Interval	Value
$0 < u' < 3$	$K_{MIX} = K_{SHC} = 0.5$
$3 < u' < 4$	$K_{MIX} = K_{SHC} = 0.8$
$u' > 4$	$K_{MIX} = K_{SHC} = 1$

Table 5.3: Calibration coefficients as function of the turbulence intensity

Once the model has been analyzed from a theoretical point of view, it is experimentally validated. In order to do that, the architecture of the Lamborghini V10, 5.0 dm^3 displacement, 40 valves, naturally aspirated, SI engine has been implemented in *GasdynPRE* interface.
At first, the engine sample is tuned according to test bench data of ducts and cylinder pressures, volumetric efficiency and torque.

Finally, the scavenging model is applied on this architecture and its goodness is appreciated also from an experimental point of view. The correlation proposed in table 5.3 for the scavenging model confirms to be the best one in predicting the unburned HC emissions, also for complex engines.

Future developments

The main areas of improvement of the proposed model concern:

- the deeper investigation of the main parameters influencing calibration coefficients;
- the increase of number of zones inside the cylinder, in order to better investigate the relative impact of mixing and through-flow.

Bibliography

[1] G Ferrari (2014), *Internal Combustion Engines*, Esculapio

[2] D.E.Winterbone & R.J.Paerson (2000), *Theory of Engine Manifold Design*, Professional Engineering Publishing

[3] D.E. Winterbone & Pearson, R.J. (1999), *Design Techniques for Engine Manifolds: Wave Action Methods for IC Engines*, Professional Engineering Pub. Limited

[4] Benson, R.S. (1982), *The thermodynamics and gas dynamics of internal combustion engines*, Clarendon Press, Oxford

[5] H.K.Versteeg & W. Malalasekera (2007), *An introduction to Computational Fluid Dynamics*, Pearson

[6] Heywood, J. B. (1998), *Internal Combustion Engine Fundamentals*, McGraw-Hill, New York

[7] Ramos, J.I. (1989), *Internal Combustion Engine Modeling*, Hemisphere, New York

[8] A.Onorati (2019) *Modelling of Automotive Propulsion Systems course notes*, Internal Combustion Engine Group, Dipartimento di Energia, Politecnico di Milano

[9] A.Onorati (2018), *Internal Combustion Engines B course notes*, Internal Combustion Engine Group, Dipartimento di Energia, Politecnico di Milano

[10] Stephen J. Chapman (2018), *Fortran for Scientists and Engineers, Fourth Edition*, McGraw-Hill Education, New York

[11] A. Onorati, T. Cerri, M. Ceccarani, D. Cacciatore (2005), *Experimental Analysis and 1D Thermo-Fluid Dynamic Simulation of a High Performance Lamborghini V10 S.I. Engine*, SAE Technical Paper Series

[12] F.Bozza & A.Gimelli (2004), *A Comprehensive 1D Model for the Simulation of a Small-Size Two-Stroke SI Engine*, SAE Technical Paper Series

[13] Xinyan Wang & Hua Zhao (2019), *A High-Efficiency Two-Stroke Engine Concept: The Boosted Uniflow Scavenged Direct-Injection Gasoline (BUSDIG) Engine with Air Hybrid Operation*, Elsevier

[14] Wai K. Cheng, Douglas Hamrin, John B. Heywood, Simone Hochgreb, Kyoungdoug Min, Michael Norris (1993), *An Overview of Hydrocarbon Emissions Mechanisms in Spark-Ignition Engines*, SAE Technical Paper Series

[15] Shigeru Onishi, Souk Hong Jo, Pan Do Jo, Satoshi Kato (1984), *Multi-Layer Stratified Scavenging (MULS) - A New Scavenging Method for Two-Stroke Engine*, SAE International Congress and Exposition, SAE Technical Paper Series

[16] S.M.Aithal (2012), *A Comparative Study of NO_x Computation Methods Coupled to Quasi-Dimensional Models in SI Engines*, Proceedings of

the ASME 2012 Internal Combustion Engine Division Fall Technical Conference, September 23-26, 2012, Vancouver, Canada

[17] Lavoie, G.A, Blumberg P.N. (1980), *A fundamental Model for Predicting Fuel Consumption, NOx, and HC Emissions of the Conventional Spark-Ignition Engines*, Combustion Science and Technology

[18] *Gasdyn theory manual* (2018), Exothermia SA

[19] *Gasdyn User Guide* (2018), Exothermia SA

[20] ANSYS Fluent Theory Guide (2013), chapter 14.1 *NO_x formation*, http://www.pmt.usp.br/ACADEMIC/martoran/NotasModelosGrad/ANSYS%20Fluent%20Theory%20Guide%2015.pdf